

# Atmosphere

Volume 13 Number 4 1975

Canadian Meteorological Society  
Société Météorologique du Canada

# Atmosphere

Volume 13 Number 4 1975

## Contents

133

The General Circulation of the Pacific Ocean  
And a Brief Account of the Oceanographic Structure of the  
North Pacific Ocean

Part 1 – Circulation and Volume Transports

*S. Tabata*

169

Effective Wind Stress over the Great Lakes  
Derived from Long-Term Numerical Model Simulations

*T.J. Simons*

180

Fourier Series on Spheres  
*George J. Boer and Leonard Steinberg*

192

An Elementary Parcel Model  
With Explicit Condensation and Supersaturation

*R.R. Rogers*

205

Book Reviews

207

Index to Volume 13

ISSN 0004-6973

Canadian Meteorological Society  
Société Météorologique du Canada

---

**The General Circulation of the Pacific Ocean  
and a Brief Account of the  
Oceanographic Structure of the North Pacific Ocean<sup>1</sup>**

**Part I – Circulation and Volume Transports**

S. Tabata

*Institute of Ocean Sciences,  
Patricia Bay,  
Environment Canada,  
1230 Government Street,  
Victoria, B.C.*

[Manuscript received 29 September 1975]

---

**ABSTRACT**

A review of the surface and subsurface circulation of the North and South Pacific Oceans is presented together with a brief review of the structures of physical oceanographic properties of the North Pacific Ocean.

Our knowledge of the distribution of surface currents and sea surface temperatures is more complete than that of other properties. Principally this is because of the greater amount of available data which has been collected by the merchant and naval ships of the world's maritime nations, emphasizing the contributions they have made to oceanography. Despite this information, however, present knowledge about major surface currents is limited to their mean velocities, except for the Kuroshio and some of the equatorial currents about

which we have some vague notions as to their variability. The intermediate water of the Pacific Ocean as a whole has been studied in detail only once. Our knowledge of the oceanic heat transport is also very limited. The flow in a meridional section in the vertical plane will require special study as it may have important bearing on the heat transported by the ocean currents. Although volume transport for the major ocean currents has been estimated, the estimates are so few and the methods used to determine the transport so inconsistent that it is difficult to make a meaningful comparison of the transport values. Estimates that vary by a factor of two are common; some vary by an order of magnitude.

---

**1 Introduction**

Having rashly accepted the invitation to speak on this general subject, I thought about the North Pacific Oceanography and how it might affect the North

<sup>1</sup>Invited lecture for the 9th CMS Congress, Vancouver, B.C., 28–30 May 1975

American continental climate. It did not take me too long to realize what I had talked myself into. Those of us living in the western coastal area are aware of the influence of the ocean on our climate; the oceanic waters modify the coastal land temperatures and are responsible for the precipitation that occurs regularly. However, there are other large-scale ocean events away from our local area that appear to be more important in affecting the continental climate. Such events may occur in areas far removed from us. Before preparing this talk, I was familiar with the oceanography of the North Pacific Ocean, but knew little about that of the equatorial belt or of the South Pacific Ocean. Yet these regions appear to be just as important, or even more important, to the North American climate than the oceanic regions closest to us. Furthermore, when one considers the atmosphere-ocean interaction of the eastern equatorial belt it is likely that the corresponding belt on the western side of the Atlantic Ocean needs to be considered. For this reason, I felt rather uneasy about giving my presentation.

Nevertheless, it is perhaps worthwhile to review the present state of knowledge concerning the circulation and structure of the ocean properties of the North and South Pacific Oceans, including the equatorial region, so that we can get an overview of our knowledge, if only to point out its deficiencies. By doing so, we can make the best use of our present knowledge as a basis to plan the next stage of investigations needed to understand the behaviour of the ocean and the complex large-scale atmosphere-ocean interaction.

I shall discuss mainly the surface and subsurface circulation of the North and South Pacific Oceans and shall add some statements regarding the structure of ocean properties of the North Pacific Ocean, and finally mention a few examples of the probable impact of the ocean on the climate.

## **2 The atmospheric circulation of the North and South Pacific Oceans**

In view of the importance oceanographers place on the wind field, I shall first describe briefly the atmospheric circulation over the Pacific Ocean.

### *a Northern Winter*

The main feature of the atmosphere over the North Pacific Ocean during the northern winter is the presence of a well-defined low-pressure system (Aleutian Low) along the Aleutian Islands and the less well-defined high-pressure system (Pacific High) centred approximately 1500 kilometres (km) west of the California Peninsula (Fig. 1a). A very well-developed high-pressure system (Siberian High) with pressures exceeding 1032 mb also occurs several thousand kilometres to the west of the Aleutian Low. Due to the presence of such a combination of atmospheric systems the winds over the North Pacific are from the north on the western side and from the south along the eastern side. In the interior of the North Pacific between the Aleutian Islands and the Hawaiian Islands near-zonal westerly winds are present. South of California the anti-cyclonic winds of the Pacific High join the North East Trade Winds where because of the occurrence of a belt of relatively weak high-pressure

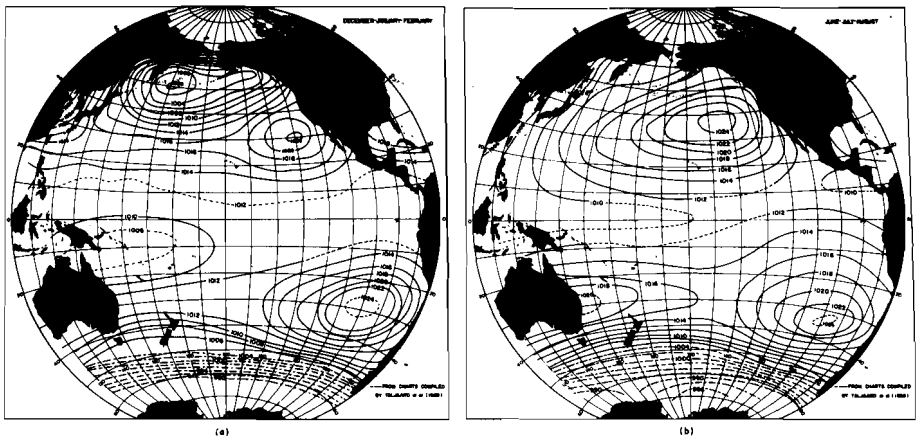


Fig. 1 Distribution of sea level atmospheric pressure (millibars) over the Pacific Ocean.  
 (a) Northern Winter  
 (b) Northern Summer

Pressure distribution over the North Pacific Ocean north of latitude  $15^{\circ}\text{N}$  are based on 22-year mean pressures (1950–71) obtained from unpublished data of the U.S. Navy Fleet Numerical Weather Center; distribution over the South Pacific Ocean, south of latitude  $50^{\circ}\text{S}$  is adapted from Taljaard *et al.*, 1969; the rest are adapted from Pilot Charts (U.S. Defence Mapping Agency Hydrographic Center, 1966; 1974).

between Latitude  $20^{\circ}$  and  $30^{\circ}\text{N}$ , the Trade Winds persist across the ocean (Mintz and Dean, 1952).

The South Pacific Ocean, on the other hand, is almost completely dominated by the presence of a well-developed high-pressure system (South Pacific High) centred approximately 3,000 km to the west of the coast of Peru. There is a relatively weak low-pressure area over northern Australia which joins the ocean-wide belt of low pressure along the Equator. An intense low-pressure area with pressures lower than 990 mb occurs over the northern part of the continent of Antarctica. To the south of Latitude  $40^{\circ}\text{S}$ , therefore, strong westerly winds are evident. Along the west coast of South America, winds are from the south, joining the Southeast Trade Winds as they approach the Equator. Moreover, there is some evidence that these Southeast Trade Winds cross the Equator, the Inter-Tropical Convergence Zone being situated at about  $2^{\circ}\text{N}$  at Longitude  $120^{\circ}\text{W}$  (Crowe, 1952).

Along the western side of the equatorial belt the winds from the Northern Hemisphere cross the Equator and because of the presence of a low-pressure area here, westerly winds are encountered in the region of northern Australia.

#### **b Northern Summer**

The most conspicuous aspect of the atmosphere over the North Pacific Ocean during the northern summer is the presence of a well-developed high pressure

system, the North Pacific High, centred approximately 2500 km west of the coast of California (Fig. 1b). It lies more than 1500 km to the north-west of the location occupied during the winter. There is also a relatively weak low-pressure area over the eastern part of Asia which extends into Bering Sea. As a consequence of these pressure systems, winds along the western side of the North Pacific are directed to the north while those along the eastern side are directed to the south, with a general eastward wind occurring to the north of Latitude  $30^{\circ}\text{N}$  in the central part and westward winds occurring south of it. Owing to the presence of the Pacific High, the northerly winds join the North-east Trade Winds. However, because the Pacific High is displaced farther to the north than during the winter, the Northeast Trade Winds are weaker than during the winter. As the winds approach the western side they veer and blow northward.

In the South Pacific Ocean the marked high-pressure system over the eastern side of the ocean is again as evident as during the northern winter. A less-intense high pressure system also occurs along the western side over Australia so that all along the latitude between Latitude  $25^{\circ}$  and  $35^{\circ}\text{S}$  a ridge of high pressure exists. Between the two high pressure systems of the North and South Pacific Oceans lies a belt of low pressure that extends across the ocean along the equatorial belt from New Guinea to Central America. As was the case in the winter, a marked low-pressure system is further evident over the continent of Antarctica. This latter system, combined with the ridge of high pressure at mid-latitudes, produces strong persistent westerly winds across a broad belt south of  $40^{\circ}\text{S}$ . There is evidence that these winds are somewhat weaker during this time than in the northern winter (Mintz and Dean, 1952; Hellerman, 1967, 1968). Due presumably to the weakening of the Northeast Trade Winds in the summer, the Southeast Trade Winds cross the Equator and the Inter-Tropical Convergence Zone is shifted about 1000 km to the north of its winter location (Crowe, 1952). Winds along the western side of the belt are from the south during this season in contrast to being from the north during the winter.

### **3 Circulation of the surface waters of the Pacific Ocean**

Our descriptive knowledge of the general circulation of the surface waters of most parts of the ocean is based largely upon the current velocity data obtained by merchant and naval ships of the maritime nations. The distribution of surface currents obtained from them are distributed as Pilot Charts mainly for the use of mariners. One of the earliest charts depicting the surface currents of the Pacific Ocean was compiled by Findlay (1853) who showed the presence of the following currents:

*The Japanese Current:* Depicted as a broad surface flow setting eastward between  $35^{\circ}$  and  $50^{\circ}\text{N}$ ; this current is now separated into the Kuroshio near the Japanese Islands, Subarctic and North Pacific Currents in the central part, and the California Current off the coast of North America. The Alaska Current is not evident, but Findlay indicates a northward coastal current off the Queen Charlotte Islands which continues along the Alaskan coast to Longitude

160°W. Part of the California Current is shown to continue along the coast of Mexico as far south as Latitude 10°S. The other part of the current is shown to feed into the westward-flowing *North Equatorial Current* which eventually turns poleward to join the Kuroshio.

*The North Equatorial Countercurrent*: Named by Findlay (1853), this is a very well placed, eastward current situated between 5° and 10°N.

*The Antarctic Current*: This is shown as a very broad, poorly-defined current setting northeastward. It differs from our present view of the current system of the South Pacific in that the set is presently considered to be to the east. Moreover, the South Pacific Current and the Antarctic Circumpolar Current now comprise the current Findlay called the Antarctic Current.

*The Cape Horn Current*: is correctly placed; so is the *Peru Current* (called Peruvian or Humboldt's Current at that time).

*The South Equatorial Current*: This is shown as a broad westward flow lying between Latitude 5°N and 25°S; until 1959 when the South Equatorial Countercurrent was discovered it was still considered to be as depicted by Findlay.

*The Australian Current*: Now called the *East Australian Current*, it is shown to originate to the south of New Caledonia. A northward-flowing current is shown along the west coast of New Zealand.

Considering that the chart was made from ships' reports from scattered observations a century and a quarter ago, it is remarkable that the major features of the circulation are present and with the exception of the details in the region north of 40°N and south of 40°S, they are in accord with our present notions of the circulation of the Pacific Ocean. Schott (1942) compiled a much improved chart based not only on ships' reports but also on observations taken by oceanographers. In fact, the Pilot Charts now available are not much better than those prepared by Schott. Distributions of surface currents derived from the more recent U.S. Pilot Charts for the Pacific Ocean are shown in Fig. 2 (U.S. Defence Mapping Agency Hydrographic Centre, 1966, 1974.)

### a *Northern Winter*

A comparison of the winter ocean circulation (Fig. 2a) with the corresponding atmospheric circulation (Fig. 1a) (surface winds are assumed to be directed at 15° to the left of the downwind direction of the geostrophic wind vector in the Northern Hemisphere and to the right in the Southern Hemisphere) shows general similarity between the two, except that the former tends to deviate somewhat to the right of the direction of the wind in the Northern Hemisphere and to the left in the Southern Hemisphere, no doubt due to the Coriolis effect. On the other hand, the southward-flowing East Kamchatka Current and the Oyashio in the Western North Pacific (Fig. 3) appear to strengthen during the winter (Hata, 1965; Arsen'ev, 1967; Hughes *et al.*, 1974) apparently in response to the increase in the northerly winds that occur during this period. However, there are major differences between the two: along the western side

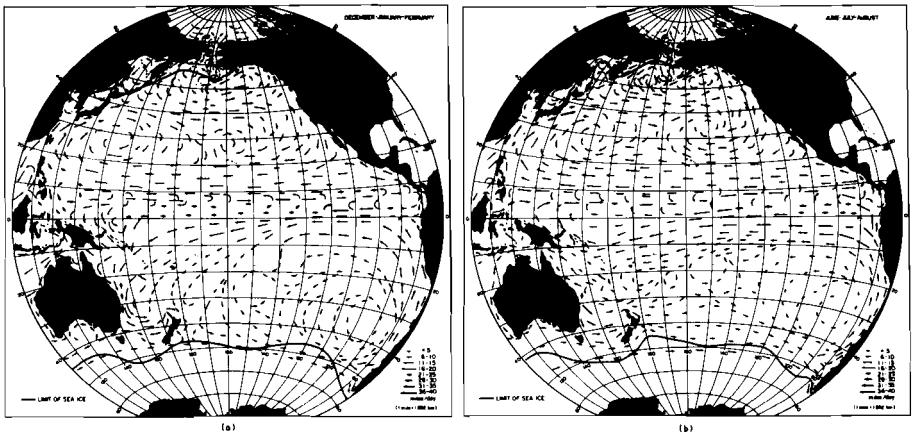


Fig. 2 Distribution of surface currents of the Pacific Ocean

(a) Northern Winter

(b) Northern Summer

Adapted from Pilot Charts (U.S. Defence Mapping Agency Hydrographic Center, 1966; 1974).

of the ocean are the intensified poleward-flowing western boundary currents such as the Kuroshio in the North Pacific and the East Australian Current in the South Pacific (Fig. 3). The Kuroshio, in particular, flows almost unimpeded in the opposite direction to that of the prevailing winds, although its speed has been noted to decrease slightly during the last quarter of the year (Taft, 1972). Along the eastern side of the North Pacific the southward-flowing branch of the Subarctic Current, the California current, flows contrary to the direction of the southerly winter winds. However, the seasonal northward-flowing Davidson Current (not shown), which is generally directly attributable to these winds also occurs along the west coast of North America coastward of the California Current. Similarly, the south-eastward-flowing New Guinea Current occurs only during the winter when persistent northerly winds prevail. Though not shown in the U.S. Pilot Charts there is a westward-flowing Antarctic Current during the winter which appears in charts published by others (for example, Schott, 1942).

It is mostly in the tropical and equatorial zones that the atmospheric and oceanic circulation show marked departure. Although the Equatorial Current along the Equator as well as both the North and South Equatorial Currents flow westward in the same general direction as the Northeast and Southeast Trade Winds there are, in this oceanic region, two narrow countercurrents symmetrical to the Equator, the North and South Equatorial Countercurrents (Fig. 3), which flow eastward against the wind. At, and very near, the Equator a strong jet-like eastward-flowing Equatorial Undercurrent (Fig. 3) is also present. The Equatorial Undercurrent (Cromwell *et al.*, 1954) and the South Equatorial Countercurrent (Reid, 1959) have only been discovered during the past two and a half decades. The South Equatorial Countercurrent, in fact,

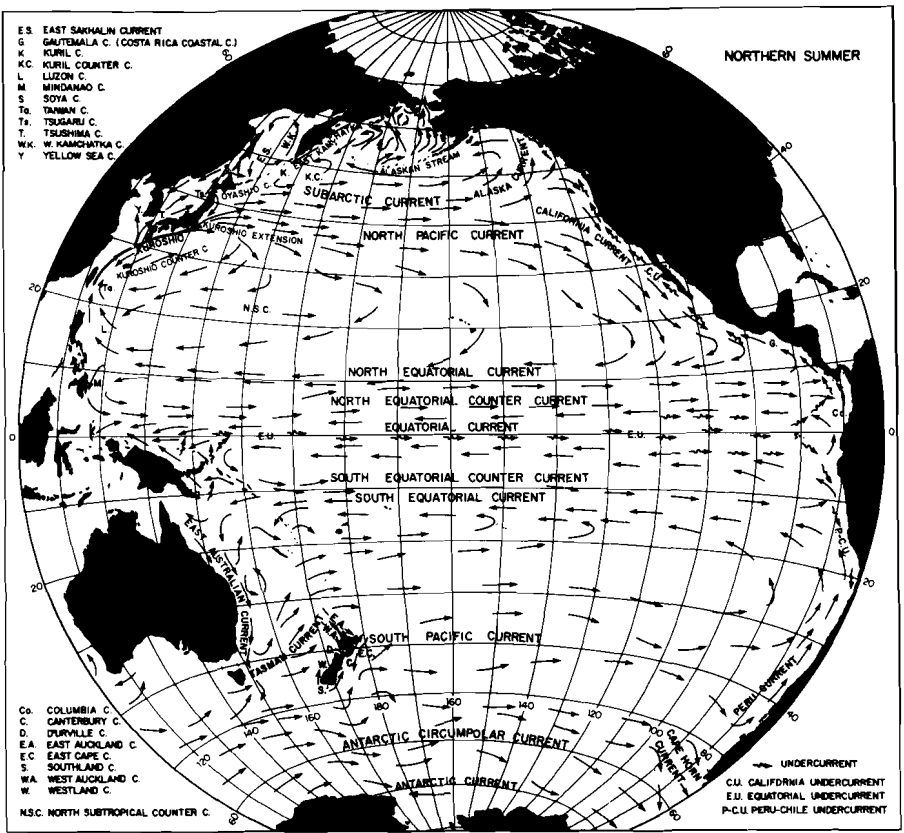


Fig. 3 Nomenclature of Currents of the Pacific Ocean during Northern Summer. During Northern Winter a narrow poleward-flowing *Davidson Current* occurs along the Pacific coast of the United States; the southeastward-flowing *New Guinea Current* occurs along the northern side of New Guinea during the winter.

is not evident in the Pilot Charts published by the U.S. authorities, but is shown to occur in the western part of the South Pacific in comparable charts published by authorities in the United Kingdom (Air Ministry, 1939) and the Netherlands (Koninklijk Nederlands Meteorologisch Institut, 1949, as quoted by Reid, 1959). A more detailed discussion of the equatorial currents will be given subsequent to consideration of the geostrophic currents and volume transports.

### b Northern Summer

The distribution of surface currents for the northern summer is shown in Fig. 2b. A comparison of this with the wind field of Fig. 1b again shows general similarity. But it is the similarity between the oceanic circulation patterns in winter and summer that is more conspicuous, although where the wind velocity changes markedly with season, this correspondence is evident in some regions.

Along the eastern side of the North Pacific the seasonal current pattern is basically unchanged except that along the coast of the United States the poleward-flowing, coastal Davidson Current is absent during the summer. Near the western end of the Equator, the southward-flowing Mindanao Current runs against the northward-blowing Southeast Trade Winds that cross the Equator and with the reversal of winds in the western Equatorial Pacific, from northerly to southerly, the New Guinea Current disappears. Moreover, the East Australian Current weakens during the northern summer (Hamon, 1965) due probably to this reversal of the equatorial winds. The westward-flowing Antarctic Current that occurs during the northern winter appears also to be present during the northern summer (Schott, 1942), but seems to be weaker than during the northern winter.

Apart from these differences, the major features of the distribution of surface currents during the summer are very similar to those during the winter.

As was mentioned earlier, the distribution of surface currents as portrayed in the various Pilot Charts are based on ships' reports. The surface current velocities indicated in these reports are derived from dead-reckoning methods in which the course (direction) and distance travelled in a time interval (course-made-good) is compared to where the ship should have travelled during that interval. The main disadvantage of this method is the uncertainty of the results arising from probable failure to account for wind effects on the ship. The other drawback of the method is the uneven spatial coverage due to the existence of established ship routes which only span certain limited areas of the ocean.

### c *Nomenclature of Currents in the Pacific Ocean*

In the previous section, reference was made to the names of some of the major currents of the Pacific Ocean. It will be useful, at this stage, however, to familiarize ourselves with the names of the other currents as some of these names will frequently turn up during the subsequent discussions. Fig. 3 shows the names of these currents and their geographical locations. Since the winter currents generally occur at the same location as the summer currents, it is not necessary to show them separately. The following two winter currents are not shown in the Figure: the *Davidson Current*, a narrow poleward-flowing current located between the west coast of the United States and the southward-flowing California Current; the *New Guinea Current*, a southeastward-flowing current that occurs along the northern coast of New Guinea. In addition, the westward-flowing Antarctic Current off the northern coast of the continent of Antarctica, though absent in the U.S. Pilot Charts, has been included in Figure 3.

This essentially completes the list of names that I have come across in the oceanographic literature. Where two or more names occurred for the same current, I have adopted those generally used by North Americans.

Most current atlases of the North Pacific indicate the zonal eastward flow to be composed of the northernmost Subarctic (or Aleutian) Current, the West Wind Drift, and the southernmost North Pacific Current. Actually, there is, as

yet, no truly valid way of distinguishing between the West Wind Drift and the Subarctic Current so we shall simply combine them into the Subarctic Current. Ever since the discovery of the Equatorial Undercurrent in 1952 and the South Equatorial Countercurrent in 1959, the naming or renaming of currents in the Equatorial Current System has not been universally agreed upon. In the past the South Equatorial Current comprised the broad westward flow occurring between the latitudes of 5°N to 20°S. Perhaps it will be reasonable to split this current and simply call the westward flow along the Equator the Equatorial Current, as Burkov (1966), Hisard *et al.* (1970), and Rotschi (1973) have already done. This leaves the westward-flowing current to the south of the South Equatorial Countercurrent unnamed. We shall call this the South Equatorial Current which then tidies up the nomenclature in the Equatorial region by its symmetry about the Equator.

Of the undercurrents, the strong, eastward ocean-wide Equatorial Undercurrent is the most prominent one. Two other undercurrents, the northward-flowing California Undercurrent in the North Pacific and the southward-flowing Peru–Chile Undercurrent, are present along the east side of the Pacific. However, these currents are generally of narrow breadth and occur at depths of only a few hundred metres.

Recent studies have also suggested the occurrence of narrow eastward-flowing countercurrents at latitudes of 20°–30° within the western part of the Pacific Ocean in both hemispheres (Yoshida and Kidokoro, 1967b). These are tentatively called the Subtropical Countercurrents.

There is no doubt as to the existence of the Equatorial Undercurrent but confirmation of the existence of the South Equatorial Countercurrent, the Subtropical Countercurrent and the South Equatorial Current (which has been separated from the Equatorial Current) awaits further study.

#### **4 Surface geostrophic currents**

Much of our knowledge about ocean circulation has been gained from the consideration of geostrophic currents. These are usually calculated relative to 1000 m depth or to the 1000 decibar level (about 990 m) since most of the oceanographic observations made in the past have not sampled beyond the depth of 1000 m. Where the baroclinic structure at levels greater than 1000 decibars is absent, the geostrophic current velocities obtained relative to the 1000 decibar surface would be acceptable. However, where structure exists, the assumption of no motion at the 1000 decibar surface may give misleading results. In areas of the western boundary currents and in high latitude regions, especially in the region of the Antarctic Circumpolar Current belt, significant structure does occur (Reed, 1970a) and as a result, surface currents based on the 1000 decibar surface may not provide accurate representation of the circulation.

The geostrophic currents determine only the baroclinic component of the ocean currents so that we also need to obtain the barotropic component if we are to know the absolute current velocity. This can be done if we can assume

that the barotropic current velocities are constant from the top to bottom of the ocean (Fofonoff, 1962). Then, if we measure the deep ocean currents at a number of locations, we can add this to the geostrophic current to obtain the total current. However, this is more easily said than done, as it is no simple matter to make sufficient numbers of deep current measurements. So, for the time being, we shall assume that the geostrophic currents obtained from routine oceanographic surveys do give a fairly accurate representation of absolute velocities.

To obtain the distribution of the geostrophic circulation over a large ocean area it is customary to construct the topography of the geopotential anomaly, in dynamic metres, relative to the 1000 decibar surface. The contour lines so constructed represent the stream lines of the current. If suitable map projections, such as the Mercator or Polar Stereographic Projections are used, the current speeds at a given latitude will be inversely proportional to the spacing between the adjacent contours. (In an Equal-Area Projection used in the accompanying charts, this does not necessarily apply as the width between the latitude circles varies with the longitude.) Moreover, as the speed of these geostrophic currents is inversely proportional to the Coriolis term, which undergoes appreciable latitudinal changes particularly as the Equator is approached, a given contour difference will yield speeds that increase equatorward. For example, a contour difference of 0.1 dynamic metre per  $1^\circ$  of latitude gives geostrophic speeds at latitudes  $50^\circ$ ,  $40^\circ$ ,  $30^\circ$ ,  $20^\circ$ ,  $10^\circ$  and  $5^\circ$  of 8, 10, 12, 18, 36 and 72 cm/sec respectively.

#### **a Northern Winter**

In Fig. 4a the topography of the geopotential anomaly relative to the 1000-decibar surface for the winter period is shown. Comparison of the surface geostrophic currents (Fig. 4a) with those of the Pilot Chart (Fig. 2a) for the corresponding period indicates that, in general, the major surface currents derived from a mapping of dynamic topography agree with those given in the Pilot Chart. The western boundary currents such as the Kuroshio and the East Australian Current, and the eastern boundary currents such as the California Current and the Peru Current are all evident; so are the Oyashio, the East Kamchatka Current, the Subarctic Current, the North Pacific Current, the Davidson Current, the New Guinea Current, the Antarctic Circumpolar Current, and the main features of the equatorial current system. There is also a suggestion of a poleward flow off southern South America corresponding to the Alaska Current in the North Pacific which is not clearly seen in the Pilot Chart. However, there are notable differences between the two distributions.

In the geostrophically based circulations, the two countercurrents, the Kuroshio Countercurrent of the North Pacific and the East Australian Countercurrent, both lie closer to their respective main currents. Also, the East Australian Countercurrent is not readily apparent in the Pilot Chart while it is clearly present in the geostrophic current. In addition, at the latitude of  $20^\circ$  to  $25^\circ$ N of the western North Pacific the geostrophic current is directed eastward

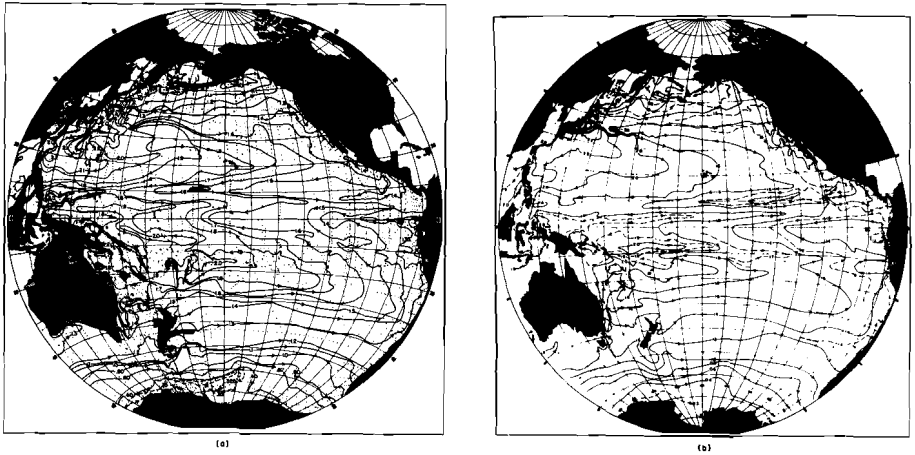


Fig. 4 Geopotential Anomaly at the sea surface relative to the 1000-decibar surface (dynamic metres) of the Pacific Ocean (from whose gradient the geostrophic flow at the surface can be calculated).

(a) Northern Winter (courtesy: Reid and Arthur, 1975)

(b) Northern Summer (courtesy: Reid, 1961) (1 dynamic metre = 10 Joules/kg)

while the Pilot Chart shows the flow to be westward. This westward flow is probably associated with the north Subtropical Countercurrent mentioned earlier. The North Equatorial Countercurrent is also wider than is indicated in the Pilot Chart. Between  $5^{\circ}$  and  $10^{\circ}\text{S}$  there is an evidence of a South Equatorial Countercurrent which does not appear in the central region. On the other hand, the large anticyclonic gyre depicted in the Pilot Chart off the coast of South America, is not evident in the geostrophic distribution. (Presumably, the above discrepancies between the two distributions for the South Pacific Ocean are due to a general lack of data in this region.) There is also the westward Antarctic Current which turns up in geostrophic circulations (e.g. Uda, 1961; Reid and Mantyla, 1971) but which is omitted from available Pilot Charts.

#### **b Northern Summer**

In Fig. 4b the distribution of geostrophic surface currents for the northern summer is shown. A comparison of this distribution with that of the Pilot Chart for the corresponding period (Fig. 2b) again shows their consistency vis-à-vis the major surface currents. Nevertheless, the pair of anticyclonic gyres evident in the North and South Pacific in the Chart are again missing from the geostrophic configuration. As during the winter, moreover, the North Equatorial Countercurrent determined through geostrophy is much broader than shown in the Chart. Contrary to the U.S. Pilot Chart, the geostrophic distribution also indicates the presence of an eastward current of oceanic extent centred around latitude  $10^{\circ}\text{S}$ . This is the South Equatorial Countercurrent mentioned earlier.

Along the western side of the Pacific, the geostrophic currents again indicate the presence of a countercurrent to the east of each of the main poleward-flows formed by the Kuroshio and the East Australian Current. During the northern summer the westward Antarctic Current appears to be absent. But Reid and Arthur (1975) believe this to be related to the fact that few data are available for the northern summer, rather than to any seasonal changes.

In general, therefore, the distribution of surface currents published in the Pilot Charts agree with those based on the geostrophic currents with regard to representing the major current systems of the Pacific Ocean, but disagree in detail in important aspects. The Kuroshio Countercurrent and the East Australian Countercurrents examined independently by Nitani (1972) and by Hamon (1965), respectively, seem to indicate that the distributions represented by the geostrophic currents are closer to values obtained by other methods such as the Geomagnetic electrokinetograph (GEK). (The GEK method makes use of the principle which considers the moving sea water to be a conducting medium cutting the earth's magnetic field thereby creating a potential difference between the two extremities of the conductor. The potential difference is measured between two conductors as they are towed behind a ship.) The Alaskan Stream which flows southwestward along the Aleutian Islands appears to be underestimated in both the Pilot Charts and the geostrophic presentation. While both indicate surface speeds of approximately 30 cm/sec, the measured speeds have been found to vary from 80 to 100 cm/sec (Reed and Taylor, 1965; Favorite, 1967), making them about three times more rapid than has been observed in the past.

One drawback to basing oceanic circulation on the geostrophic currents alone is that they do not take into consideration the direct effect of winds. Therefore, it is possible that in regions of strong winds the actual currents will be stronger or weaker than the calculated currents, depending on the direction of the winds. Similarly, ships' reports are likely to contain errors due to the influence of wind on the ship's drift. At the moment it is not possible to determine which presentation offers the truer picture and therefore for the time being we need to consider both of these presentations in order to depict the surface ocean circulation.

In general, we can think of the surface current pattern in the Pacific Ocean as composed of a number of idealized interlocking gyres, symmetrical about the Equator, some of which are closed and others which are not. These gyres are:

(a) *The Subarctic cyclonic gyre* (closed), delineated by the southward East Kamchatka Current and Oyashio, the eastward zonal Subarctic Current, the northward Alaska Current and the westward Alaskan Stream.

(b) *The North Subtropical anticyclonic gyre* (closed), delineated by the northward Kuroshio, the eastward zonal North Pacific Current, the southward California Current and the westward North Equatorial Current. It is to be noted, however, that the California Current is essentially a part of the Sub-

arctic Current and that most of the eastward North Pacific Currents turns southward before approaching the coast of North America.

(c) *The North Tropical cyclonic gyre* (closed), delineated by the southward Mindanao Current, the eastward zonal North Equatorial Countercurrent, the returning northward current off the coast of Central America and the westward zonal North Equatorial Current.

(d) *The North Equatorial anticyclonic gyre* (closure uncertain), which includes the zonal eastward North Equatorial Countercurrent and the westward Equatorial Current.

(e) *The South Equatorial anticyclonic gyre* (closure uncertain), which includes the zonal eastward South Equatorial Countercurrent and the zonal westward Equatorial Current.

(f) *The South Tropical cyclonic gyre* (closure uncertain), which includes the zonal westward South Equatorial Current and the zonal eastward South Equatorial Countercurrent.

(g) *The South Subtropical anticyclonic gyre* (closed), delineated by the southward East Australian Current, the eastward zonal South Pacific Current, the northward Peru Current and the westward zonal South Equatorial Current.

(h) *The Subantarctic cyclonic gyre* (apparently closed); this gyre is formed by the Antarctic Circumpolar Current but its closure is dependent on the existence of a return westward Antarctic Current which we know little about.

Of these gyres, three in the North Pacific Ocean (Subarctic Gyre, North Subtropical Gyre and North Tropical Gyre) and two in the South Pacific Ocean (South Subtropical and South Subantarctic Gyre) appear to have a reasonably certain existence. However, the existence of the others, particularly the equatorial gyres, is uncertain; in point of fact, they may not be gyres at all.

## 5 Geostrophic Currents at Subsurface Depths

Reid and Arthur (1975) have recently shown that the pattern of distribution of surface geostrophic currents recognized at the sea surface, especially the Subarctic and the Subantarctic gyres and the two Subtropical gyres, are present, though in reduced form, to depths as great as 3000 m. Below this only the Subarctic and Subantarctic gyres and the two western boundary currents in the South Pacific can be identified. They further indicated that the subtropical gyres below the sea surface appear to shift poleward at greater depths and that there is a broad eastward flow (relative to the deep water) in the lower latitudes and a poleward flow in the middle and high latitudes along the eastern boundaries.

## 6 Circulation of the Intermediate Water

There has been but one study made on the circulation of water in the intermediate layers of the combined North and South Pacific Oceans although similar studies have been conducted for various smaller regions. Reid (1965)

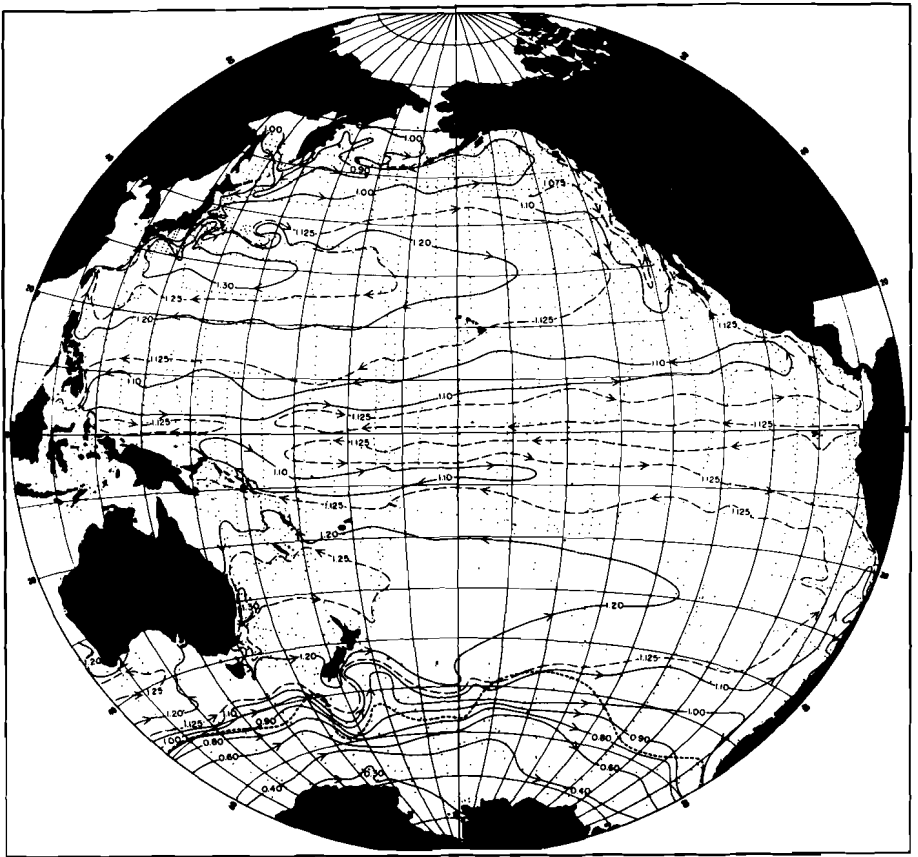


Fig. 5 Acceleration Potential (dynamic metres) relative to the 1000-decibar surface of the Pacific Ocean (from whose gradient the geostrophic flow can be calculated on the surface where the density is approximately  $1.0268 \text{ g-cm}^3$ ). (Courtesy: Reid, 1965) (1 dynamic metre = 10 Joules/kg)

used data taken over a span of a century, beginning with the early information gathered by the historic *Challenger* expedition up to those collected to 1962, and examined the geostrophic flow along constant potential density surfaces (isentropic surfaces). The surfaces chosen varied in depth from approximately 100 m in the Subarctic region to about 1000 m in the Subtropical region.

Fig. 5 shows the topography of the acceleration potential (sometimes called the isentropic stream function) for the isentropic surface approximated by isopycnal surface of density  $1.0268 \text{ gm/cm}^3$ . The contour lines denote the stream lines of the geostrophic currents along the isentropic surface. A comparison of these currents with those at the surface (Fig. 4) indicates that many of the features represented by the flow of intermediate waters are similar to those at the surface. Important differences do occur, however. Firstly, the poleward-flowing undercurrents on the eastern side of the ocean, the California Undercurrent of the North Pacific and the Peru–Chile Undercurrent, are un-

mistakably present in Reid's diagrams. The South Equatorial Countercurrent is also clearly shown and lies somewhat north of the position occupied at the surface. Because of its obvious manifestation in the subsurface layers some investigators claim that the South Equatorial Countercurrent may essentially be a subsurface current (Tsuchiya, 1968). Absent from Reid's presentation is the Equatorial Undercurrent. However, this is because the undercurrent is centred at a depth of approximately 100 m which is much shallower than the depth for which the currents of Figure 5 have been derived. Nor is there any sign of the Subtropical Countercurrents except for the eastward-flow evident to the north of New Zealand which Yoshida and Kidokoro (1967) claim might be connected with the Countercurrent. At intermediate depths the North Equatorial Current extends about 500 km north of its boundary occupied at the surface and in the south the boundary of the South Equatorial Current extends almost 1000 km more to the south of its boundary at the surface.

### **7 Circulation of the Deep and Bottom Waters**

Compared to our knowledge of the circulation of the surface and intermediate waters the circulation of the deep and bottom waters is still poorly known. As one might expect, this is principally due to lack of deep measurements which are difficult to make because of the requirement for specialized heavy duty equipment and specially-made tapered steel cables; they are also very time consuming. As a result, most oceanographic surveys do not include deep measurements in their routine sampling programs. Much of our knowledge concerning the deep water circulation is therefore based on water mass analysis and observations of the change in the distribution of water properties, particularly of potential temperature, salinity and dissolved oxygen content. Only at one location in the Pacific have deep bottom current velocities been measured, in the Tonga Trench.

Unlike the Atlantic Ocean, the Pacific Ocean has only one source of deep-bottom water – the Antarctic Ocean. Because the deep-bottom waters of the Pacific are more homogeneous than any of the other oceans, this deep-bottom water is simply designated as The Pacific Deep Water (Montgomery, 1958; Cochrane, 1958). It is not pure Antarctic Bottom Water but is a mixture, although the water formed at the Antarctic comprises more than 50% of the mixture (Gordon, 1971). The main source of Antarctic Bottom Water is in the Weddell Sea adjacent to the Atlantic Ocean but minor sources are found in the Ross Sea region adjacent to the Pacific Ocean and in the region of Amery Ice Shelf adjacent to the Indian Ocean (Gordon, *ibid*). Basically, the Pacific Deep Water is believed to be a mixture of the water flowing down the continental shelf of Antarctica and the water of the Antarctic Circumpolar Current (Sverdrup *et al.*, 1942). There is even some evidence of deep water formed in the North Atlantic Ocean being mixed into this Deep Water (Reid *et al.*, 1968).

As early as over a century ago there were suggestions that the deep bottom waters had origins outside of the Pacific Ocean (Prestwick, 1871, as quoted

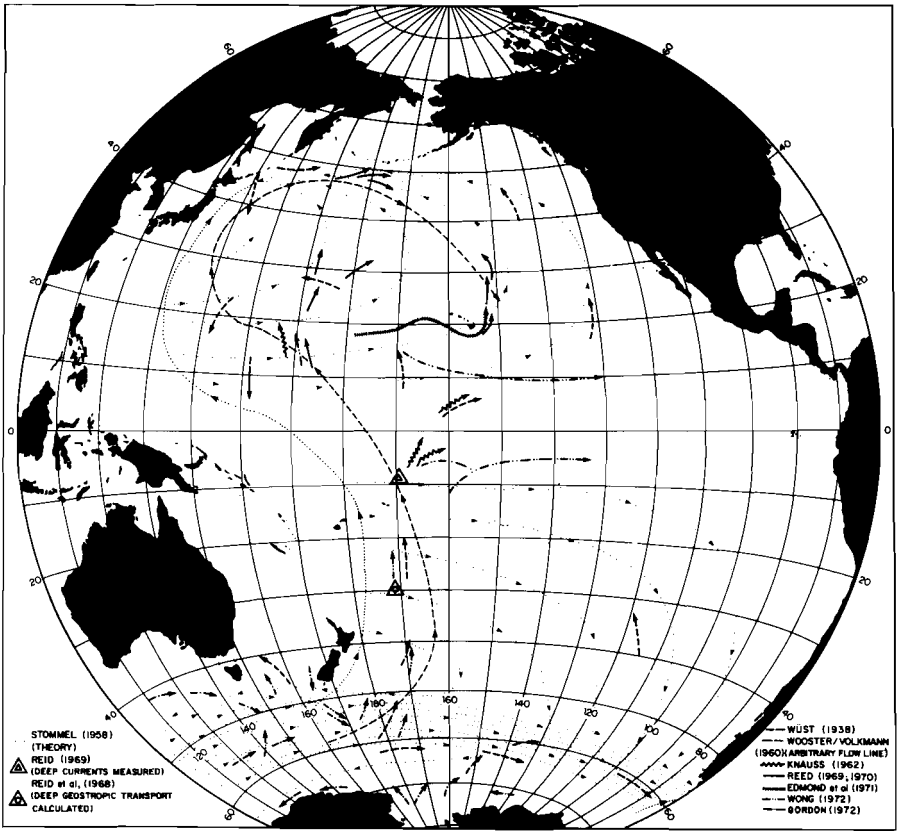


Fig. 6 Deep Bottom Currents of the Pacific Ocean as deduced by a number of sources.

by Reid, 1969), and as early as 1929 Wüst (Wüst, 1929, as quoted by Reid, 1969) had traced the cold bottom waters of the western North Pacific Ocean to the Antarctic Circumpolar Current. More recently, from 1960 onward, several investigators have examined, among other things, temperature, potential temperature, salinity, dissolved oxygen content and radio carbon ( $C^{14}$ ) and have shown that the earlier beliefs were correct. They have further demonstrated that the bulk of the Pacific Deep Water flows northward along the western side of the ocean, mainly along the Tonga-Kermadec Trench (lying east of New Zealand) (Wooster and Volkman, 1960; Knauss, 1962; Gordon, 1972; Wong, 1972). Reid *et al.* (1968) have examined a detailed oceanographic section taken along latitude  $28^{\circ}15'S$  and have estimated that the latter current forms a relatively strong northward-flowing deep current, less than 100 km wide, which is confined to depths of 2500 to 4500 m. They estimated the volume transport of this northward flow to be 8 to 12 sverdrups (a sverdrup is equivalent to  $10^6 \text{ m}^3/\text{sec}$ ). This value compares with 12 to 15 sverdrups obtained by Bolin and Stommel (1961) from consideration of the

steady-state budget of heat, mass, salt and radio carbon, and with 15 to 25 sverdrups obtained by Knauss (1962) based on the distribution of temperature, salinity and carbon 14 data. Further south along the latitude  $43^{\circ}15'S$  section, Reid *et al.* (1968) failed to observe such an intensified current. In Fig. 6 the direction of the deep-bottom currents determined by the various investigators are shown. Northward flow is seen to occur along the eastern side of New Zealand, whereupon approaching the Equator, a part continues northward or northwestward while the remainder veers eastward (Knauss, 1962; Wong, 1972). Edmond *et al.* (1971) indicate that an eastward flow also occurs just south of the Hawaiian Islands, and then turns to flow northward. According to the work of Reed (1969) this northerly flow appears to continue northward until at least latitude  $35^{\circ}N$ . The main northerly flow, however, seems to occur further west along Longitude  $170^{\circ}E$  (Knauss, 1962; Reid, 1969; Wong, 1972). More recently Reed (1970) has shown that the deep water which has flowed northward can continue eastward along the southern side of the Aleutian Islands.

The only location in the Pacific where deep bottom current measurements have been made is situated in the Tonga Trench at Latitude  $9^{\circ}S$ , Longitude  $169^{\circ}W$  in a region northeast of the Samoa Islands (Reid, 1969). The deep channel here appears at depths greater than 5000 m. It is only 50 km and 200 km wide at depths of 5000 and 4000 m, respectively. The highest average speed of this current, 15 cm/sec, was observed at a depth of 4800 m and was directed toward north-northeast with maximum speeds reaching as high as 20 cm/sec. Even at a depth of 3 m above the bottom (5275 m) a northerly current with speed slightly less than 5 cm/sec was observed.

Stommel (1957) has proposed a simple thermocline circulation model of such abyssal circulation that is compatible with the wind-driven circulation above the main thermocline. It is this circulation pattern (Stommel, 1958) which appears in Fig. 6. An intensified northerly abyssal current is depicted in this hypothetical model which generally agrees with observations.

In the preceding three sections I have attempted to outline the present status of knowledge on the horizontal circulation of the surface, intermediate and deep bottom water. Very little is known about the temporal variations of these currents, except for those that have been examined within 500 km of the coast. Even for these, detailed information on even the annual variations of the currents is not available.

## **8 Volume Transport of Water**

The ocean currents transport huge quantities of heat and salt from one place to another and for this reason the volume transport of water, rather than the surface speed of the currents, has more significance to the overlying atmosphere. At the surface and intermediate levels, the warm, saline waters are transported poleward with the larger western boundary currents (Kuroshio, East Australian Current) and Equatorward by the eastern boundary currents (California Current, Peru Current). The surface current speed and the volume

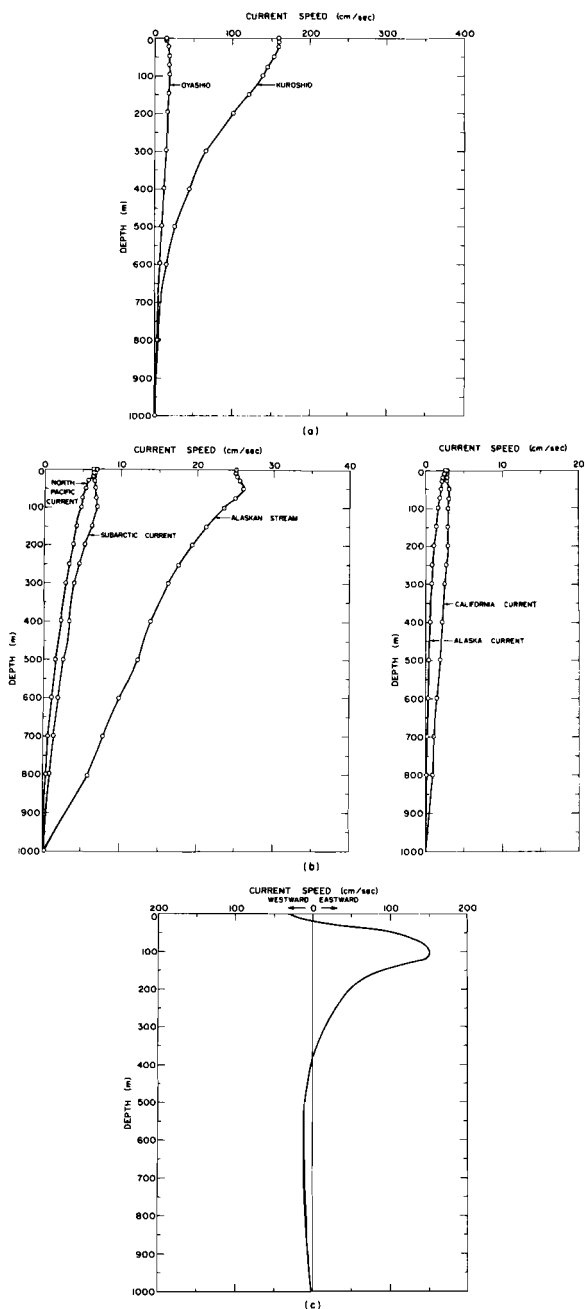


Fig. 7 Geostrophic Current Velocity Structures (cm/sec) of some of the major currents of the Pacific Ocean: (a) *Kuroshio* and *Oyashio*. (b) *North Pacific Current*, *Subarctic Current*, *Alaskan Stream*, *California Current* and *Alaska Current*. (c) *Equatorial Current* and *Equatorial Undercurrent* (Adapted from Knauss, 1960).

transport are generally correlated and therefore in many cases the substitution of current speed for implied transport is applicable. However, the velocity structures vary with different currents and it is dangerous to assume that this correlation can be taken for granted. A few examples will be shown to demonstrate this. In Fig. 7a are shown the vertical geostrophic velocity structures of the Kuroshio and the Oyashio. While the speed of the Kuroshio drops to about  $\frac{1}{2}$  of the surface speed at a depth of 500 m, the Oyashio, although a much smaller current, possesses  $\frac{3}{4}$  of the surface speed at 500 m. Fig. 7b shows the vertical velocity structures of the main currents of the North Pacific. The current speed at a depth of 500 m for the North Pacific Current and the Alaskan Stream is one half of the surface value whereas the corresponding value for the Alaska Current is  $\frac{1}{5}$  and for the California Current  $\frac{3}{5}$ . This comparison is by no means complete as even within the same current the ratio of the current speed at the surface and 500 m can vary from location to location at a given time and from time to time at the same location. It is when there is an appreciable subsurface current that the reliance of the volume transport upon the surface current could be downright wrong. The best example can be seen from the current velocity structure at the Equator shown in Fig. 7c, where not only is the current direction reversed but the subsurface velocity is much greater.

Estimates of the volume transport of the major currents of the Pacific Ocean have been made by Sverdrup *et al.* (1942) using data collected prior to 1942 and these values will be later compared to the more recent estimates. There is only one study that I am aware of that shows the distribution of the volume transport (relative to the 1500 decibar surface) for the entire Pacific Ocean. This has been prepared by Burkov (1966). His chart, which uses only the February data, is shown in Fig. 8. Comparison of the distributions of volume transport indicated in this chart with that of the surface geostrophic currents obtained by Reid and Arthur (1975) for the winter shows that the gross features of both are similar. The major difference, as expected, occurs along the equatorial belt where Burkov (1966) added the contribution of the Equatorial Undercurrent which gave a net transport to the east. Another difference is present in the South Pacific between the Latitude  $20^{\circ}$  and  $30^{\circ}$ S where the volume transport is westward while the surface current is eastward. The transport, however, is consistent with the direction of the currents at the intermediate level (Reid, 1965) which suggests that in this region the transports in the intermediate depths contribute more to the integrated transport than do the surface currents. In order to show the comparison between these transports with those derived from the application of Sverdrup's theory (Sverdrup, 1947; Fofonoff, 1962) the Sverdrup transport obtained by the consideration of the mean wind stress (Burkov, 1966) is shown in Fig. 9. Although the magnitudes of transports so obtained are somewhat smaller than those indicated in the observed geostrophic transports (Fig. 8), the main features are consistent with the "observed" ones except at the Equator and near the region of the boundary currents, which is to be expected.

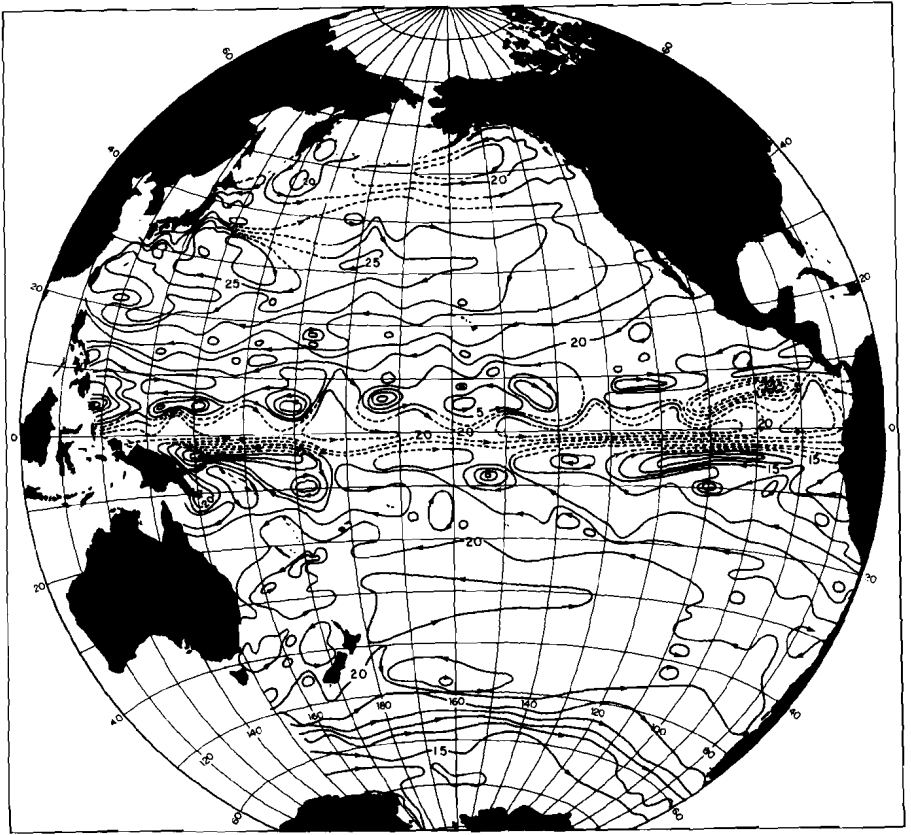


Fig. 8 Geostrophic Transport relative to the 1500-decibar surface in the Pacific Ocean for February. The Transport between adjacent isolines is 10 sverdrups (Adapted from Burkov, 1966).

In Fig. 10, a chart showing estimates of transports determined by various investigators, is shown. The values determined prior to 1942 are distinguishable by the brackets around them. These calculations (Table I) are practically all the ones that have been made to date and show how few estimates there are. The main feature of the magnitudes shown here is that, while relative agreement is present between the estimates for the same current, it is not uncommon to detect magnitudes that differ by a factor of 2 and in some cases by an order of magnitude. The most conspicuous feature of this illustration is that, while many transport values are available for the Kuroshio and the Equatorial region, they are almost non-existent in the South Pacific except for the few values estimated for the Cape Horn Current and the East Australian Current.

The Antarctic Circumpolar Current appears to transport the greatest amount of water in the Pacific Ocean. Since an early estimation of 120 sverdrups, no

TABLE 1. Sources of Information on the Volume Transport Estimates for the Pacific Ocean

*North Pacific Ocean:*

Alaska Current: (Sverdrup *et al.*, 1942; Bennett, 1959; Fofonoff and Tabata, 1966, NORPAC 1955 data, NORPAC Committee, 1960).

Alaskan Stream: (Bennett, 1959; Favorite, 1967; Ingraham and Favorite, 1968; Ohtani, 1970).

California Current: (Sverdrup *et al.*, 1942; Wooster and Reid, 1963; Wyrтки, 1966; Pavlova, 1966; NORPAC 1955 data, NORPAC Committee, 1960).

East Kamchatka Current: (Arsen'ev, 1967; Ohtani, 1970; Reid, 1973; Hughes *et al.*, 1974).

Kuril Current: (Hirano, 1957; Hata, 1965).

Kuroshio: (Sverdrup *et al.*, 1942; Masuzawa, 1967; 1972; Worthington and Kawaii, 1972).

Kuroshio Countercurrent: (Masuzawa, 1967; Nitani, 1972).

Luzon Current: (Nitani, 1972).

Mindanao Current: (Sverdrup *et al.*, 1942; Masuzawa, 1968; Nitani, 1972).

North Pacific Current: (Sverdrup *et al.*, 1942; NORPAC 1955 data, NORPAC Committee, 1960).

North Subtropical Countercurrent: (Uda and Hasunuma, 1969).

Oyashio: (Hirano, 1957; Sugiura, 1959; Hata, 1965).

Subarctic Current: (Sverdrup *et al.*, 1942; NORPAC 1955 data, NORPAC Committee, 1960).

Taiwan Current: (Nitani, 1972).

Transport through Bering Strait: (Coachman and Aagard, 1966).

Transport through passes along Aleutian Islands: (Favorite, 1974; Takenouti and Ohtani, 1974; Hughes *et al.*, 1974).

*South Pacific Ocean:*

Peru Current: (Sverdrup *et al.*, 1942; Wooster and Reid, 1963; Wyrтки, 1966).

East Australian Current: (Hamon, 1965; 1970).

Antarctic Circumpolar Current: (Sverdrup *et al.*, 1942).

Cape Horn Current: (Clowes, 1933; Sverdrup *et al.*, 1942; Ostapoff, 1960; 1961; Reid and Nowlin, 1971; Mann (pers. comm.) 1975).

South Subtropical Countercurrent: (Hamon, 1965; Stanton, 1973).

*Equatorial Pacific Ocean:*

North Equatorial Current: (Sverdrup *et al.*, 1942; Montgomery and Stroup, 1962; Masuzawa, 1964; 1967; Wyrтки, 1966).

North Equatorial Countercurrent: (Sverdrup *et al.*, 1942; Knauss and Pepin, 1959; Knauss, 1961; Tsuchiya, 1961; Montgomery and Stroup, 1962; Wyrтки, 1966; Wyrтки and Kendall, 1967; Masuzawa, 1967).

Equatorial Current: (Montgomery and Stroup, 1962; Wyrтки, 1966; Hisard *et al.*, 1970; Magnier *et al.*, 1973).

South Equatorial Countercurrent: (Wooster, 1961; Jarrige, 1968).

*Undercurrents:*

Equatorial Undercurrent: (Knauss, 1960; Montgomery and Stroup, 1962; Wyrтки, 1966; Masuzawa, 1967; Jones, 1969; Hisard *et al.*, 1970; Rotschi, 1970; Tsuchiya, 1970; 1972; Magnier *et al.*, 1973; Taft and Jones, 1973).

California Undercurrent: (Wooster and Jones, 1970).

Peru-Chile Undercurrent: (Wooster and Gilmartin, 1961).

attempt has been made to determine additional values. However, there have been several estimates made for the Cape Horn Current through Drake Passage where the transport was found to vary from 90 to 237 sverdrups. A recent set of current measurements made in Drake Passage indicates that the net transport might even be zero (K. Mann, private communication). A suggestion of no net transport, with eastward transport of 40 sverdrups in the upper layers and a westward transport of same magnitude in the lower layers was previously made by Ostapoff (1960).

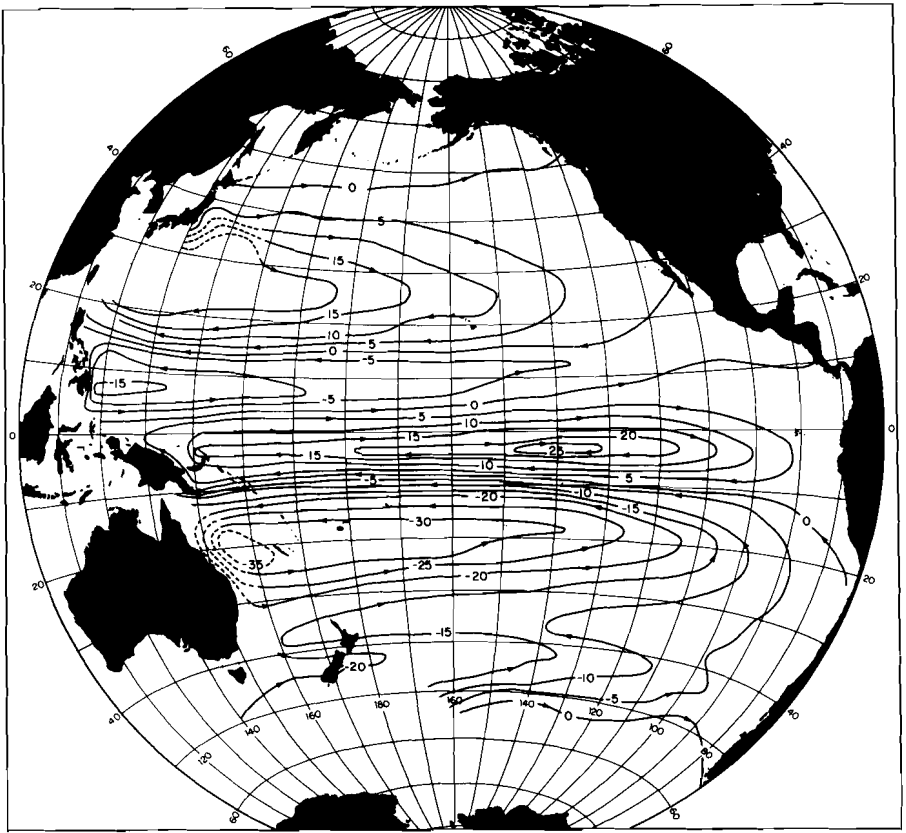


Fig. 9 Mean Sverdrup-Mass Transport in the Pacific Ocean. The Transport between adjacent isolines is 5 sverdrups (Adapted from Burkov, 1966).

In the equatorial region the total westward transport by the North Equatorial Current and the Equatorial Current is approximately 40 to 120 sverdrups. The eastward transport of the combined flow of the three countercurrents, the North Equatorial Countercurrent, the Equatorial Undercurrent and the South Equatorial Countercurrent is similar (30 to 120 sverdrups) to the volume of westward transport.

Where the westward North Equatorial Current approaches the Philippine Islands, it splits to form the northward Kuroshio and the southward Mindanao Current. A little more than one-half of the volume contained in the North Equatorial Current flows as the Kuroshio while the rest goes into the Mindanao Current (Nitani, 1972) which then feeds into the return flow of the North Equatorial Countercurrent. Masuzawa (1964) has noted that the transport of the North Equatorial Current increases progressively from the longitude of the Hawaiian Islands to off the Philippine Islands by approximately 40 sverdrups so that the total volume transport before separation can be greater than 100

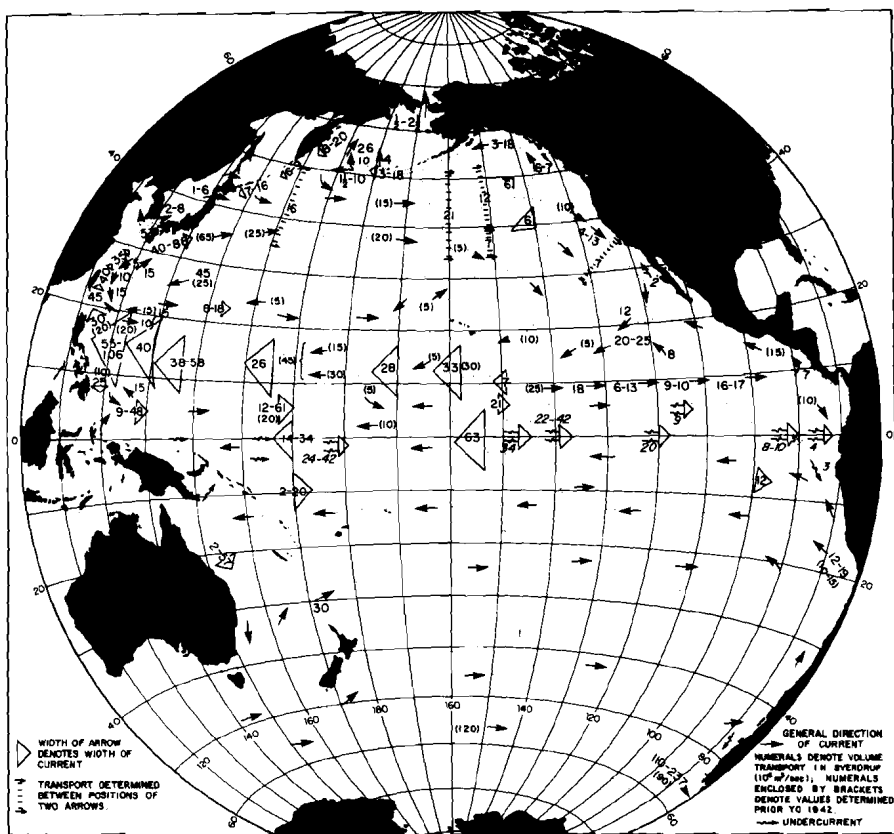


Fig. 10 Volume Transport of Water (sverdrups) of the various current systems as determined to date.

sverdrups. The implication of this increase is that a considerable amount of water must be fed into the North Equatorial Current by the Subtropical gyre, of which the Kuroshio is a part. Earlier estimates of the Kuroshio have placed the transport at 40 to 65 sverdrups, but more recent measurements have indicated that it is considerably greater than this, as high as 88 sverdrups (Worthington and Kawai, 1972). The Kuroshio is the most important current in the North Pacific Ocean and is also the most studied current of the Pacific. It is a narrow, swift flow with speeds reaching 270 cm/sec (Maritime Safety Agency, 1971). It is about 100 km wide and several hundred metres thick.

The southward transport of water by the Kuroshio Countercurrent is about one quarter of the northerly transport of the Kuroshio (Nitani, 1972). This Countercurrent, considered at one time as part of the Subtropical gyre, appears to be quite distinct from it, although the part of the Kuroshio that veers to form the gyre is often included as the Countercurrent. While the Kuroshio transports the warm water poleward along the western side of the North

Pacific, the cold Kuril Current–Oyashio transports from 6 to 16 sverdrups equatorward. There are indications that the latter transports might be greater during winter (Hata, 1965). The East Kamchatka Current transports from 8 to 20 sverdrups and feeds into the Kuril Current–Oyashio system. Because transport of the East Kamchatka Current appears to be larger than that of the Kuril Current – Oyashio it is believed that an appreciable amount of the former must feed into the eastward Subarctic Current. The combined Subarctic Current and the North Pacific Current appears to transport at least 20 sverdrups according to estimates made from the NORPAC data of Summer 1955 (NORPAC Committee, 1960). About one-half of this volume can be assigned to the Subarctic Current. It is possible that by using a reference level greater than the 1000 decibar surface, the transport may be considerably greater as Bennett (1959) has noted for some areas of the Gulf of Alaska.

The North Pacific Current appears to turn southward long before it approaches the North American coast whereas the Subarctic Current continues to flow eastward to the vicinity of the coast where it splits to form the northward Alaska Current and the southward California Current. At Longitude  $150^{\circ}\text{W}$ , an eastward volume transport of at least 12 sverdrups is indicated; one half of this goes into the Alaska Current and the other half into the California Current.

Observations along "Line P" between Station P (Lat.  $50^{\circ}\text{N}$ , Long.  $145^{\circ}\text{W}$ ) and the coast indicate that, relative to the 1000-decibar surface, about 7 sverdrups is transported northward – extending the reference level to the 3500-decibar surface doubles this estimate. Contrary to what one would expect, however, no clear indication of a winter strengthening of geostrophic transport off the B.C. coast has been noted (Fofonoff and Tabata, 1966). The main current in this region, the Alaska Current, continues northward then backs and feeds into the intensified, narrow (200 km) Alaskan Stream. Bennett (1959) originally suggested that the transport of the Stream was at least 18 sverdrups, a figure borne out by subsequent observations which have indicated it to vary from 5 to 20 sverdrups (Ohtani, 1965; Favorite, 1967; Ingraham and Favorite, 1968; Favorite, 1974). Measurements made off Adak Island (situated approximately 20 km east of the International Date Line in the Aleutian Chain) show that during the winter the transport may double that of summer (Ingraham and Favorite, 1968). For the most part the Alaskan Stream flows westward along the Aleutian Islands, although a portion of it does enter the Bering Sea through the deeper passes between the islands (Favorite, 1967). Near the terminus of the Aleutian chain, however, the bulk of the westward transport also enters the Bering Sea at a region east of the Komandorskii Islands (300 km east of Kamchatka Peninsula). This northward flow is estimated to be from 10 to 26 sverdrups. As some water, about 4 sverdrups, also enters the current before it reaches Komandorskii Island (Favorite, 1974), there must be some cross-stream flow taken from the eastward flowing Subarctic Current to sustain this northward transport.

The water that flows into the Bering Sea generally conforms to the cyclonic

circulation there, so that only a fraction of it finds its way northward into the Arctic Ocean ( $\frac{1}{2}$  to  $2\frac{1}{2}$  sverdrups). Therefore, the main portion of the Alaskan stream water eventually feeds into the relatively strong East Kamchatka Current. Hughes *et al.* (1974) have proposed that, in light of water balance considerations, 28 sverdrups must enter the Bering Sea through Near Strait east of Komandorskii Island during both winter and summer. However, because the East Kamchatka Current seems to transport as much as 35 sverdrups in winter and 20 sverdrups in summer, about 5 sverdrups must be lost from the Bering Sea in summer through the other passes of the Aleutian Islands and that 10 sverdrups must be gained by the Sea during the winter through these same passes.

Returning to a discussion of the eastern end of the Subarctic Current, we find that its southward-turning branch, the California Current, which is a part of the large anticyclonic gyre of the North Pacific, continues southward off the coast of the United States transporting from 4 to 13 sverdrups until it finally feeds into the North Equatorial Current before reaching the coast of Mexico. There is, however, some suggestion that the California Current can extend as far as the coast of Central America before it joins the North Equatorial Current (Tsuchiya, 1974). Further, an appreciable amount of the flow from the North Equatorial Countercurrent is fed back into the North Equatorial Current (Tsuchiya, 1968, 1974).

The poleward-flowing California Undercurrent is a relatively small current, having a breadth of about 20 km and thickness of about 300 m; one set of volume transport estimates yields a value of only 2 sverdrups (Wooster and Jones, 1970). It flows along the continental slope and the water characteristics suggests that it may have its origin in the North Equatorial Countercurrent. Tibby (1941) analyzed the deep waters along the Pacific Coast of the U.S. and found that off California the deep water contained about 50% equatorial water while the remainder was Subarctic water. Off the coast of Oregon the percentage of equatorial water drops to 35%. This water probably is fed by that part of the North Equatorial Countercurrent that does not join the North Equatorial Current.

It has been postulated that the poleward-flowing Davidson Current (or the California Countercurrent, which it is sometimes called) might be due to the surfacing of the California Undercurrent (Sverdrup *et al.*, 1942) when the northerly winds weaken or disappear. But the association of these two currents is still uncertain.

The poleward-flowing Davidson Current is a seasonal current that occurs during October through February along the Pacific coast of the United States and extends from the coast of southern California to northern Washington and is likely to extend even further northward (Burt and Wyatt, 1964; Schwartlose, 1964; Boisvert, 1969; Wyatt *et al.*, 1972). It is a relatively narrow current with the breadth generally within 200 km, although it can exceed 300 km (Burt and Wyatt, 1964). It has a mean speed of approximately 10 cm/sec but can reach values as high as 100 cm/sec (Wyatt *et al.*, *ibid*) in November. On the

other hand, Boisvert (1969) has noted that the maximum speed is reached generally in January.

The currents and transports in the Southern Pacific Ocean, except for the East Australian Current, are poorly documented. Some studies have been conducted off the South American coast and there have been appreciable amounts of data collected off the coast of Peru and Chile but little of the data is widely available. At this stage it is perhaps sufficient to note that the Peru Current is the southern counterpart of the California Current and the Peru-Chile Countercurrent, which transports about 3 sverdrups (Wooster and Gilmartin, 1961), is the southern counterpart of the California Countercurrent. The Peru Current is, however, wider in breadth than the California Current and appears to transport about twice the volume of water (Wooster and Reid, 1963). White (1969) showed that part of the transport that splits from the eastward-flowing Equatorial Undercurrent flows southward as far as 5°S off Peru. It is possible that this flow may contribute to the Peru-Chile Undercurrent (the southern counterpart of the California Undercurrent) but it is more likely that its source water is the South Equatorial Countercurrent.

We shall return to the equatorial region later, but first we shall conclude our discussion of the currents in the South Pacific by describing the pertinent features of the East Australian Current.

The East Australian Current is the southern counterpart of the Kuroshio. Though its features are less spectacular, it is nevertheless a major current transporting water at the rate of 12 to 57 sverdrups (Hamon, 1965, 1970) and having surface speeds comparable to the Kuroshio (200 cm/sec). It has a width of about 150 km and appears to be fed by the westward-flowing waters of the South Equatorial Current, which, the data of Wyrcki (1966) and Reid (1961, 1965) suggest, feeds into the East Australian Current via the Coral Sea. Scully-Power (1973), on the other hand, claims, on the basis of one set of data, that only 10% of the flow into the Coral Sea is associated with South Equatorial Current through this area and that most of the water originates with the South Equatorial Current but comes from south of New Caledonia. Studies by Hamon (1965, 1970), however, indicate that the East Australian Current is fed by water from the area to the north of New Caledonia. Apparently the only safe statement one can make on this subject is that during the northern winter, at least, the origin of this water appears to be the equatorial region (Burkov, 1966; Reid and Arthur, 1975). Irrespective of its origin, we do know that part of the Current continues to flow poleward along the eastern coast of Australia to as far as Tasmania and that there is a significant northward-flowing countercurrent just east of the Current which subsequently turns eastward. Hamon (1970), upon inspection of the details of the flow, argues that the East Australian Current is not a well-defined current but is a series of strong anticyclonic eddies that gradually moves poleward. Apparently no cruise data has shown it to be continuous along the coast at any one time. Monthly sea level heights, measured at Lord Howe Island, between Australia

and New Zealand, show variations of  $\pm 30$  cm which is attributed to the effect of the major water movements associated with the current (Hamon, 1965).

Not all the currents I have mentioned so far have been confirmed beyond all reasonable doubt. For example, the eastward Subtropical Countercurrent, which supposedly flows between latitudes  $20^{\circ}$ – $25^{\circ}$ N, has not yet been confirmed. Nevertheless, since it has been suggested that it has a counterpart in the Atlantic Ocean at similar latitudes it is perhaps worthwhile to comment upon it, if only to instigate further programs to clarify its existence. Interest in this current developed after Yoshida and Kidokoro (1967a, 1967b), upon examining the distribution of wind stress over the Pacific Ocean and the wind-driven Sverdrup type transports, noted the occurrence of a narrow belt of eastward-flowing currents in the North Pacific. They concluded that the formation of such a current is to be expected and explained it was associated with the trough in the curl of the wind stress, analogous to the explanation given for the occurrence of the equatorial countercurrents which also lie in the trough in the curl of the wind stress. Such an eastward current has been noted in the past (Uda, 1955; Yamanaka *et al.*, 1965) and was evident in the Pilot Charts prepared by the Japanese Hydrographic Department based on data collected between 1924 and 1934 (Japanese Hydrographic Department, 1936). Uda and Hasunuma (1969) re-examined all the previous pertinent data and concluded that such a current does indeed occur and that it can transport as much as 18 sverdrups. Other evidence also support the existence of such a current (Seckel, 1968; Robinson, 1968, 1969; Reed, 1970c). In the distribution of surface geostrophic currents prepared by Burkov (1966) and Reid and Arthur (1975) a suggestion of this current is indicated for the winter period. In the Atlantic, Voorhis and Hersey (1964) observed similar eastward-flowing current in the Sargasso Sea. In the South Pacific Ocean, the eastward-flowing current, which continues from the previously mentioned northward-flowing countercurrents of the East Australian Current, is thought to be associated with this Subtropical Countercurrent (Yoshida and Kidokoro, 1967b). Observations made along longitude  $170^{\circ}$ E indicate that such an eastward current exists in the Southern Hemisphere also (Merle *et al.*, 1969; Rotschi, 1973). The recent atlas of surface currents of the South Pacific Ocean published by the authorities of the United Kingdom (Meteorological Office, 1967) indicates a weak eastward flow between  $20^{\circ}$  and  $30^{\circ}$ S in the region west of  $140^{\circ}$ W during all seasons.

So many studies have been made on the equatorial current system during the past two decades following the discovery of the Equatorial Undercurrent in 1952 that it might be worthwhile to give it more attention than the others, since even the South Equatorial Countercurrent was only discovered a decade and a half ago.

The most conspicuous feature of the equatorial current system is the presence of the well-defined zonal flows that extend from one side of the ocean to the other except, of course, near the continents. The two westward currents on the poleward side, the North Equatorial Current and the South Equatorial Current,

are fed by the wind-driven currents of the Subpolar and Subtropical waters. The North Equatorial Current is a broad current, about 1000 km wide, which transports approximately 20 sverdrups at the eastern side. Of this, about one half comes from the California Current and the other half from return flow of the Equatorial Countercurrent (Sverdrup, *et al.*, 1947). The North Equatorial Current is further reinforced by the addition of water from the north via the North Pacific Current (subtropical gyre), so that by the time it arrives off the Philippine Islands it can be transporting well over 100 sverdrups (Masuzawa, 1964). This transport is twice as large as had been estimated previously.

The South Equatorial Current also appears to be a broad current, although its transport is not really known. Judging from values interpolated from the chart of Burkov (1966) (Fig. 8) it is somewhat smaller than that of the North Equatorial Current. However, since the Peru Current can feed up to 20 sverdrups into it, it may in fact be as large as the northern counterpart.

The westward Equatorial Current is also a broad current having a width of approximately 1000 km, lying between 5°N and 5°S, and is estimated to transport as much as 63 sverdrups (Montgomery and Stroup, 1962; Hisard *et al.*, 1970; Magnier *et al.*, 1973). It is believed to be principally driven by the Southeast and Northeast Trade Winds. Surprisingly, it is one of the least studied of the equatorial currents. Imbedded in the Equatorial Current is the jet-like eastward Equatorial Undercurrent whose core is at a depth of approximately 100 m. This current is symmetrical about the Equator and has a core velocity exceeding 150 cm/sec (Knauss, 1960, 1966) and a volume transport estimated to be between 19 and 42 sverdrups (Knauss, *ibid*; Montgomery and Stroup, 1962; Tsuchiya, 1970; Knauss and Pepin, 1959). The origin of this current is believed to be in the region of the Coral Sea, or near the Solomon Islands (Tsuchiya, 1967, 1968, 1970) or north of New Guinea (Hisard *et al.*, 1970; Rotschi, 1973). At the western extremity of the current, the flow in the upper oceanic layers has at times been observed to reverse with the reversal of the winds although the currents below the thermocline remain unaffected (Rotschi, 1973). The Undercurrent is also known to reach the surface when the Trade Winds are weak (Jones, 1969). Moreover, Taft and Jones (1973) have indicated that the Undercurrent is weakest when the Southeast Trades are strongest and when the Equatorial Current is strongest. On the contrary, Wyrтки (1974a, 1974b) has noted that the Undercurrent is in phase with the Equatorial Current above, being strongest in Spring and weakest in Autumn. These two statements are not in accord and therefore more observations are needed to clarify them. Finally, at its eastern terminus more water of this Undercurrent is discharged to the north than to the south (Tsuchiya, 1967).

Of the two eastward-flowing countercurrents, the North Equatorial Countercurrent (situated between the westward-moving North Equatorial Current and the westward-moving Equatorial Current) is more well-developed than the South Equatorial Countercurrent. It occurs in a relatively narrow belt between 3 and 8°N and its transport varies from 12 to 61 sverdrups (Montgomery and Stroup, 1962; Knauss and Pepin, 1959; Tsuchiya, 1961; Knauss, 1961; Wyrтки

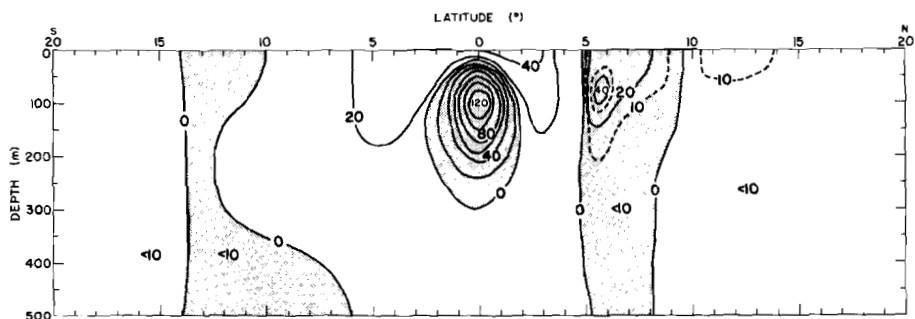


Fig. 11 Cross-section of current velocities for Central Equatorial Pacific (cm/sec) at Longitude 140°W. The values are Geostrophic Velocities (relative to 1000-metre surface) except near the Equator where measured values were used. The shaded portion indicates Eastward flow (Adapted from Knauss, 1963).

and Kendall, 1967; Masuzawa, 1967). Knauss (1961) has noted that transport values should be considered with caution as he has observed a change from 60 sverdrups to practically zero within a span of 11 months. The South Equatorial Countercurrent has only been thoroughly examined since its discovery in 1959 (Reid, 1959, 1961, 1965; Wooster, 1961; Tsuchiya, 1968; Jarrige, 1968; Rotschi, 1973). It has already been discussed in more detail earlier in this paper so it should be sufficient to say that it is a much less-developed current than its northern counterpart and is only about one half as wide. Estimates of its transport varies from 2 to 20 sverdrups (Wooster and Gilmartin, 1961; Jarrige, 1968). In Fig. 11 the cross-section of the equatorial currents in the Central Equatorial Pacific is shown. All the equatorial currents discussed are depicted. It is to be noted that the South Equatorial Countercurrent being weaker than the other equatorial currents can be sensitive to forces that govern the circulation in the equatorial belt. One illustration by Reid and Arthur (1975) indicates that while it appears to be present along the western and eastern side of the ocean it is missing in the central part. In a situation like this it is possible that the South Equatorial Current may cross the position occupied by the South Equatorial Countercurrent and merge with the Equatorial Current.

There is a body of evidence which suggests that the Equatorial Undercurrent and the North Equatorial Countercurrent have a common origin (Tsuchiya, 1961). This region is considered to be somewhere north of New Guinea (Burkov and Ovchinnikov, 1960; Rotschi, 1973) or in the area of the Coral Sea (Tsuchiya, 1967, 1968). Tsuchiya (1970) also suggests that the South Equatorial Countercurrent may also originate from the same general area. Merle *et al.* (1973) have further examined the origin of these currents and have indicated that the Equatorial Undercurrent has 2 cores at its western extremity – one at 100 m and another at 200 m, and that only the deeper core has its origin in the south. Since the North Equatorial Current splits near the Philippines, with about half its transport going to form the northward Kuroshio

and the other half going to form southward Mindanao Current, and since most of the latter flow presumably feeds into the returning North Equatorial Countercurrent, there must be roughly 25 to 50 sverdrups within the North Equatorial Current which can feed into the North Equatorial Countercurrent. This magnitude is somewhat similar to the estimated volume transport of the North Equatorial Countercurrent (Fig. 10) and therefore this transport can be accounted for by the consideration of the contribution from the North Equatorial Current alone. The contribution from the water south of the Equator feeding into the North Equatorial Countercurrent must therefore be relatively small.

Not much is known about the seasonal variation of these equatorial currents although Wyrтки (1974a, 1974b) has observed that the North Equatorial Current and the North Equatorial Countercurrent are both strongest in the Autumn and weakest in Spring. The strength of these currents are apparently strongly influenced more by the position of the Trade Winds than by their strength. When the Northeast Trades are strong and in a southerly position during the first half of the year, both the North Equatorial Current and the North Equatorial Countercurrent are weak. However, when the Northeast Trades are weaker but in a more northerly position during the second half of the year, both currents are strong. Tsuchiya (1974) has further shown that there is a good correlation between the position of the North Equatorial Countercurrent and that of the atmosphere's Intertropical Convergence Zone, supporting Wyrтки's (1974a, 1974b) view that the position of the Trade Winds are more important than the velocity in determining the distribution of currents.

In general, most of the currents in the equatorial current system can be explained through a consideration of the Ekman-Sverdrup type of wind-driven transports. The westward North and South Equatorial Currents are attributed to the wind-driven transports that bring in subpolar and subtropical waters toward the Equator and then force them westward, as mentioned earlier. The two countercurrents, the North and South Equatorial Countercurrents are directed generally against the prevailing Trade Winds. This is not an unexpected result and Yoshida (1961) has indicated that their presence can be explained from a consideration of the wind-driven transport alone. In particular, their occurrences are attributable to the existence of the trough in the curl of the wind stress.

The occurrence of the Equatorial Undercurrent apparently arises as a consequence of the tilt in the sea level caused by the piling up of wind-driven water at the western part of the Equator – the mean sea level along the western side is 70 to 80 cm higher than in the east (Fig. 4). The horizontal pressure gradient caused by this tilt in the sea level causes a downstream baroclinic flow along the Equator and is often given as the driving force of the Equatorial Undercurrent. While such an explanation is reasonable, it still does not fully explain the occurrence of the Undercurrent. After all, this current extends  $2^\circ$  to  $3^\circ$  north and south of the Equator and, therefore, flows in a region where the Coriolis effect becomes significant. In point of fact, the geostrophic balance is valid as close as  $\frac{1}{2}^\circ$  to the Equator (Knauss, 1960; Montgomery and Stroup,

1962). This is only 55 km away from the Equator! The explanation for the Undercurrent is further provided for by the effect of wind-driven circulation. Just north of the Equator, the Northeast Trades will drive the surface water to the west, by nature of the Ekman drift current theory. However, the net Ekman transport is to the north. Similarly, just south of the Equator the Southeast Trade Winds, while transporting surface water to the west, will provide a net southward transport. Hence, a compensating geostrophic flow should result below the Ekman layer which feeds into the undercurrent. Actually, because of the presence of the higher sea level on the western side this slope will permit the meridional geostrophic flow to be directed toward the Equator anyway, and this water can feed into the undercurrent.

More recently, Taft *et al.* (1973) have observed that the Equatorial Undercurrent and the winds in the vicinity of Christmas Island undergo fluctuations with a periodicity of 3 to 4 days. Since periodicity in the fluctuations in the winds and sea level of 4 to 5 days has been observed over the central Pacific (Groves, 1956; Groves and Miyata, 1967), there is some speculation as to whether the Equatorial Undercurrents are excited by these winds. In fact, Philander (1973), having reviewed the various theories and models of the Equatorial Undercurrents, has expressed reservations as to the apparent successes of the theories and models which do not allow interaction of the Undercurrent with planetary waves generated at the Equator or with such waves propagating equatorward from the higher latitudes. Thus, even though the simple models of the equatorial circulation appear to explain the occurrence of the Undercurrent, there are still a large number of unexplained questions related to its dynamics.

---

## References

- AIR MINISTRY, 1939: South Pacific Ocean Currents. M.O. 435. Marine Meteorological Office, London. 11 figures, 8 plates.
- ARSEN'EV, V.S. 1967: Currents and water masses of the Bering Sea (in Russian with English summary). *Izd. Nauka*, Moscow (Transl., 1968, Nat. Mar. Fish. Service, Northwest Fish. Center, Seattle, Wash.), 135 pp.
- BENNETT, E.B., 1959: Some oceanographic features of the north-east Pacific Ocean during August 1955. *J. Fish. Res. Bd. Canada*, **16**, 565–633.
- BOISVERT, WILLIAM E., 1969: Major currents off the west coasts of North and South America. Navy Oceanogr. Office, Wash. D.C. Tech. Rept. TR-221, 34 pp.
- BOLIN, B. and H. STOMMEL, 1961: On the abyssal circulation of the World Ocean. IV. Origin and rate of circulation of deep water as determined with aid of traces. *Deep Sea Res.*, **8**, 95–110.
- BURKOV, V.A., 1966: Structure and Nomenclature of Pacific Ocean Currents. *Okeanologiya*, **4**, 1–10.
- and I.M. OVCHINNIKOV, 1960: Structural features of zonal flows and the meridional circulation of water in the central Pacific Ocean in the winter in the northern hemisphere. *Akad. Nauk. S.S.S.R., Tr. Inst. Okeanol.* **40**, 93–107.
- BURT, WAYNE V. and BRUCE WYATT, 1964: Drift bottle observations of the Davidson Current off Oregon. *Studies on Oceanography* (K. Yoshida, editor), Univ. of Wash. Press, 560 pp, 156–165.
- COACHMAN, L.K. and K. AAGAARD, 1966: On

- the water exchange through Bering Strait. *Limnol. and Oceanography*, **11**, 44–59.
- COCHRANE, JOHN D., 1958: The frequency distribution of water characteristics in the Pacific Ocean. *Deep Sea Research*, **5**, 111–127.
- CROMWELL, T., R.B. MONTGOMERY, and E.D. STROUP, 1954: Equatorial Undercurrent in the Pacific Ocean revealed by new methods. *Science*, **119**, 648–649.
- CROWE, P.R., 1952: Wind and weather in the equatorial zone. Publ. Inst. British Geogr. Trans and Papers, No. 17, London, 23–76.
- EDMOND, J.M., Y. CHUNG, and J.G. Sclater, 1971: Pacific bottom water: Penetration east around Hawaii. *J. Geophys. Res.*, **76**, 8089–8097.
- FAVORITE, FELIX, 1967: The Alaskan Stream. International North Pacific Fisheries Com., Bull. No. 21, 53 pp, 1–20.
- 1974: Flow into the Bering Sea through Aleutian Island passes. Oceanography of the Bering Sea with emphasis on renewable resources (D.W. Hood and E.J. Kelly, editors), Occasional Publ. No. 2, Inst. of Marine Sciences, Univ. Alaska, 623 pp, 1–37.
- FINDLAY, A.G., 1853: Oceanic currents, and their connection with the proposed Central-America Canals. *J. Roy. Geogr. Soc.*, **23**, 217–240.
- FOFONOFF, N.P., 1962: Dynamics of ocean currents. *The Sea* (Ideas and observations on progress in the study of the seas (M.N. Hill, general editor)), Vol. 1, Interscience Publishers, 864 pp, 323–395.
- and S. TABATA, 1966: Variability of oceanographic conditions between Ocean Station P and Swiftsure Bank of the Pacific Coast of Canada. *J. Fish. Res. Bd. Canada*, **23**, 825–868.
- GORDON, ARNOLD L., 1971: Oceanography of Antarctic Waters. *Antarctic Oceanology*, Vol. 15, Antarctic Research Series (J.L. Reid, editor); Published by American Geophys. Union, 169–203.
- 1972: Spreading of Antarctic Bottom Waters II. Studies in Physical Oceanography (A.L. Gordon, editor), Gordon and Breach Science Publishers, New York, London, Paris, 232 pp, 1–17.
- GROVES, G.W., 1956: Periodic variations of sea level induced by equatorial waves in the easterlies. *Deep Sea Res.*, **3**, 248–252.
- and M. MIYATA, 1967: On weather-induced long waves in the equatorial Pacific. *J. Mar. Res.*, **25**, 115–126.
- HAMON, B.V., 1965: The East Australian Current, 1960–1964. *Deep Sea Res.*, **12**, 899–921.
- 1970: Western boundary currents in the South Pacific. Scientific Exploration of the South Pacific (Warren S. Wooster, editor), Nat. Acad. Sciences, Wash. D.C., 257 pp, 50–59.
- HATA, KATSUMI, 1965: Seasonal variation of the volume transport in the Oyashio area. *J. Oceanogr. Soc. Japan*, **21**, 193–201.
- HELLERMAN, S., 1967: An updated estimate of the wind stress on the world ocean. *Monthly Weather Review*, **95**, 607–626.
- 1968: Corrections to tables published in **95** (1967). *Monthly Weather Review*, **96**, 63–74.
- HIRANO, T., 1957: The oceanographic study on the Subarctic region of the northwestern Pacific Ocean – 1. On the water systems in the Subarctic region. *Bull. Tokai Regional Fish. Res. Lab.*, **15**, 23–46.
- HISARD, PHILIPPE, JACQUES MERLE and BRUNO VOITURIEZ, 1970: The Equatorial Undercurrent at 170° E in March and April, 1967. *J. Mar. Res.*, **28**, 281–303.
- HUGHES, F.W., L.K. COACHMAN and K. AAGAARD, 1974: Circulation, transport and water exchange in the western Bering Sea. Oceanography of the Bering Sea with emphasis on renewable resources (D.W. Hood and E.J. Kelly, editors), Occasional Publ. No. 2, Institute of Marine Science, Univ. Alaska, 623 pp, 59–98.
- INGRAHAM W. JAMES, JR. and F. FAVORITE, 1968: The Alaskan Stream south of Adak Island. *Deep Sea Res.*, **15**, 493–496.
- JAPANESE HYDROGRAPHIC DEPARTMENT, 1936: Current charts of the North Pacific Ocean, No. 6031A, 6031B, 6031C, 6031D. (Available from Maritime Safety Agency, Tokyo, Japan.)

- JARRIGE, FRANCOIS, 1968: On the eastward flow of water in the Western Pacific South of the Equator. *J. Mar. Res.*, **26**, 286–289.
- JONES, J.H., 1969: Surfacing of the Pacific Equatorial Undercurrent: Direct observation. *Science*, **163**, 1449–1450.
- KNAUSS, JOHN A., 1960: Measurements of the Cromwell Current. *Deep Sea Res.*, **6**, 265–286.
- 1961: The structure of the Pacific Equatorial Countercurrent. *J. Geophys. Res.*, **66**, 143–155.
- 1962: On some aspects of the deep circulation of the Pacific. *J. Geophys. Res.*, **67**, 3943–3954.
- 1963: Equatorial Current Systems. *The Sea, Ideas and Observations on Progress in the Study of the Seas* (M.N. Hill, general editor); Volume 2, Interscience Publishers, 554 pp, 235–252.
- 1966: Further measurements and observations on the Cromwell Current. *J. Mar. Res.*, **24**, 205–240.
- and ROBERT PEPIN, 1959: Measurements of the Pacific Equatorial Countercurrent. *Nature*, **183**, 380–382.
- Koninklijk Nederlands Meteorologisch Instituut, 1949: No. 124 (quoted by Reid, 1959).
- MAGNIER, Y., H. ROTSCHI, P. RUAL and C. COLIN, 1973: Equatorial circulation in the western Pacific (170°E). *Prog. In Oceanogr.*, **6** (B.A. Warren, editor), Pergamon Press, 193 pp, 29–46.
- MASUZAWA, JOTARO, 1964: Flux and water characteristics of the Pacific North Equatorial Current. *Studies on oceanography* (K. Yoshida, editor), Univ. of Wash. Press, 560 pp, 121–128.
- 1967: An oceanographic section from Japan to New Guinea at 137°E in January 1967. *The Oceanogr. Mag.*, **19**, 95–118.
- 1968: Second cruise for CSK *Ryofu Maru*, January to March 1968. *The Oceanogr. Mag.*, **20**, 173–185.
- MERLE, JACQUES, HENRI ROTSCHI and BRUNO VOITURIEZ, 1969: Zonal circulation in the tropical western South Pacific. *Bull. of the Japanese Soc. of Fisheries Oceanogr. Special No.* (Prof. Uda's Commemorative papers), 91–98.
- METEOROLOGICAL OFFICE, 1967: Quarterly surface currents of the South Pacific Ocean. *Met. O.* 435 (2nd edition) H.M.S.O., London, 25 pp.
- MINTZ, YALE and GORDON DEAN, 1952: The observed mean field of motion of the atmosphere. *Geophysical Research Papers*, No. 17, Geophysics Research Directorate, Air Force Cambridge Research Center, Cambridge, Mass. 66 pp.
- MONTGOMERY, R.B., 1958: Water characteristics of the Atlantic Ocean and of the world ocean. *Deep Sea Res.*, **5**, 134–148.
- and E.D. STROUP, 1962: Equatorial waters and currents at 150°W in July–August 1952. *The Johns Hopkins Oceanogr. Studies*, No. 1, the Johns Hopkins Press, 68 pp.
- NITANI, HIDEO, 1972: Beginning of the Kuroshio. *Kuroshio, its physical aspects.* (Henry Stommel and Kozo Yoshida, editors), Univ. Tokyo Press, Tokyo, 517 pp, 129–163.
- NORPAC COMMITTEE, 1960: *Oceanic Observations of the Pacific, 1955*, NORPAC data (Norris W. Rakestraw, Joseph L. Reid, Philip Rudnick and Warren S. Wooster, editors). Univ. Cal. and Univ. Tokyo Press, Berkeley and Tokyo. 532 pp.
- OSTAPOFF, F., 1960: On the mass transport through the Drake Passage. *J. Geophys. Res.*, **65**, 2861–2868.
- 1961: A contribution to the problem of Drake Passage circulation. *Deep Sea Res.*, **8**, 111–120.
- PRESTWICK, J., 1871: *Q.J. Geol. Soc. London*, **27**, 30. (Quoted by Reid, 1969).
- PHILANDER, S.G.H., 1973: Equatorial Undercurrent: Measurements and Theories. *Rev. Geophys. and Space Physics*, **11**, 513–570.
- REED, R.K. and N.E. TAYLOR, 1965: Some measurements of the Alaskan Stream with parachute drogues. *Deep-Sea Res.*, **12**, 777–784.
- 1969: Deep-water properties and flow in the central north Pacific. *J. Mar. Res.*, **27**, 24–31.
- 1970a: Geopotential topography of deep levels in the Pacific Ocean. *J. Oceanogr. Soc. Japan*, **26**, 331–339.
- 1970b: On the anomalous deep-water south of the Aleutian Islands. *J.*

- Mar. Res.*, **28**, 371-372.
- 1970c: On Subtropical currents and thermal structure in the central North Pacific. *J. Oceanogr. Soc. Japan*, **26**, 183-184.
- REID, J.L., 1959: Evidence of a South Equatorial Countercurrent in the Pacific Ocean. *Nature*, **184**, 209-210.
- 1961: On the geostrophic flow of the surface of the Pacific Ocean with respect to the 1000-decibar surface. *Tellus*, **13**, 489-502.
- 1965: Intermediate waters of the Pacific Ocean. The Johns Hopkins Oceanographic Studies, No. 2, The Johns Hopkins Press: 85 pp.
- 1969: Preliminary results of the measurements of deep currents in the Pacific Ocean. *Nature*, **221**(5183), 843.
- and ROBERT S. ARTHUR, 1975: Interpretation of Maps of Geopotential Anomaly for the Deep Pacific Ocean. (Submitted to the *Journal of Mar. Res.* for publication.)
- and ARNOLD W. MANTYLA, 1971: Antarctic work of the *Aries* expedition. *Antarctic J., U.S.*, **6**, 111-113.
- and WORTH D. NOWLIN, 1971: Transport of water through the Drake Passage. *Deep Sea Res.*, **18**, 51-64.
- HENRY STOMMEL, E. DIXON STROUP and BRUCE A. WARREN, 1968: Detection of a deep boundary current in the western South Pacific. *Nature*, **217**, 937.
- ROBINSON, M.K., 1968: Bathythermograph (BT) data confirms theoretical prediction of Subtropical Countercurrent (abstract). *Trans. Amer. Geophys. Union*, **49**, 702.
- 1969: Theoretical predictions of Subtropical Countercurrents confirmed by bathythermograph (BT) data. *Bull. of the Japanese Soc. of Fisheries Oceanogr.* 151-121. Special No. (Prof. Uda's Commemorative Papers).
- ROTSCHI, HENRI, 1970: Variations of Equatorial Currents. Scientific Exploration of the South Pacific (Warren S. Wooster, editor), Nat. Acad. Sciences, Wash. D.C., 257 pp, 75-83.
- 1973: Hydrology at 170°E in the South Pacific. Oceanography of the South Pacific, 1972. Compiled by Ronald Fraser, New Zealand Nat. Comm. for UNESCO, Wellington, 524 pp, 113-128.
- SCHWARTZLOSE, R.A., 1964: Nearshore currents of the western United States and Baja California as measured by drift bottles. Prog. Rep. Calif. Dept. Fish. Game, 1 July 1960 to 30 June 1962, Rept. No. 9, 15-22.
- SCHOTT, G., 1942: Grundlagen einer Weltkarte der Meereströmungen. *Ann. Hydr. Mar. Met.*, 329-340.
- SCULLY-POWER, P.D., 1973: Oceanography of the Coral Sea: The Winter Regime. Oceanography of the South Pacific 1972 (Compiler, Ronald Fraser) New Zealand Nat. Com. for UNESCO, Wellington, 524 pp, 129-135.
- SECKEL, G.R., 1968: A time-sequence oceanographic investigations in the North Pacific Trade-Wind Zone. *Trans. Am. Geophys. Union*, **49**, 377-387.
- STANTON, B.R., 1973: Circulation along the eastern boundary of the Tasman Sea. Oceanography of the South Pacific (R. Fraser, compiler) New Zealand, Nat. Com. for UNESCO, Wellington, 524 pp, 142-147.
- STOMMEL, H., 1957: A survey of ocean current theory. *Deep-Sea Res.*, **4**, 149-184.
- 1958: The abyssal circulation. *Deep-Sea Res.*, **5**, 80-82.
- SUGIURA, J., 1959: On the currents south of Hokkaido in the western North Pacific. *The Oceanogr. Mag.*, **11**, 1-11.
- SVERDRUP, H.U., 1947: Wind-driven currents in a baroclinic ocean; with application to the Equatorial Currents of the eastern Pacific. *Proc. Nat. Acad. Sciences*, **33**, 318-326.
- MARTIN W. JOHNSON and RICHARD H. FLEMING, 1942: *The Oceans: Their physics, chemistry and general biology*. Prentice-Hall, Inc., New York, 1087 pp.
- TAFT, B.A., B.M. HICKEY, C. WUNSCH and D.J. BAKER, JR., 1974: Equatorial Undercurrent and deeper flows in the central Pacific. *Deep Sea Res.*, **21**, 403-430.
- and JAMES H. JONES, 1973: Measurements of the Equatorial Undercurrent in the eastern Pacific. *Prog. in Oceanogr.*, **6** (B.A. Warren, editor), Pergamon Press, 193 pp, 47-110.
- TIBBY, RICHARD B., 1941: The water masses off the west coast of North America.

- J. Mar. Res.*, **4**, 112-121.
- TSUCHIYA, MIZUKI, 1961: An oceanographic description of the Equatorial Current System of the western Pacific. *Oceanogr. Mag.*, **13**, 1-30.
- 1967: Distribution of salinity, oxygen content, and thickness of 160 cl/t of thermocline anomaly in the Inter-tropical Pacific Ocean. *Studies Tropical Oceanogr.*, Miami, **5**, 37-41.
- 1968: Upper waters of the Inter-tropical Pacific Ocean. The Johns Hopkins Oceanographic Studies, No. 4, The Johns Hopkins Press, 50 pp.
- 1970: Equatorial circulation in the South Pacific. Scientific Exploration of the South Pacific (Warren S. Wooster, editor), U.S. Acad. Sciences, Wash. D.C., 257 pp, 69-74.
- 1972: A subsurface North Equatorial Countercurrent in the eastern Pacific Ocean. *J. Geophys. Res.*, **77**, 5981-5986.
- 1974: Variation of the surface geostrophic flow in the eastern Inter-tropical Pacific Ocean. *Fish. Bull.*, **72**, 1075-1085.
- UDA, MICHITAKA, 1955: On the Subtropical Convergence and the Currents in the Northwestern Pacific. *Rec. Oceanogr. Works Japan*, new-series 2, 141-150.
- 1961: Deep circulation in the Antarctic Ocean. Antarctic Record, No. 11, Ministry of Educ., Tokyo: 831-835.
- and K. HASUNUMA, 1969: The eastward Subtropical Countercurrent in the Western North Pacific Ocean. *J. Oceanogr. Soc. Japan*, **25**, 201-210.
- U.S. DEFENCE MAPPING AGENCY HYDROGRAPHIC CENTER, 1966: Atlas of Pilot Charts. South Pacific and Indian Oceans. H.O. Pub. No. 107 (formerly H.O. Pub. No. 577), 16 sets of charts.
- 1974: Pilot Charts of the North Pacific Ocean. 12 sets of charts (January through December). H.O. 55 (formerly H.O. Pub. No. 1401).
- VOORHIS, A.D. and J.B. HERSEY, 1964: Oceanic thermal fronts in the Sargasso Sea. *J. Geophys. Res.*, **69**, 3809-3814.
- WHITE, W.B., 1969: The Equatorial Undercurrent, the South Equatorial Countercurrent, and their extensions in the South Pacific Ocean east of the Galapagos Islands during February-March 1967. Rept. 69-4T, Texas A & M, University College Station, Texas. 74 pp.
- WONG, C.S., 1972: Deep zonal water masses in the Equatorial Pacific Ocean inferred from anomalous oceanographic properties. *J. Geophys. Res.*, **77**, 7196-7202.
- WOOSTER, WARREN S., 1961: Further evidence of a Pacific South Equatorial Countercurrent. *Deep Sea Res.*, **8**, 294-297.
- and M. GILMARTIN, 1961: The Peru-Chile Undercurrent. *J. Mar. Res.*, **19**, 97-112.
- and JAMES H. JONES, 1970: California Undercurrent off Northern Baja California. *J. Mar. Res.*, **28**, 235-250.
- and J.L. REID, 1963: Eastern boundary currents The Sea, Ideas and observations in Progress in the study of the Seas. (M.N. Hill, general editor), Vol. 2. Interscience Publishers, 554 pp, 253-280.
- and GORDON H. VOLKMANN, 1960: Indications of deep Pacific circulation from the distribution of properties at five kilometres. *J. Geophys. Res.*, **65**, 1239-1249.
- WORTHINGTON, L.V. and HIDEO KAWAI, 1972: Comparison between deep actions across the Kuroshio and the Florida Current and Gulf Stream. Kuroshio, Its Physical Aspects. 1972. (Henry Stommel and Kozo Yoshida, editors), Univ. Tokyo Press, 517 pp, 371-385.
- WÜST, G., 1929: Schichtung und Tiefenzinkulation des Pazifischen Ozeans auf Grund zweier Längsschnitte. Veroff. Inst. f. Meereskunde, Univ. Berlin, N.F. Reihe A. No. 20, 1, Berlin (quoted by Reid, 1969).
- WYATT, BRUCE, WAYNE V. BURT and JUNE G. PATTULLO, 1972. Surface currents off Oregon as determined from drift bottle returns. *J. Phys. Oceanogr.*, **2**, 286-293.
- WYRTKI, KLAUS, 1966: Oceanography of the eastern Equatorial Pacific Ocean. *Oceanogr. Mar. Biol. Ann. Rev.* (Harold Barnes, editor), **4**, 33-68.
- 1974a: Sea level and the seasonal fluctuations of the Equatorial currents in the western Pacific Ocean. *J. Phys. Oceanogr.*, **4**, 91-103.
- 1974b: Equatorial currents in the

- Pacific, 1950 to 1970 and their relations to the Trade Winds. *J. Phys. Oceanogr.*, **4**, 372-380.
- and ROBERT KENDALL, 1967: Transports of the Pacific Equatorial Countercurrent. *J. Geophys. Res.*, **72**, 2073-2076.
- YAMANAKA, HAJIME, NOBORU ANRAKU and JIRO MORITA, 1965: Seasonal and long-term variations in oceanographic conditions in the western North Pacific Ocean. *Rept. of Nankai Regional Fisheries Laboratory*, No. 22, 35-69.
- YOSHIDA, KOZO, 1961: Some calculations in the Equatorial circulation. *Records of Oceanogr. Works in Japan*, **6**, 101-105.
- and TOSHIKO KIDOKORO, 1967a: A Subtropical Countercurrent in the North Pacific. *J. Oceanogr. Soc. Japan*, **23**, 88-91.
- 1967b: A Subtropical Countercurrent (II) - A prediction of eastward flows at lower Subtropical Latitudes. *J. Oceanogr. Soc. Japan*, **23**, 231-246.
-

---

# Effective Wind Stress over the Great Lakes Derived from Long-Term Numerical Model Simulations

T.J. Simons

*Canada Centre for Inland Waters  
Burlington, Ontario*

[Manuscript received 8 August 1975, in revised form 15 October 1975]

---

## ABSTRACT

Numerical models were used to compute water circulations throughout the 1970 shipping season for Lake Erie and for the 1972 International Field Year on Lake Ontario. Simultaneous computations of surface elevations were compared with observed water levels to adjust the model re-

sults after the fact. As a by-product of these simulations, effective stress coefficients over water can be estimated. The results support earlier evidence that the effective wind stress over water is larger than indicated by atmospheric boundary layer measurements.

---

## 1 Introduction

In recent years increased concern with the aquatic environment has lent considerable impetus to dynamical simulation of large water bodies. The shift of emphasis from the classical storm surge problem to modern water quality models has been accompanied by a change of time scales from days to years. An interesting by-product of such long-term simulations is the opportunity to evaluate certain physical parameters under different environmental conditions. An example is the aerodynamic drag coefficient over water as derived from comparisons of observed and computed water levels and currents.

It is known that the choice of method for estimating stress coefficients may have a considerable effect on the outcome of the study. The matter has been reviewed in a number of publications and a comparative study has been made recently by Wieringa (1974). Since the latter includes an extensive bibliography of earlier studies, the list of references will be kept to a minimum in the present report. A study of this literature leads to the conclusion that drag coefficients derived from atmospheric boundary layer measurements tend to be lower than corresponding values inferred from changes of water levels.

Two types of hydrodynamical models are commonly used to estimate effective wind stress over water from wind set-up. The first one is based on steady-state solutions of the familiar Ekman equations, whereas the second employs numerical techniques to compute water transports and surface elevations as a function of time and space. The first method has been applied to Lake Erie

by Keulegan (1953) and to Lake Ontario by Donelan *et al.* (1974b). Platzman (1963) used the numerical procedure in a study of selected storm episodes on Lake Erie.

The results discussed in the present paper have been obtained from numerical models of Lake Erie and Lake Ontario, but the time scales involved are much longer than the typical storm-surge periods usually considered in this regard. Actually, the purpose of the computations was to simulate water circulations throughout the 1970 shipping season on Lake Erie and the 1972 International Field Year on Lake Ontario, in the framework of interdisciplinary study projects on these lakes. In view of the availability of extensive series of water levels computed in the course of these simulations, it appears of some interest to compare the resulting drag estimates with previous determinations.

## 2 Some notes on wind induced water set-up

Inasmuch as the slope of a water surface reflects the action of the wind stress integrated over the whole water body and over a substantial time interval, it would seem to be an ideal indicator of effective drag coefficients over water. However, for a proper interpretation of the results of such computations, it is necessary to evaluate the dynamical relationships between wind stress and surface slope. In particular in the present case, it is essential to place the results in the proper perspective, since the accuracy of the deduced drag estimate is not necessarily proportional to the complexity of the model.

The basic characteristics of the response of a water body to wind forcing are readily illustrated by considering an elongated lake with uniform cross section, aligned with the wind. In the steady state the surface slope will balance the surface stress and bottom friction, thus leading to the conventional set-up relationship

$$\rho g H \frac{dh}{dx} = \tau_s - \tau_b \quad (1)$$

where  $x$  is the coordinate along the lake axis,  $h$  is the surface elevation,  $H$  is the depth,  $g$  the earth's acceleration,  $\rho$  the density of water,  $\tau_s$  the surface stress, and  $\tau_b$  the bottom stress (from the water to the lake bottom). The resulting estimate of the drag coefficient is thus affected by any assumptions regarding bottom stress.

A theoretical estimate of bottom stress follows immediately from the classical Ekman solutions, which express water transports in terms of surface stress (drift current) and surface slope (gradient current). Since mass conservation requires that the water transport, integrated over a cross section of the channel, must vanish, the Ekman theory gives a steady-state relation between set-up and wind stress averaged over the width of the lake. By recourse to (1), the following expression for bottom stress in shallow water results:

$$\bar{\tau}_b = \tau_s \left[ 1 - \frac{3\overline{HH^2}}{2\overline{H^3}} \right] \quad (2)$$

where the bar denotes an average over the width of the channel. For constant depth, this equation gives  $\bar{\tau}_b = -\tau_s/2$ ; for a sinusoidal cross section  $\bar{\tau}_b = -\tau_s/8$ . In either case the bottom stress produces an additional set-up according to (1), but the effect is less in the second case because the bottom currents run against the wind only in the deeper parts of the lake. This is illustrated in Fig. 1 which displays the current distribution for a sinusoidal channel with positive values indicating currents running with the wind.

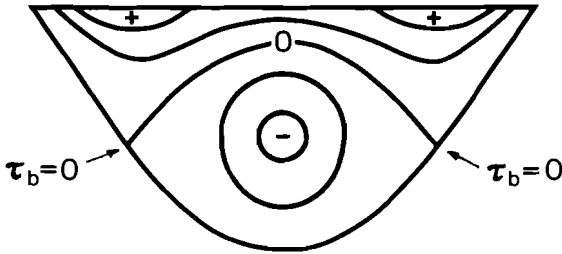


Fig. 1 Shallow water Ekman solution for a long channel with sinusoidal cross-section aligned with the wind. Positive values indicate currents running with the wind.

Different estimates of bottom stresses follow from other assumptions regarding vertical momentum diffusion, or if the flow is taken to be turbulent instead of laminar. For practical applications of (1) it is usually assumed that the bottom friction produces an additional set-up of the order of 10 percent of the set-up caused by the surface stress (see, e.g., Bretschneider, 1967). Unfortunately, this ambiguity is not eliminated if the conventional steady-state relationship is replaced by a time-dependent numerical model, allowing for any lake bathymetry and wind forcing. In particular, a vertically integrated model such as the familiar storm surge model requires that the bottom stress be related to the vertically averaged water transport. Theoretical formulations such as those proposed by Nomitsu (1934) and Platzman (1963) are closely related to the foregoing steady-state solutions. Thus the bottom friction appears in the model equations as an increase in the wind stress. On the other hand, a detailed analysis of a multilayered model of Lake Ontario (Bennett, 1974) indicates a reduction of set-up by bottom stress. The latter is also the case if the foregoing analysis of bottom friction in a sinusoidal channel is extended to deeper lakes, using the complete Ekman solutions summarized by Welander (1957).

In addition to the uncertainties associated with bottom stress simulations, any model is subject to errors caused by shore effects. Probably the most troublesome are the effects of radiation stresses summarized by Longuet-Higgins and Stewart (1964). Donelan *et al.* (1974b) investigated this problem for the Lake Ontario data base used in the present study and excluded all cases that might be subject to this type of error. The present analysis will be based on the complete data set and it will be shown that the results are fully

consistent with the earlier study. Nevertheless, it is understood that this and other problems associated with water level measurements will affect the present stress determination to the same degree as the conventional set-up method. The main purpose of this study is to compare results from a time-dependent numerical model versus the steady-state approach. In that context it is imperative to consider the spatial resolution of a numerical model since the sloping bottom near the shore makes a significant contribution to the total set-up. An estimate of this effect is readily obtained from steady-state relationships.

Assume that the bottom is a linear function of  $x$  and let the  $x$ -axis be directed from the water to the land such that the beach intersects the mean water level at  $x = 0$ . The total water depth from the free surface to the bottom can then be written as  $H = -\beta x + h$  where  $\beta$  is positive, and (1) becomes

$$H \frac{dH}{dx} + \beta H - \gamma = 0 \quad \gamma \equiv \frac{(1 + \alpha)\tau_s}{g} \quad (3)$$

where the coefficient  $\alpha$  represents the bottom stress as a fraction of the wind stress. If the depth at the first interior grid point of the numerical model is denoted by  $H_0$  and the surface elevation at the shore is indicated by  $h_s$ , then solution of (3) by standard methods leads to

$$h_s = \frac{\gamma}{\beta} \ln \frac{H_0 - \gamma/\beta}{h_s - \gamma/\beta} \quad (4)$$

For Lake Erie, the grid spacing of the present model is 6.67 km, whereas  $\alpha = 0.5$  according to Ekman theory for shallow water, hence  $\gamma/\beta = 10^8 \tau_s/H_0$  in c.g.s. units. If  $H_0 = 500$  cm, then  $h_s$  is approximately  $10 \times \tau_s$  for  $\tau_s$  of order unity. For comparison, the total Buffalo – minus – Toledo set-up computed by the numerical model is of the order of  $25 \times \tau_s$  in c.g.s. units. Thus, the numerical model would tend to under-estimate the water set-up and hence would lead to an over-estimate of the drag coefficient.

### 3 Computational procedures

The results presented in the following were derived from numerical models of large water bodies very similar to contemporary models of the atmosphere. Thus, solutions of lake circulations and surface elevations are obtained by step-wise time integration of the dynamical equations of motion and the continuity equation on a three-dimensional array of grid points. Input parameters are the bottom topography and shoreline configuration, observed temperature configurations derived from ship surveys, and the distribution of wind stress at the water surface as a function of space and time. Output parameters are the values of water levels and currents in any desired location and at any desired time.

For Lake Erie a vertically-integrated model was run throughout the 1970 shipping season and a two-layer model was applied during the summer months. For Lake Ontario all computations were made with a four-layer model. The numerical-dynamical aspects of the simulations have been presented else-

where (Simons, 1974, 1975). The resolution of the Lake Erie model is 6.67 km, the grid spacing of the Lake Ontario model is 5 km. In the two-layer and four-layer models the bottom friction is formulated in terms of the square of the currents in the bottom layer with a proportionality constant equal to  $2.5 \times 10^{-3}$ . In the homogeneous model, the bottom stress is related to the vertically-integrated transport by a coefficient which is inversely proportional to the square of the depth. A more theoretical formulation as discussed before, would augment the effective surface stress, which will be taken into account in the interpretation of results.

For the Lake Erie study, synoptic stress fields over the lake were obtained from wind observations at six meteorological stations on the periphery of the lake. The stations selected for this study were Windsor, Long Point and Port Colbourne in Ontario, Toledo and Cleveland in Ohio; and Erie, Pennsylvania. The procedure for estimating effective surface stresses over water followed Platzman's (1963) treatment of the subject. Thus, variations of stress coefficients due to station exposure and surface roughness were ignored. For the Lake Ontario study, observations from eleven meteorological buoys taken at a height of 4 m above the surface, were available throughout the period of simulation. All stresses were assumed to be related to the wind by the usual quadratic law, and the horizontal interpolations employed weighting functions inversely proportional to the square of the distance. A constant drag coefficient of  $2.4 \times 10^{-3}$  was used for all simulations; hence the model solutions must be adjusted after the fact by comparing observed and computed water levels. Although the models are to some extent nonlinear, the solutions vary with wind stress in nearly linear fashion.

The analysis of Lake Ontario water levels is complicated by the large depth of the lake which results in typical changes of surface elevations of a few centimetres or less. The inverse barometric effect leads to surface slopes of comparable magnitude. In addition, the semi-diurnal lunar tide of the order of 1 cm shows up quite markedly in the water level records. It is necessary, therefore, to correct for these effects. Surface pressures were interpolated to the 5-km grid mesh of the model on the basis of shore-based observations at eight first-order meteorological stations. The corresponding water levels at each grid point were then computed by imposing the condition that the total water mass of the lake be conserved. The semi-diurnal tide was removed by a high-precision digital band-reject filter.

Lake Ontario water level records are dominated by high-frequency oscillations corresponding to free surface modes, the slowest of which has a period of 5 h. Although these are, in principle, reproduced by the numerical model, the errors inherent in the simulation of free oscillations might lead to spurious interpretation of the more direct effects of wind forcing. Therefore, the comparison of observed and computed set-up was carried out not only for the original hourly data but also after removing these oscillations by a digital filter. A comparison was also made of water levels averaged over periods ranging from 5 h to one day. The resulting relationships between observed and com-

puted set-up were remarkably similar, but the correlation coefficients obviously increased with averaging period.

In order to reduce an effective drag coefficient over water from the present numerical simulations, the distribution of points on a plot of observed versus computed water set-up is approximated by a linear relationship. Once this relationship has been determined, the original drag coefficient is multiplied by the slope of this line to give the best estimate of actual wind stress. It is common to estimate the relation between two variables by linear regression, but this leads to two different lines depending on the choice of dependent and independent variable. When both variables are subject to error, a unique linear relationship is presented by the maximum likelihood estimate (see, e.g., Kendall and Stuart, 1970). If  $X$  and  $Y$  are two observable random variables with sample covariance  $S_{xy}$ , sample variances  $S_x^2$  and  $S_y^2$ , and error variances  $S_\epsilon^2$  and  $S_\delta^2$ , respectively, then the slope coefficient of the maximum likelihood relationship is

$$\frac{S_y^2 - \lambda S_x^2 + [(S_y^2 - \lambda S_x^2)^2 + 4\lambda S_{xy}^2]^{1/2}}{2S_{xy}} \quad (5)$$

where  $\lambda = S_\delta^2/S_\epsilon^2$  is the ratio of the error variances. It is clear that the above estimate is bounded from below by the regression coefficient of  $Y$  on  $X$  ( $S_\epsilon^2 \rightarrow 0$ ), and from above by the reciprocal of the regression coefficient of  $X$  on  $Y$  ( $S_\delta^2 \rightarrow 0$ ).

#### 4 Estimates of aerodynamic drag coefficients

The foregoing procedure to derive effective drag coefficients from numerical model simulations may be applied to any pair of water level stations at opposing ends of a lake. For elongated water bodies such as Lake Erie and Lake Ontario, the surface slope along the main axis of the lake may be expected to be most sensitive to wind forcing. Thus the stations selected for the present analysis are Toledo and Buffalo on Lake Erie and Burlington and Oswego on Lake Ontario. Furthermore, the data were divided into different classes in order to isolate effects of air-water stability and periods of high winds. Within each class, the correlation between observed and computed set-up was computed, and the drag coefficient was estimated from the slope of the linear relationship.

Fig. 2 shows effective stress coefficients for Lake Erie during 1970 as a function of the time of the year. The results are shown at weekly intervals, but the statistical analyses are based on overlapping periods of four weeks of daily-mean water levels. The correlation coefficients attest to a nearly linear relationship between observed and computed set-up, and consequently the results are not very sensitive to the estimate of the ratio of error variances. The range of stress coefficients corresponding to linear regression of observed on computed set-up, and vice versa, is indicated by the length of the vertical bars. The solid lines refer to the vertically-integrated model; the dashed bars correspond to the two-layer model.

In consideration of the foregoing discussion, the following adjustments to the

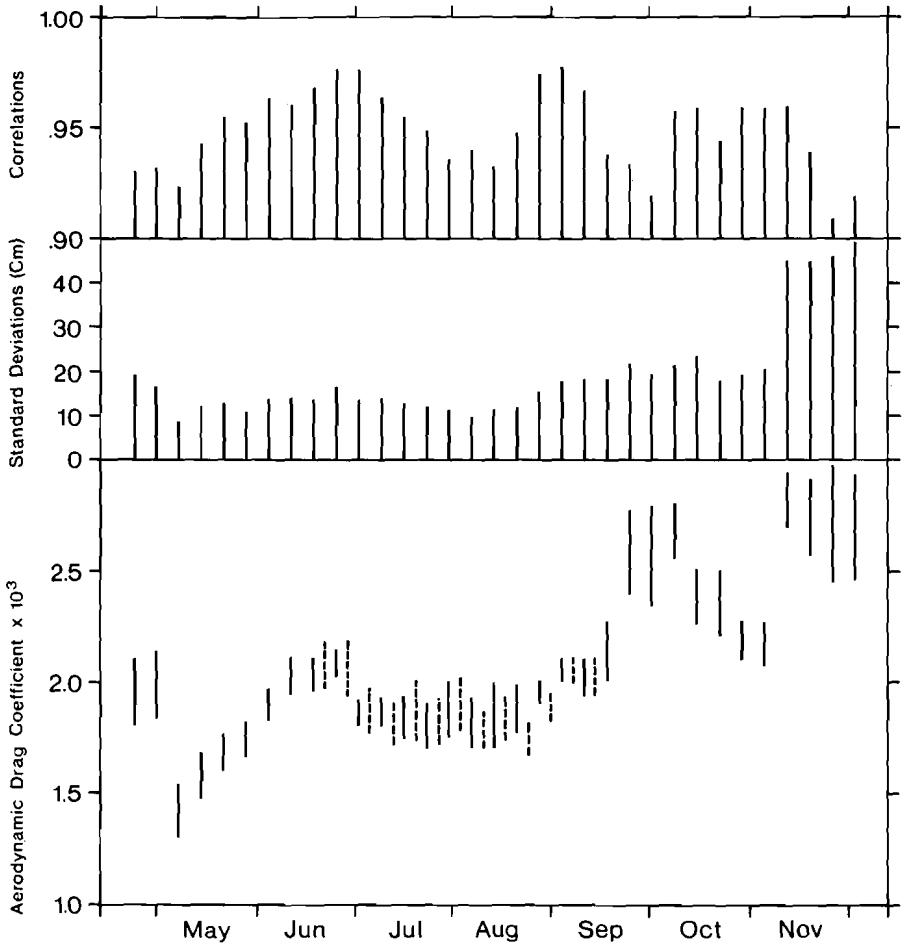


Fig. 2 Correlations between observed and computed set-up and deduced aerodynamic drag coefficients for Lake Erie at weekly intervals during 1970. Surface stress over water computed from shore-based wind observations.

model output were incorporated in Fig. 2. Since Lake Erie is shallow in terms of Ekman theory, a theoretical formulation of bottom stress as suggested by Platzman (1963) would lead to a considerable increase of computed water levels. Although empirical studies indicate that the effect is smaller than suggested by this theory, for the lake as a whole one would expect corrections of the order of 10 percent. Thus estimates of stress coefficients derived from the homogeneous model were reduced by that amount. Estimates of resolution errors relating to the effects of a sloping bottom near the shore, would lead to corrections of similar magnitude and again result in a lower drag estimate. Thus the wind stress coefficients deduced from the homogeneous model were reduced by 20 percent, those from the two-layer model by 10 percent.

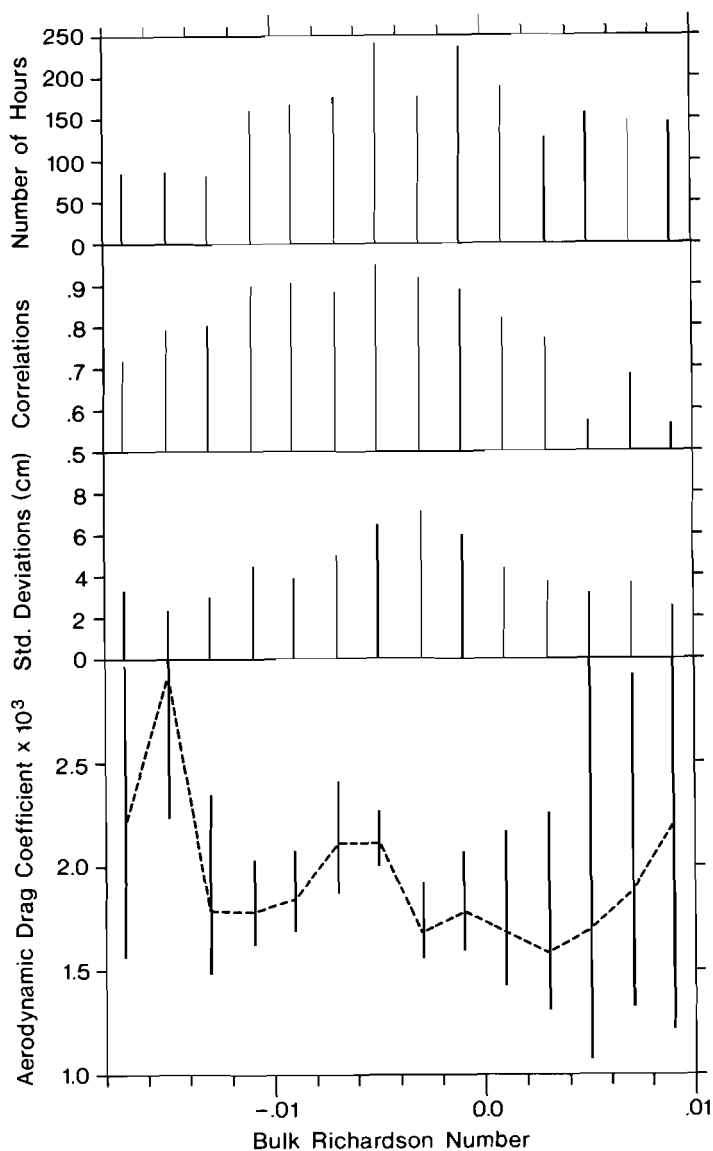


Fig. 3 Correlations between observed and computed set-up and corresponding drag coefficients for Lake Ontario during 1972 as a function of bulk Richardson number. Surface stress over water computed from buoy observations at 4 m above the water.

Although the necessary information on the atmospheric boundary layer is not available, Fig. 2 would appear to indicate significant effects of stability on stress over water (see also Hsu, 1974). Thus there is a gradual increase in drag coefficients from the stable spring periods to the unstable fall season. By November, the coefficient tends to diminish again and the subsequent increase is probably related to the high wind activity. This may be inferred from the

graph of the standard deviations of observed set-up computed for each period. There is a considerable body of evidence to suggest an increase of drag coefficients for strong winds (see, e.g., Wieringa, 1974). As a matter of interest, it may be added that Platzman's simulations of Lake Erie storms yielded an estimate of  $3.2 \times 10^{-3}$  for the effective stress coefficient over water in relation to shore-based wind observations.

A statistical analysis of Lake Ontario water levels as a function of time did not lead to meaningful results, mostly because a number of months during 1972 were characterized by very calm weather. However, data from the meteorological buoy network on Lake Ontario during the 1972 International Field Year make it possible to compute the stability of the atmospheric boundary layer and to classify our results accordingly. The stability parameter used is the bulk Richardson number discussed by Donelan *et al.* (1974a). As an example, Figure 3 shows results of statistical analyses for values of this index between  $-0.02$  and  $0.01$  at intervals of  $0.002$ , based on 5-hourly averages of water levels. Because of the low correlations, the choice of dependent and independent variables has considerable effect on the slope of the straight line used to approximate the relation between observed and computed set-up. The range of stress coefficients corresponding to the two linear regression lines is again displayed by vertical bars. The dashed line connects the maximum likelihood estimates for the case of equal normalized error variances in observed and computed set-up, that is,  $\lambda = 1$  in (5).

As in the case of Lake Erie, the estimates shown in Figure 3 have been corrected for resolution errors. In this case, the correction was based on the form in which the depth appears if the steady-state relation (1) is integrated over the whole lake. The corresponding "effective" depth computed from the 5-km bathymetry of the model was compared with available data on a 2-km grid. The corresponding reduction of stress coefficients was about 6 percent. No corrections are made for bottom stress, since all results were obtained from a four-layer model, which presumably incorporates a better formulation of bottom friction than a one-layer model.

The results obtained here should be compared with stress calculations made by Donelan *et al.* (1974b) from the same data base. These authors used the conventional steady-state set-up formula, but applied very stringent selection criteria to the data in order to ensure that the underlying assumptions were mostly satisfied. These conditions were satisfied for a total of approximately 400 hours during the 1972 Field Year. The stability classification adopted by these authors identified about half of the cases as unstable and one quarter as stable. A linear regression of set-up on wind-squared resulted in a drag coefficient of  $1.45 \times 10^{-3}$ , whereas a linear regression of wind-squared on set-up would give a value of  $2.22 \times 10^{-3}$ , the correlation being 0.81 for all data taken together.<sup>1</sup>

<sup>1</sup>In the final version of their paper, Donelan *et al.* (1974b) elected to adopt the lower bound on the drag coefficient for reasons given in their paper. Furthermore the wind-averaging procedure was modified, resulting in a slight reduction of the coefficient to  $1.35 \times 10^{-3}$ .

In order to achieve an exact comparison, an analysis was done on the results from the present numerical model for the same hours selected by Donelan's program. The two corresponding coefficient estimates were  $1.62 \times 10^{-3}$  and  $2.09 \times 10^{-3}$  with a correlation of 0.88, fully consistent with the steady-state results in the framework of the maximum likelihood theory.

With regard to stability effects, Fig. 3 appears rather inconclusive since the correlations rapidly deteriorate towards both sides of the stability scale. As shown by the standard deviations, this is largely due to small values of wind set-up outside the range of weakly unstable configurations. Within the latter range, the increase of drag coefficient with instability is not very pronounced, but it should be noted that these coefficients refer to over water winds at a height of 4 m. Since the wind shows less variation with height under unstable conditions, the coefficient would decrease with stability when referred to a higher level.

## 5 Summary and conclusion

Estimates of effective aerodynamic drag coefficients over water, derived from long-term numerical model simulations of Lake Erie and Lake Ontario, are in general agreement with results from the conventional steady-state relationship between wind and surface slope. Comparison of the two methods for an identical data base give consistent results, while the improvement in correlation coefficients does not appear proportional to the increase in effort. Estimates of stress coefficients relating to wind observations at 4 m above the surface of Lake Ontario, appear to average out to  $1.85 \times 10^{-3}$ , assuming a comparable normalized error in wind and water levels. Drag coefficients over Lake Erie referring to routine observations at shore-based meteorological stations, are of similar magnitude in spring and early summer, but increase to an average value of  $2.5 \times 10^{-3}$  during the stormy, unstable, fall season.

The present calculations confirm earlier evidence that the effective stress over water is larger than indicated by atmospheric boundary layer measurements. Donelan's (1975) theoretical formulation of the interaction between surface waves and the atmospheric boundary layer shows a pronounced increase of drag coefficients if the wave field is not fully adjusted to the wind. Since boundary layer observations are biased towards periods of steady winds, it might be expected that such measurements underestimate the effective stress over water. It is thus felt that the higher drag coefficients should be used if a first estimate of surface stress is required.

## Acknowledgements

The atmospheric observations on Lake Ontario were collected and analyzed under direction of F.C. Elder; the stability classifications were based on a program of M.A. Donelan. The physical and statistical interpretation of the results benefitted from discussions with M.A. Donelan and A. El-Shaarawi.

---

## References

- BENNETT, J., 1973: On the dynamics of wind-driven lake currents. *J. Phys. Ocean.*, **4**, 400-414.
- BRETSCHNEIDER, C.L., 1967: Storm surges. *Advances in Hydrosience*, V.T. Chow, Ed., Academic Press, **4**, 341-419.
- DONELAN, M.A., 1975: On the coupling between wind and waves. Canada Centre for Inland Waters, 42 pp.
- DONELAN, M.A., K.N. BIRCH and D.C. BEASLEY, 1974a: Generalized profiles of wind speed, temperature and humidity. *Internat. Assoc. Great Lakes Res., Conf. Proc.* **17**, 369-388.
- DONELAN, M.A., F.C. ELDER and P.F. HAMBLEN, 1974b: Determination of the aerodynamic drag coefficient from wind set-up. *Internat. Assoc. Great Lakes Res., Conf. Proc.* **17**, 718-788.
- HSU, S.A., 1974: On the log-linear wind profile and the relationship between shear stress and stability characteristics over the sea. *Boundary-Layer Meteorology*, **6**, 509-514.
- KEULEGAN, G.H., 1953: Hydrodynamic effects of gales on Lake Erie. *J. Res. Natl. Bur. Standards*, **50**, 99-109.
- KENDALL, M.G. and A. STUART, 1970: The advanced theory of statistics, **2**: Inference and relationship, 3rd ed., Hafner Publishing Co., New York, 391-407.
- LONGUET-HIGGINS, M.S. and R.W. STEWART, 1964: Radiation stresses in water waves, a physical discussion with applications. *Deep Sea Res.*, **11**, 529-562.
- NOMITSU, T., 1934: Coast effect upon the ocean current and the sea level. *II. Changing State. Memoirs, College of Science, Kyoto Imp. Univ.*, **A17**, 249-280.
- PLATZMAN, G.W., 1963: The dynamical prediction of wind tides on Lake Erie. *Meteorol. Monographs*, **4**, No. 26, 44 pp.
- SIMONS, T.J., 1974: Verification of numerical models of Lake Ontario. Part I. Circulation in Spring and Early Summer. *J. Phys. Ocean.*, **4**, 507-523.
- SIMONS, T.J., 1975: Continuous dynamical computations of water transports in Lake Erie for the year 1970. *J. Fish. Res. Bd. Can.*, **33** (in press).
- WELANDER, P., 1957: Wind action on a shallow sea: some generalizations of Ekman's theory. *Tellus*, **9**, 45-52.
- WIERINGA, J., 1974: Comparison of three methods for determining strong wind stress over Lake Flevo. *Boundary-Layer Meteorology*, **7**, 3-19.
-

---

# Fourier Series on Spheres

George J. Boer

and

Leonard Steinberg

*Atmospheric Environment Service, Downsview, Ontario*

[Manuscript received 9 June 1975; in revised form 20 October 1975]

---

## ABSTRACT

A spectral representation consisting of a two-dimensional Fourier series for use on a sphere is described.

The method is applied to the advection of a passive scalar field over the poles and is compared to the pseudo-

spectral and grid-point representations.

The results show that the double Fourier series method compares favourably with both the pseudo-spectral and grid-point schemes.

---

## 1 Introduction

A method of representing scalar and vector component fields on the sphere by means of two-dimensional series has been developed and applied to the test problem of advection of a conical shape with a non-divergent flow field.

The method grew out of the pseudo-spectral approach of Merilees (1973) and resembles the method of Orszag (1974) although it was developed independently.

The results of the advection calculation using double Fourier series is compared with both the pseudo-spectral method and the "conservative" grid point scheme obtained using the second order Arakawa Jacobian (Arakawa, 1966).

## 2 Fourier Series Representation

The representation of a scalar or vector field in terms of an expansion in simple functions has a number of advantages for computational purposes. Among these are the analytic nature of the representation and the ability to calculate derivatives and integrals accurately. It may also be possible, given suitable expansion functions, to do unaliased calculations, to maintain accuracy in a least squares sense, and to maintain certain conservative properties inherent in the continuous physical system. For Fourier series, the existence of a fast transform routine is an important consideration.

It is common to represent a scalar field in terms of a truncated Fourier series expansion in longitude (the usual meteorological notation is used):

$$A(\lambda, \phi) = \sum_{|p| \leq \infty} A_p(\phi) e^{ip\lambda} \quad (2.1)$$

The least squares approximation to the function is obtained for

$$A_p = \frac{1}{2\pi} \int_0^{2\pi} A e^{-ip\lambda} d\lambda \quad (2.2)$$

The expression for  $A$  is often decomposed further by representing the  $A_p(\phi)$  in terms of associated Legendre functions. The resulting spherical harmonic expansion is in terms of functions which are orthogonal with respect to area weighting over the sphere. The orthogonality of the expansion functions implies many desirable properties for theoretical and numerical treatment of atmospheric motions.

While spherical harmonics have desirable properties from several points of view, they are somewhat difficult to use in numerical computations. Fourier series, on the other hand, are particularly simple both analytically and numerically and are amenable to fast transform techniques. Complications arise, however, since a Fourier series representation is not orthogonal with respect to area weighting on the sphere.

Consider  $A_p(\phi)$  in eqn. (2.1), with the zero of "latitude" taken at the south pole so that  $\phi \in [0, \pi]$ .  $A_p(\phi)$  may be expanded in terms of a sine or cosine series in this interval. Such a representation, while it will converge to  $A_p(\phi)$  in the interval if sufficient terms are retained in the expansion, may exhibit Gibb's phenomenon and need not converge when differentiated term by term.

It is possible, however, to expand  $A_p(\phi)$  in a Fourier series which is properly convergent in  $[0, \pi]$  and which may be differentiated term by term. A simple demonstration of this is as follows. Given  $A(\lambda, \phi)$  defined in the "primary", region,  $\lambda \in [0, 2\pi]$ ,  $\phi \in [0, \pi]$ , extend the definition of  $A$  to the region  $\lambda \in [0, 2\pi]$   $\phi \in [0, 2\pi]$  thus:

$$A'(\lambda, \phi) = \begin{cases} A(\lambda, \phi) & , \quad \phi \in [0, \pi] \\ A(\lambda + \pi, 2\pi - \phi) & , \quad \phi \in [\pi, 2\pi]. \end{cases} \quad (2.3)$$

Then  $A'$  is continuous (if  $A$  is) and periodic with period  $2\pi$  in both  $\lambda$  and  $\phi$ . Moreover,  $A' = A$  in the primary region. This definition for  $A'$  is just that used by Merilees (*loc cit*) to obtain periodic functions in  $\phi$  for pseudo-spectral calculations. For a given  $\lambda$ ,  $A'(\lambda, \phi)$  is the value of  $A$  which would be traced out following a meridian of longitude completely around the globe.

Since  $A'$  is continuous and periodic it may be represented as a double Fourier series

$$A' = \sum_{|p| \leq N} \sum_{|q| \leq M} A'_{pq} e^{ip\lambda} e^{iq\phi} \quad (2.4)$$

$$A'_{pq} = \frac{1}{4\pi^2} \int_0^{2\pi} \int_0^{2\pi} A' e^{-ip\lambda} e^{-iq\phi} d\lambda d\phi. \quad (2.5)$$

This series is everywhere well behaved, possesses derivatives and integrals which may be obtained by operating term by term on the series and, in particular, represents the scalar in the primary region.

It can be easily shown that the symmetry of  $A'$  in the extended region together with the specification that  $A'$  is real leads to the following relations among the coefficients:

$$\begin{aligned} A'_{p-q} &= (-1)^p A'_{pq}, \\ A'_{-pq} &= (-1)^p A'^*_{pq}, \\ A'_{-p-q} &= A'^*_{pq}. \end{aligned}$$

The Fourier series (2.4) may be written to apply to the primary region in the form

$$A(\lambda, \phi) = \sum_{|p| \leq N} \sum_{q=0}^M \delta A_{pq} e^{ip\lambda} F_p^{-q} \quad (2.7)$$

where

$$F_p^{-q} = e^{iq\phi} + (-1)^p e^{-iq\phi} \quad (2.8)$$

$$\delta = \begin{cases} \frac{1}{2}, & q = 0 \\ 1, & q \neq 0 \end{cases} \quad (2.9)$$

whence

$$A_{pq} = \frac{1}{4\pi^2} \int_0^{2\pi} \int_0^\pi A e^{-ip\lambda} F_p^{-q} d\phi d\lambda. \quad (2.10)$$

If  $A$  is to be single valued at the poles,  $\phi = 0, \pi$  it follows that

$$\begin{aligned} \sum_{|p| \leq N} \sum_{q=0}^M \delta A_{pq} (1 + (-1)^p) e^{ip\lambda} &= \text{const} \quad , \phi = 0 \\ \sum_{|p| \leq N} \sum_{q=0}^M \delta A_{pq} (1 + (-1)^p) (-1)^q e^{ip\lambda} &= \text{const}, \phi = \pi \end{aligned} \quad (2.11)$$

and therefore that

$$\sum_{q \text{ even}} \delta A_{pq} = \sum_{q \text{ odd}} A_{pq} = 0; \quad p \neq 0, \quad p \text{ even}$$

is a necessary condition on the coefficients. Equations (2.7-2.11) define the representation of a scalar on the sphere in terms of a two-dimensional Fourier series.

The Fourier series representation of a vector component is obtained in an analogous way. To obtain continuity in the extended region a change of sign is required, i.e.,

$$u'(\lambda, \phi) = \begin{cases} u(\lambda, \phi) & , \phi \in [0, \pi] \\ -u(\lambda + \pi, 2\pi - \phi) & , \phi \in [\pi, 2\pi] \end{cases} \quad (2.12)$$

The resulting Fourier series is of the form

$$\begin{aligned} u &= \sum_{|p| \leq N} \sum_{q=0}^M \delta U_{pq} e^{ip\lambda} F_{p+1}^{-q} \\ U_{pq} &= \frac{1}{4\pi^2} \int_0^{2\pi} \int_0^\pi u e^{-ip\lambda} F_{p+1}^{-q} d\phi d\lambda \end{aligned} \quad (2.13)$$

and similarly for  $v$ . The necessary conditions at the poles may be obtained by representing  $u$  and  $v$  in terms of the polar stereographic components  $U_s$  and  $V_s$  as follows:

$$\begin{aligned} u &= -U_s \sin \lambda + V_s \cos \lambda \\ v &= -U_s \cos \lambda - V_s \sin \lambda \end{aligned}$$

where  $U_s, V_s$  behave as scalars in terms of spherical polar representation. At the poles

$$u = \sum_{|p| \leq N} \sum_{q=0}^M \delta U_{pq} e^{ip\lambda} (1 + (-1)^{p+1}) = \frac{1}{2}(We^{i\lambda} + W^*e^{-i\lambda}) \quad , \phi = 0$$

$$v = \sum_{|p| \leq N} \sum_{q=0}^M \delta V_{pq} e^{ip\lambda} (1 + (-1)^{p+1}) = \frac{i}{2}(We^{i\lambda} - W^*e^{-i\lambda}) \quad , \phi = 0$$

$$u = \sum_{|p| \leq N} \sum_{q=0}^M \delta U_{pq} e^{ip\lambda} (1 + (-1)^{p+1})(-1)^q = \frac{1}{2}(We^{i\lambda} + W^*e^{-i\lambda}), \phi = \pi$$

$$v = \sum_{|p| \leq N} \sum_{q=0}^M \delta V_{pq} e^{ip\lambda} (1 + (-1)^{p+1})(-1)^q = \frac{i}{2}(We^{i\lambda} - W^*e^{-i\lambda}), \phi = \pi$$

$$W = V_s + iU_s$$

so that we require

$$\left. \begin{aligned} \sum_{q \text{ even}} \delta U_{pq} = \sum_{q \text{ odd}} U_{pq} = 0 \\ \sum_{q \text{ even}} \delta V_{pq} = \sum_{q \text{ odd}} V_{pq} = 0 \end{aligned} \right\} |p| \neq 1, p \text{ odd.} \quad (2.14)$$

For  $|p| = 1$

$$\begin{aligned} \sum_{q=0}^M 2\delta U_{1q} = \frac{W}{2}, \quad \sum_{q=0}^M 2\delta V_{1q} = \frac{iW}{2} \quad (\text{For } \phi = 0) \\ \sum_{q=0}^M 2\delta U_{1q}(-1)^q = \frac{W}{2}, \quad \sum_{q=0}^M 2\delta V_{1q}(-1)^q = \frac{iW}{2} \quad (\text{For } \phi = \pi) \end{aligned} \quad (2.15)$$

and

$$\sum_{q \text{ even}} \delta U_{1q} = i \sum_{q \text{ even}} \delta V_{1q}; \quad \sum_{q \text{ odd}} U_{1q} = i \sum_{q \text{ odd}} V_{1q}.$$

The equations above give an expansion of a scalar or vector component field on the globe in terms of double Fourier series. The useful features of such an expansion have been alluded to at the beginning of the section. The drawback of this representation is that the expansion functions are not orthogonal with respect to area weighting on the sphere and, therefore, the expansion coefficients are not those appropriate to a least squares representation and do not exhibit the condition of finality. The coefficients are those appropriate to a least squares representation for a weighting function of unity (rather than the cosine of latitude as in area weighting). These disadvantages may be outweighed by the accuracy and ease of calculation with Fourier series using the FFT.

### 3 The simple advection case

The simplest non-trivial test of the method is that of the passive advection of a scalar field by a non-divergent flow field. The equation of motion is

$$\frac{\partial A}{\partial t} + \frac{u}{a \sin \phi} \frac{\partial A}{\partial \lambda} + \frac{v}{a} \frac{\partial A}{\partial \phi} = 0 \quad (3.1)$$

or in terms of a stream function  $\psi$

$$V = k \times \nabla \psi$$

$$\frac{\partial A}{\partial t} + \frac{1}{a^2 \sin \phi} \left( -\frac{\partial \psi}{\partial \phi} \frac{\partial A}{\partial \lambda} + \frac{\partial \psi}{\partial \lambda} \frac{\partial A}{\partial \phi} \right) = 0 \quad (3.2)$$

The flow field chosen was that of solid rotation about an axis lying in the equatorial plane of the spherical coordinate system. Such a flow field requires the computation method to account successfully for the convergence of the meridians and the behaviour at the pole during the advection of the passive scalar over the poles. The stream function chosen was

$$\psi = -a^2\omega \sin \phi \cos \lambda \quad (3.3)$$

whence

$$u = -a\omega \cos \phi \cos \lambda \quad (3.4)$$

$$v = a\omega \sin \lambda.$$

The scalar field chosen was conical in shape with a base which formed a circle on the sphere. The defining expression is

$$A(\lambda, \phi) = \begin{cases} A_0(1 - R/R_0), & R \leq R_0 \\ 0, & R > R_0 \end{cases} \quad (3.5)$$

$$R = 2a[\sin^2 \phi \sin^2(\lambda - \lambda_0)/2 + \sin^2(\phi - \phi_0)/2]^{1/2}$$

where  $A_0$  is the height of the cone and  $R_0$  is the radius of the circular base of the cone;  $\phi_0$  and  $\lambda_0$  are the latitude and longitude of the central axis of the cone.

Equation (3.1) was rewritten in the form

$$\frac{\partial A}{\partial t} + \frac{1}{a} \left( u \frac{\partial \hat{A}}{\partial \lambda} + v \frac{\partial A}{\partial \phi} \right) = 0 \quad (3.6)$$

where  $\hat{A} = A/\sin \phi$ . It may be shown that if  $A$  is represented in terms of a double Fourier series expansion (2.7) with the conditions (2.11), then  $\hat{A}$  may be expanded in a series of the form

$$\hat{A} = \sum_{|p| \leq N} \sum_{q=0}^M \delta \hat{A}_{pq} e^{ip\lambda} F_{p+1}^q \quad (3.7)$$

where the  $\hat{A}_{pq}$  are expressed in terms of the  $A_{pq}$  as shown in Appendix I.

The transformed equation (3.6) can be written most compactly in the form

$$\frac{d}{dt} A_{pq} + \frac{1}{a} \sum_{|\alpha|, |\beta| \leq N} \{ i\alpha \hat{A}_{\alpha\beta} U_{p-\alpha q-\beta} + i\beta A_{\alpha\beta} V_{p-\alpha q-\beta} \} = 0 \quad (3.8)$$

Coefficients with negative values in the second subscript are defined as previously indicated, i.e. for a variable which behaves as a scalar

$$A_{\alpha-\beta} = (-1)^\alpha A_{\alpha\beta}$$

and for a variable which behaves as a vector component

$$V_{\alpha-\beta} = (-1)^{\alpha+1} V_{\alpha\beta}.$$

The equation was integrated using central differences in time and the convolution terms were calculated using the transform method of Orszag (1971a) (see also Orszag (1971b)).

Linear stability analysis of the problem gives the stability restriction that, approximately,

$$\Delta t \leq |\tan \phi| / \omega p_{\max}.$$

In order to meet the stability requirement while retaining a reasonable time step, Fourier filtering in the  $\lambda$  direction was performed poleward of  $60^\circ$  latitude ( $\phi_0 = 30^\circ, 150^\circ$ ). The maximum zonal wave number retained was,  $p_{\max}$ , where

$$p_{\max} \leq \left| \frac{\tan \phi}{\tan \phi_0} \right| N, \quad \phi < 30^\circ, \quad \phi > 150^\circ.$$

A value of  $\omega = 2.40885 \times 10^{-6} \text{ sec}^{-1}$  was chosen to give an advection velocity which would move the apex of the cone one grid interval in an integral number of time steps of 1 hour. The stability condition for this value of  $\omega$  and for  $N = 32$  requires, approximately,  $\Delta t \leq 1.4$  hours.

The Fourier filtering also automatically maintains the conditions (2.11). These conditions are imposed in the filtering procedure simply by the condition that  $p_{\max} = 0$  at the poles, i.e. that the filtered variable is a constant at the poles.

The conservation of "total  $A$ " was tested by calculating

$$\int_0^{2\pi} \int_0^\pi A \sin \phi d\phi d\lambda = 2\pi \sum_{\substack{q=0 \\ q \text{ even}}}^M 4\delta A_{0q} / (1 - q_2).$$

It is not obvious that "total  $A$ " should be conserved in the truncated system (3.8) although it will be seen that is is, to good approximation, at least in the cases tested.

#### 4 Comparison with other numerical methods

The same calculations were carried out using two other methods; a finite difference formulation of equation (3.2) using the Arakawa second order Jacobian (Arakawa, 1966) and a pseudo-spectral formulation of equation (3.1) after Merilees (1973).

The equation used in the finite difference case was

$$\begin{aligned} & \frac{A_{nm}^{\tau+1} - A_{nm}^{\tau-1}}{2\Delta t} \\ & + \frac{1}{a^2 \sin \phi_m (12\Delta^2)} \{ \psi_{n+1m} (A_{nm-1} + A_{n+1m-1} - A_{nm+1} - A_{n+1m+1}) \\ & + \psi_{n-1m} (A_{nm+1} + A_{n-1m+1} - A_{nm-1} - A_{n-1m-1}) \\ & + \psi_{nm+1} (A_{n+1m} + A_{n+1m+1} - A_{n-1m} - A_{n+1m-1}) \\ & + \psi_{nm-1} (A_{n-1m} + A_{n-1m-1} - A_{n+1m} - A_{n+1m-1}) \\ & + \psi_{n+1m+1} (A_{n+1m} - A_{nm+1}) + \psi_{n+1m-1} (A_{nm-1} - A_{n+1m}) \\ & + \psi_{n-1m+1} (A_{nm+1} - A_{n-1m}) + \psi_{n-1m-1} (A_{n-1m} - A_{nm-1}) \} = 0 \end{aligned}$$

The pseudo-spectral equations used can be written in the form

$$\frac{A_{nm}^{\tau+1} - A_{nm}^{\tau-1}}{2\Delta t} + \frac{u_{nm}}{a \sin \phi_m} \frac{\partial A}{\partial \lambda} \Big|_{nm} + \frac{v_{nm}}{a} \frac{\partial A}{\partial \phi} \Big|_{nm} = 0$$

where the net of grid points is defined as

$$\begin{aligned} \lambda_n &= \frac{\pi}{N} n, \quad n = 0, 1, \dots, 2N - 1 \\ \phi_m &= \frac{\pi}{M} (m + 1/2), \quad m = 0, 1, \dots, M - 1. \end{aligned}$$

TABLE 1. Characteristics of different advection calculations.

Type of calculation	Resolution	$\Delta t$ (hrs.)	No. of Revolutions	Approx. CPU Time (sec.)	Apex Value
Double Fourier	64	0.5	1	1995	7.90
	64	1.0	1	998	7.60
			2		7.50
	32	1.0	1	173	7.85
	16	1.0	1	43	7.74
Pseudo-spectral	64	1.0	1	170	7.62
			2	becomes unstable	
(with Fourier chopping)	64	1.0	1		7.57
Finite difference			2	333	7.40
	64	1.0	1		6.89
			2	55	6.14
(no polar filtering)	64	0.1	1	127	7.05

and the derivatives are evaluated as described by Merilees (*loc cit*). An alternative pseudo-spectral formulation can be defined in terms of a series representation of the form (2.7) and (2.13) and will of course be identical to Merilees' scheme.

## 5 Discussion of results

Little effort was made to optimize the calculation using the Fourier series method other than the use of Orszag's (1971) convolution method for calculating the two non-linear products involved. The same FFT subroutine was used in both Fourier methods. Advective calculations with a number of resolutions and time steps were performed for the several methods.

Table 1 summarizes the results of several such calculations. The results are for 512 hours at which time the cone should have completed one revolution, and after 1024 hours at which time the cone should have completed two revolutions. The cone is initially situated at the equator for the Fourier series case and is displaced one-half a grid distance from the equator in the pseudo-spectral and finite difference cases. In the two Fourier methods the resolution listed in the table is  $2N$  (equivalent to the number of grid points involved in a discrete transform). In all cases  $M = N$ . For the finite difference calculation, the resolution is the number of grid points around a latitude circle. The number of points in the north-south direction is one half this number.

In all cases the "mass" of the cone, i.e. the mean value of  $A$  was conserved to  $10^{-11}$  in the spectral calculations and to  $10^{-4}$  in the pseudo-spectral calculations.

Fig. 1 gives a north-south profile through the cone after 512 hours (one revolution) with  $\Delta t = 1$  hr for the cases: (a) double Fourier series method,  $2N = 64$ ; (b) double Fourier series method,  $2N = 32$ ; (c) double Fourier series method,  $2N = 16$ ; (d) pseudo-spectral method,  $2N = 64$ ; and (e) second order Arakawa/Jacobian,  $\Delta\lambda = \Delta\phi = 2\pi/64$ . The cone has been advected over both poles and should have returned to its original position indicated by the light solid lines in the figure. It is apparent from the figures that:

- (i) both the shape of the cone and its position are very well treated by the double Fourier series and pseudo-spectral methods while the second order finite difference calculation is clearly inferior.
- (ii) even the low resolution double Fourier series calculation ( $2N = 16$ ), where computation times become comparable to times for finite difference methods, gives very good results.
- (iii) in the double Fourier and pseudo-spectral cases, the point of the cone suffers some distortion. This is due primarily to time truncation error. The inset of Fig. (1a) gives the shape of the cone apex with  $\Delta t$  reduced to 0.5 hr. In this case the tip of the cone is rather well represented.

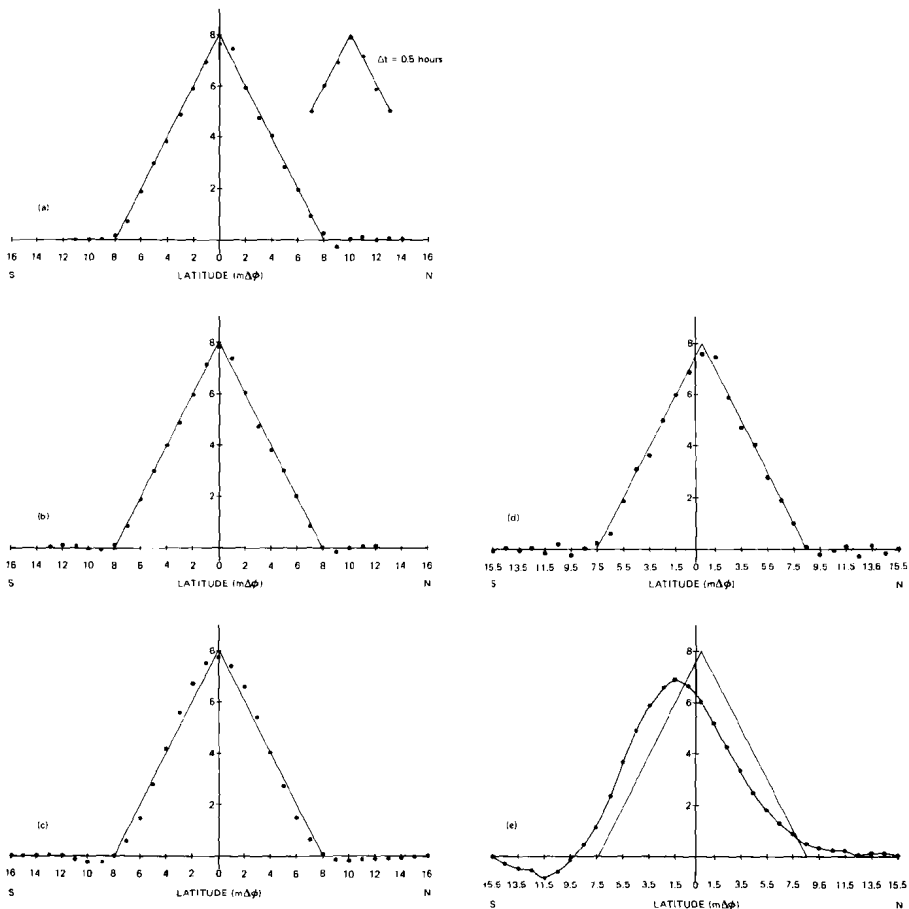


Fig. 1 North-South profile through the cone after one complete revolution about the sphere with  $\Delta t = 1$  hr. (a) double Fourier method with  $N = 32$ , (b) double Fourier method with  $N = 16$ , (c) double Fourier method with  $N = 8$ , (d) Pseudo-spectral method  $N = 32$  (e) second order finite difference method with  $\Delta \lambda = \Delta \phi = 2\pi/64$ . Note that the initial position of the cone is displaced one half a grid length from the equator in the pseudo-spectral and grid point methods.

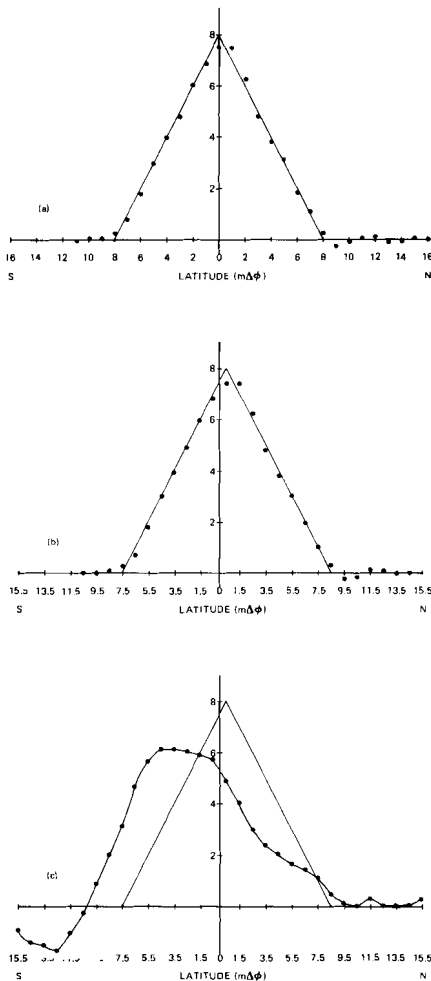


Fig. 2 North-South profile through the cone after two complete revolutions about the sphere with  $\Delta t = 1$  hour: (a) double Fourier method with  $N = 32$ , (b) Pseudo-spectral method with  $N = 32$  and Fourier chopping, (c) second order finite difference method with  $\Delta\lambda = \Delta\phi = 2\pi/64$ .

Fig. 2 gives a north-south profile through the cone after 1024 hrs. (2 revolutions again with  $\Delta t = 1$  hr. for the double Fourier series and pseudo-spectral cases ( $2N = 64$ ) and the second order grid point method. The shape and position of the cone has deteriorated very little from the previous case for the double-Fourier and pseudo-spectral calculations. The grid point calculations displays increased distortion.

In the case of a cone advected by such a simple flow field one might expect the pseudo-spectral scheme to give results comparable to the double Fourier scheme. After one revolution this is essentially the case as indicated in Fig. 1(d). For longer times, however, aliasing effects begin to dominate the solution. Fig. 3

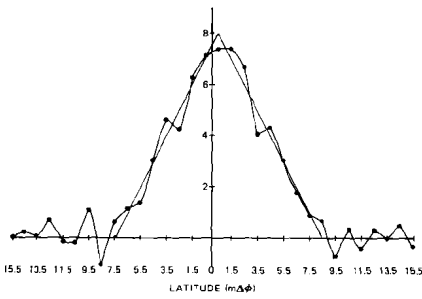


Fig. 3

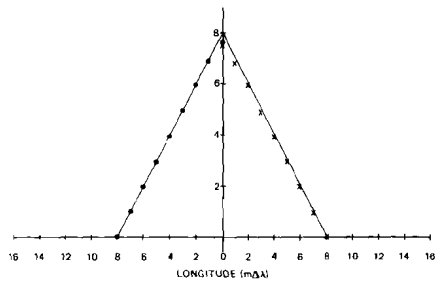


Fig. 4

Fig. 3 North-South profile through the cone after one and one-half revolutions about the sphere with  $\Delta t = 1$  hour. Pseudo-spectral method with  $N = 32$  but no Fourier chopping.

Fig. 4 East-West profile through the cone after one complete revolution (dots) and after two complete revolutions (crosses) about the sphere with  $\Delta t = 1$  hr. Double Fourier method with  $N = 32$ .

indicates the result after 768 hours (one and one-half revolutions). The solution continues to deteriorate rapidly thereafter. In this case at least, it is easy to control the aliasing by Fourier chopping as proposed by Merilees (*loc. cit.*). The result of Fig. 2(b) has been obtained by chopping the high wave number one-third of the spectrum at 64 hour intervals.

The east-west profile of the cone is symmetric for the double Fourier method and very accurately maintained as indicated in Fig. 4 where the points plotted on the 'left' half of the cone are for one revolution while those on the 'right' are for two revolutions.

Finally, it should be pointed out that the apparent difference in efficiency between pseudo-spectral and double Fourier series methods as indicated in the table can be reduced considerably. The program used for calculating cross-product series in the double Fourier calculation was rather general in form. The calculations of  $u(\partial \hat{A} / \partial \lambda)$  and  $v(\partial A / \partial \phi)$  were done independently and the fact that  $U_{pq}$  and  $V_{pq}$  were constant in this case was not used to speed up the calculations.

## 6 Summary

A method of representing scalar and vector components on the sphere in terms of two-dimensional Fourier series has been used in the simple test calculation of passive advection of a conical shape. The cone is advected several times around the sphere in a meridional direction so as to pass over both poles. The results are compared with similar calculations using pseudo-spectral and grid point methods. The double Fourier series method gives good results, even at low resolution, and is not complicated by the aliasing problems inherent in the pseudo-spectral calculation or by the inaccuracies inherent in the grid-point scheme.

It should be noted that in the absence of proof of the conservation of quadratic quantities in this numerical scheme, it is not possible to claim that non-

linear instabilities must necessarily be absent in the calculation for this or for more nonlinear “meteorological” flow situations. The two-dimensional Fourier series calculation exhibited no non-linear instability behaviour, however while the pseudo-spectral calculation became unstable. This suggests at least, that the method is less prone to aliasing errors, as might be expected in view of the way in which the nonlinear terms are calculated. It is conceivable that some conservation statements may be possible of proof which, while not guaranteeing exact conservation of quadratic quantities with area weighting on the sphere, will guarantee the boundedness of these quantities and hence the absence of non-linear instabilities. Such proofs however are not obvious.

While little effort was made to optimize the double Fourier calculations with respect to computer time, the accuracy of the method at low resolution compared to grid point schemes at “greater” resolution suggests that for similar accuracy the double Fourier series method may well be as efficient. In the case where storage is more of a constraint than computation time, the double Fourier method could be very attractive compared to grid point methods. In more complicated cases, the shallow water equations for instance, there appears to be no reason why semi-implicit time differencing could not be employed to yield a significant increase in efficiency.

For all schemes used here, polar filtering was used to control the time step and to maintain computational stability. The desirability of polar filtering in more complicated cases is by no means clear. It may prove to be necessary and/or desirable to maintain stability by some other method such as implicit time differencing.

The double Fourier series method applied to the sphere has a number of desirable features compared to pseudo-spectral and grid point methods as mentioned above. Compared to the more usual spherical harmonic representation the ease of calculation using the FFT must be weighed against the “pole problem” and the fact that the expansion functions are not orthogonal with respect to area weighting on the sphere. A more definitive comparison of the various methods must await more meteorologically realistic calculations.

**Appendix**

Fourier series representation of  $\hat{A} = A/\sin \phi$ .

Given a scalar

$$A = \sum_{|p| \leq N} \sum_{q=0}^M \delta A_{pq} e^{i p \lambda} F_p^q$$

$$\sum_{q \text{ even}} \delta A_{pq} = \sum_{q \text{ odd}} A_{pq} = 0, p \text{ even}, p \neq 0, \tag{A1}$$

we wish to determine the Fourier series representation of  $\hat{A} = A/\sin \phi$ . It is apparent that  $\hat{A}$  must have a formal expansion like that of a vector component.

$$\hat{A} = \sum_{|p| \leq N} \sum_{q=0}^M \delta \hat{A}_{pq} e^{i p \lambda} F_{p+1}^q$$

and

$$\hat{A}_{pq} = \frac{1}{4\pi^2} \int_0^{2\pi} \int_0^\pi \frac{A}{\sin \phi} e^{-i p \lambda} F_{p+1}^{-q} d\phi d\lambda$$

$$\begin{aligned}
&= \frac{1}{4\pi^2} \sum_{|\alpha| \leq N} \sum_{\beta=0}^M \delta A_{\alpha\beta} \int_0^{2\pi} e^{i(\alpha-p)\lambda} d\lambda \int_0^\pi \frac{F_\alpha^\beta F_{p+1}^{-q}}{\sin \phi} d\phi \\
&= \frac{1}{2\pi} \sum_{\beta=0}^M \delta A_{p\beta} \int_0^\pi \frac{F_p^\beta F_{p+1}^{-q}}{\sin \phi} d\phi
\end{aligned}$$

for

$$\begin{aligned}
\int_0^\pi \frac{F_p^\beta F_{p+1}^{-q}}{\sin \phi} d\phi &= 2i \int_0^\pi \frac{\sin(\beta-q)\phi}{\sin \phi} d\phi \\
&\quad + 2i(-1)^{p+1} \int_0^\pi \frac{\sin(\beta+q)\phi}{\sin \phi} d\phi \\
&= 2i \left\{ \begin{array}{l} 0; \beta = q, \beta - q \text{ even} \\ \pi; \beta - q \text{ odd}, > 0 \\ -\pi; \beta - q \text{ odd}, < 0 \end{array} \right\} \\
&\quad + 2i(-1)^{p+1} \left\{ \begin{array}{l} 0; \beta + q \text{ even} \\ \pi; \beta + q \text{ odd} \end{array} \right\}
\end{aligned}$$

we have

$$\hat{A}_{pq} = \left\{ \begin{array}{l} -2i \sum_{\substack{\beta=1 \\ \beta \text{ odd}}}^{q-1} A_{p\beta}; p \text{ even}, q \text{ even} : 2i \sum_{\substack{\beta=q+1 \\ \beta \text{ odd}}}^{M-1} A_{p\beta}; p \text{ odd}, q \text{ even} \\ -2i \sum_{\substack{\beta=0 \\ \beta \text{ even}}}^{q-1} \delta A_{p\beta}; p \text{ even}, q \text{ odd} : 2i \sum_{\substack{\beta=q+1 \\ \beta \text{ even}}}^M A_{q\beta}; p \text{ odd}, q \text{ odd} \end{array} \right.$$

The condition (A1) on  $A_{pq}$  implies that

$$\hat{A}_{pq} = 0, q \geq M$$

so that  $\hat{A}$  is expressible in a double Fourier series with the same number of terms as  $A$ .

This formal derivation gives relations for  $\hat{A}_{pq}$  which are also those obtained by equating terms in the series for  $\hat{A}$  and  $A \sin \phi$  and solving the resulting sets of equations subject to the conditions (A1). The case for  $p = 0$  however is anomalous. The series derivation, or the consideration that  $A/\sin \phi$  is singular for  $\phi \rightarrow 0, \pi$  shows that the values for  $A_{0q}$  are indeterminate. This is not a problem in the transformed equation of motion in the case treated here since  $A$  enters as a derivative with respect to  $\lambda$ , i.e., as  $ip\hat{A}_{pq}$ , so that the term is well defined for  $p = 0$ .

## References

- ARAKAWA, A., 1966: Computational design for long term numerical integration of the equation of fluid motion: two-dimensional incompressible flow. Part I. *Comp. Phys.* **1**, 119-143.
- MERILEES, P.E., 1973: The pseudo-spectral approximation applied to the shallow water equations on a sphere. *Atmosphere*, **11**, 13-20.
- ORSZAG, S.A., 1971 a: Numerical simulation of incompressible flows within simple boundaries. 1. Galerkin (spectral) representations. *Stud. Appl. Math.*, **50**, 293-327.
- 1971 b: Numerical simulation of incompressible flows within simple boundaries: accuracy. *J. Fluid Mech.*, **49**, 75-112.
- 1974: Fourier series on Spheres. *Mon. Wea. Rev.*, **102**, 56-75.

---

# An Elementary Parcel Model with Explicit Condensation and Supersaturation

R.R. Rogers

*Department of Meteorology, McGill University, Montreal*

[Manuscript received 1 April 1975; in revised form 24 October 1975]

---

## ABSTRACT

The development of droplet size, supersaturation, and temperature in an ascending, unmixed parcel of cloudy air was investigated using a numerical model in which condensation and supersaturation are explicitly calculated. Of particular interest was the steady-state value which the supersaturation attains, and the time required to reach this value. The results were found to be in reasonable agreement with an approximate analytical solution of the equations that predicts a steady-state supersaturation equal to  $G(p, T)U/\nu r$ , where  $G(p, T)$  is a known

thermodynamic function of temperature and pressure,  $U$  is the updraft speed (assumed constant),  $\nu$  is the number of droplets per unit mass of air (assumed constant), and  $r$  is the droplet radius. The approach to this limiting value is very nearly exponential, with a time constant equal to  $G(p, T)/Q_1\nu r$ , where  $Q_1$  is a function of temperature. Without giving up the possibility of approximate analytical solutions, the equations can be elaborated to allow an accelerating updraft or to simulate the effects of rapid droplet coalescence.

---

## 1 Introduction

As an exercise for an undergraduate course in cloud physics, a computer model was devised for tracing the development of droplet size and supersaturation in an ascending air parcel. The students ran repeated experiments with the model, varying the initial conditions, in order to determine how quickly a steady value of supersaturation is reached and on what this value depends. Not surprisingly, the results showed systematic dependences on such parameters as updraft speed, droplet size and concentration, and initial temperature. In every case a quasi-steady-state value of supersaturation was approached very quickly, suggesting that some of the factors in the differential equation for the rate of change of supersaturation could be regarded as constant during the short time required to reach the steady state. An analytical solution based on this approximation was found to be in agreement with results from the computer model.

The model is a useful teaching aid, combining a number of fundamental thermodynamic and cloud physical processes. Included are adiabatic expansion, diffusional growth, latent heating, and changes in supersaturation, all with the

correct dependence on temperature and pressure. Equally important, the results of the numerical experiments, and the analytical approximations they suggest, provide insight into the factors influencing the course of supersaturation in natural clouds. The model predictions are apparently consistent with results from more elaborate calculations, such as those of Squires (1952) and Young (1974).

## 2 The Model

A parcel of air containing a population of equal-sized cloud droplets ascends at a constant speed. Pressure decreases at the hydrostatic rate, supersaturation is created, and the droplets grow by condensation-diffusion. The released latent heat raises the temperature of the air, with the heat content of the droplets being neglected. The saturation ratio is accounted for explicitly, by comparing the rate at which supersaturation is produced by the updraft with the rate at which it is depleted by condensation. During the process, the droplet mixing ratio is constant: no new droplets are created by the activation of condensation nuclei; none is lost by coalescence.

### a Initial Conditions

The following parameters are specified initially:

- (1) droplet radius,  $r_0$
- (2) droplet concentration,  $\nu_0$  per unit mass or  $n_0$  per unit volume
- (3) updraft speed,  $U$
- (4) temperature,  $T_0$
- (5) pressure,  $p_0$
- (6) saturation ratio,  $S_0$

From these parameters are calculated the initial values of air density  $\rho_0$ , liquid water mixing ratio  $\chi_0$ , and liquid water concentration  $M_0$ , using the relationships

$$\rho_0 = p_0/R'T_0$$

$$\chi_0 = \frac{4}{3}\pi\rho_L\nu_0r_0^3$$

$$M_0 = \rho_0\chi_0$$

where  $R'$  is the gas constant for air and  $\rho_L$  is the density of water.

### b Changes in the Various Quantities

#### (1) Drop size.

It is assumed that the droplets are large enough for the solution and curvature terms in the diffusional growth equation to be neglected. The equation is then

$$\frac{dr}{dt} = \frac{\sigma}{r}, \quad (1)$$

where

$$\sigma = \frac{S - 1}{F_k + F_d}. \quad (2)$$

$F_k$  and  $F_d$  are thermodynamic factors given by (cf. Mason, 1971)

$$F_k = \frac{L^2 \epsilon \rho_L}{KR'T^2}$$

$$F_d = \frac{R'T \rho_L}{\epsilon D e_s(T)}$$

where  $L$  is the latent heat of condensation,  $\epsilon = 0.622$  is the ratio of the gas constants of air and water,  $K$  is the coefficient of thermal conductivity of air,  $D$  is the diffusion coefficient of water vapor in air, and  $e_s(T)$  is the equilibrium vapor pressure over a plane water surface at temperature  $T$ . Computational details in evaluating these factors are explained in the Appendix. Ventilation effects are small for the droplet sizes considered and are neglected.

When a time step  $\Delta t$  is taken, the new radius is obtained by integrating (1):

$$r_1 = \sqrt{r_0^2 + 2\sigma_0 \Delta t}, \quad (3)$$

where  $\sigma_0$  is the value of  $\sigma$  determined by the initial values of temperature, pressure, and saturation ratio.

(2) Liquid water content.

The droplet mixing ratio  $\nu_0$  is assumed constant. Therefore, after time step  $\Delta t$  the liquid water mixing ratio is given by

$$\chi_1 = \chi_0 + \Delta\chi_1 = \frac{4}{3}\pi\rho_L\nu_0 r_1^3. \quad (4)$$

(3) Pressure.

The change in pressure in time  $\Delta t$  is given by

$$\Delta p_1 = p_1 - p_0 = \frac{dp}{dt} \Delta t = -\rho_0 g U \Delta t, \quad (5)$$

where  $\rho_0$  is the initial density,  $U$  the updraft speed, and  $g$  the acceleration of gravity.

(4) Temperature.

From the first law of thermodynamics, the differential equation linking temperature, pressure, and condensed water is

$$\frac{dT}{T} - \frac{R'}{c_p} \frac{dp}{p} = \frac{L}{c_p T} d\chi. \quad (6)$$

Therefore the temperature after  $\Delta t$  is given by

$$T_1 = T_0 \exp \left[ \frac{L}{c_p T_0} (\chi_1 - \chi_0) + \frac{R'}{c_p} \ln \frac{p_1}{p_0} \right]. \quad (7)$$

(5) Density.

$$\rho_1 = p_1 / R' T_1. \quad (8)$$

(6) Liquid water content.

$$M_1 = \rho_1 \chi_1. \quad (9)$$

(7) Saturation ratio.

The differential equation which describes the change in saturation ratio, as adapted from Fletcher (1962, p. 128), is

$$\frac{dS}{dt} = Q_1 U - \rho Q_2 \frac{d\chi}{dt} \quad (10)$$

where  $Q_1$  and  $Q_2$  are thermodynamic factors given by

$$Q_1 = \frac{Lg\epsilon}{R'c_p T^2} - \frac{g}{R'T}$$

$$Q_2 = \frac{R'T}{\epsilon e_s} + \frac{\epsilon L^2}{c_p T p}$$

The change in  $S$  in time  $\Delta t$  is calculated from

$$\Delta S_1 = S_1 - S_0 = \bar{Q}_1 U \Delta t - \bar{\rho} \bar{Q}_2 \Delta \chi_1, \quad (11)$$

where  $\Delta \chi_1 = \chi_1 - \chi_0$ ,  $\bar{\rho} = \frac{1}{2}(\rho_1 + \rho_0)$ , and  $\bar{Q}_1$  and  $\bar{Q}_2$  denote the thermodynamic factors evaluated at  $T = \frac{1}{2}(T_0 + T_1)$  and  $p = \frac{1}{2}(p_0 + p_1)$ . It was found that the integrations were considerably more accurate when these averages were used in place of the initial values, especially in the case of density.

A sequence of time steps is taken and the development of  $r$ ,  $T$ ,  $S$ , and the other calculated variables is thereby followed. It was found that time steps of one second or less are required for accuracy and computational stability.

### 3 Results

The main point of this study was to determine the course of supersaturation in an ascending cloudy parcel, and to investigate its dependence on such parameters as updraft speed, droplet size and concentration, and initial temperature. Each of these parameters was varied (in addition to several others) and a number of calculations were carried out over times ranging from a few seconds to several minutes.

#### a Standard Case

The standard experiment, against which the various results were compared, is defined by the following initial conditions, which are thought to be representative of the lower levels of rapidly developing cumulonimbus clouds of the Canadian Prairies:

$$r_0 = 8 \mu\text{m}$$

$$n_0 = 200 \text{ cm}^{-3}$$

$$U = 10 \text{ m/s}$$

$$T_0 = 7^\circ\text{C}$$

$$p_0 = 800 \text{ mb}$$

$$S_0 = 1.00.$$

For these conditions the initial values of water content are  $\chi_0 = 0.43 \text{ g/kg}$  and  $M_0 = 0.43 \text{ g/m}^3$ , as the air density is  $1 \text{ kg/m}^3$ .

Fig. 1 shows the development of droplet radius and supersaturation during the first 20 s (200 m) of ascent. A peak supersaturation of 0.97 per cent is reached at 7 s, after which the supersaturation gradually decreases. The droplet size in-

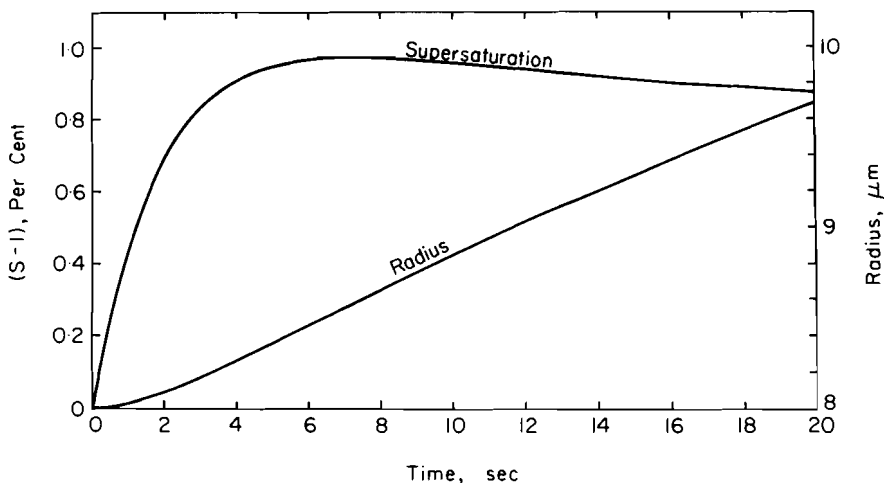


Fig. 1 Development of droplet size and supersaturation in the standard case, defined by:  $r_0 = 8 \mu\text{m}$ ,  $n_0 = 200 \text{ cm}^{-3}$ ,  $U = 10 \text{ m/sec}$ ,  $T_0 = 7^\circ\text{C}$ ,  $P_0 = 800 \text{ mb}$ ,  $S_0 = 1.0$ .

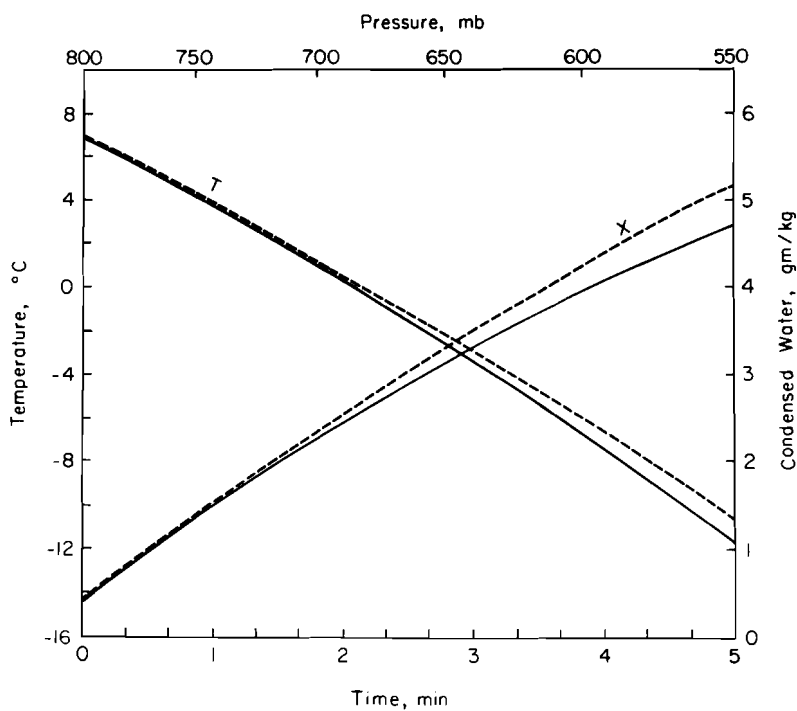


Fig. 2 Temperature and liquid water mixing ratio in the standard case (solid curves). The dashed curves are for temperature and condensed water in pseudoadiabatic ascent.

creases relatively slowly during the first second, owing to the low values of supersaturation. After the peak supersaturation is reached, the droplet growth curve becomes approximately parabolic, as would be expected from (1) if  $\sigma$  were constant.

In Fig. 2 the parcel temperature and liquid water mixing ratio are plotted for the first five minutes (3 km) of ascent. Shown for comparison (dashed) are the temperature for pseudoadiabatic ascent and the liquid water content for a saturated adiabatic process. Because all the vapor excess over equilibrium does not condense out in the model, it gives temperatures and water contents that deviate progressively from the adiabatic values. For the case of  $S = 1.0$  (no supersaturation) the curves would be coincident.

## b Effect of Varying the Initial Conditions

### (1) Supersaturation.

Figs. 3 and 4 illustrate the influence of initial supersaturation on the development of droplet size and supersaturation. Fig. 3 shows that in about 10 s the supersaturation reaches essentially the same value in all cases, regardless of its initial value. A sustained, quasi-steady value is reached, followed by a gradual decrease. In these examples the curves are indistinguishable after 15 s. Because droplet growth rate is proportional to supersaturation, the cases with high initial saturation ratios produce larger drops, as shown in Fig. 4. These cases also pro-

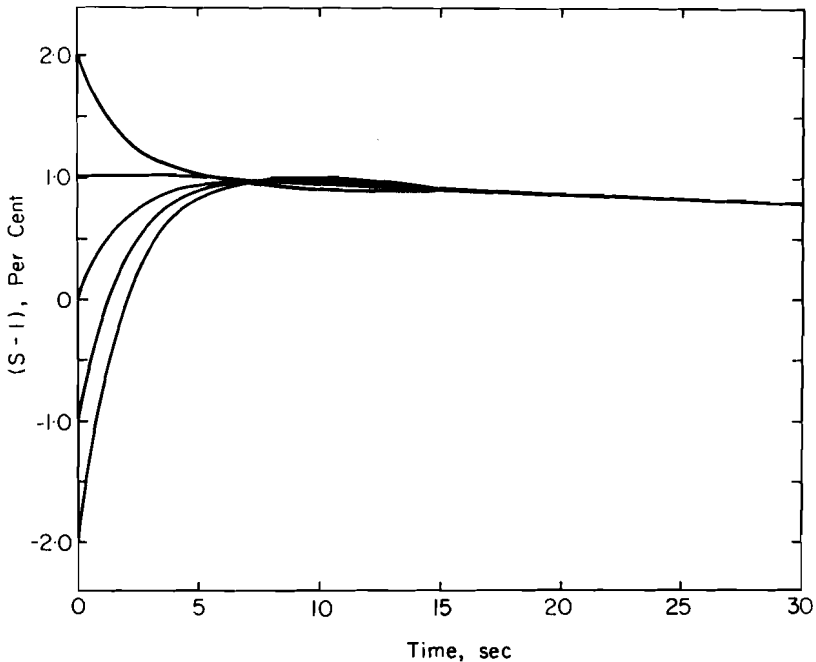


Fig. 3 The progress of supersaturation from different initial values. All other parameters are as in the standard case.

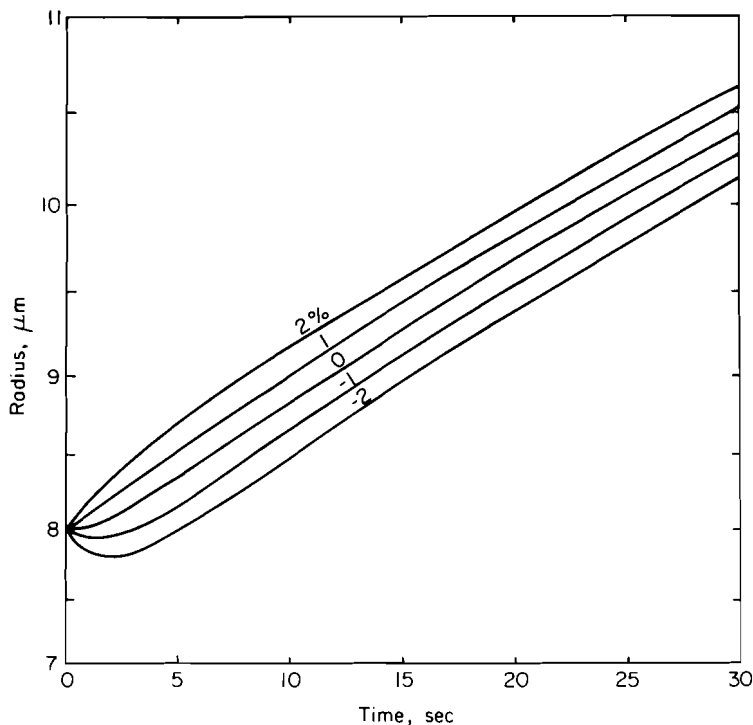


Fig. 4 Development of drop radius as a function of initial supersaturation. These curves correspond to the cases in Fig. 3. The ordinate scale is linear in  $r^2$ ; the curves would therefore be straight lines for  $\sigma$  in (1) a constant.

duce slightly higher liquid water contents and temperatures, because of the faster initial condensation rates.

(2) Updraft speed.

The development of supersaturation is shown in Fig. 5 for vertical velocities ranging from 1 to 15 m/s. The faster the updraft, the higher the peak supersaturation and the faster the initial increase in supersaturation.

(3) Other variables.

By individually varying the other parameters that define the initial conditions it was found that the quasi-steady, limiting supersaturation increases with

- (a) decreasing  $n_0$
- (b) decreasing  $r_0$
- (c) decreasing  $T_0$
- (d) increasing  $p_0$

In every case, it was found that the approach to the limiting supersaturation could be approximated as exponential, especially at the earliest times. Fig. 6 illustrates this effect for the cases in which  $n_0$  was varied. Plotted as a function of time for each case is  $\ln[(s_\infty - s)/(s_\infty - s_0)]$ , where  $s = (S - 1)$  is the supersaturation at time  $t$ ,  $s_0$  is the initial supersaturation (in all these cases, zero), and  $s_\infty$  is the quasi-steady, limiting supersaturation. Straight lines imply exponential

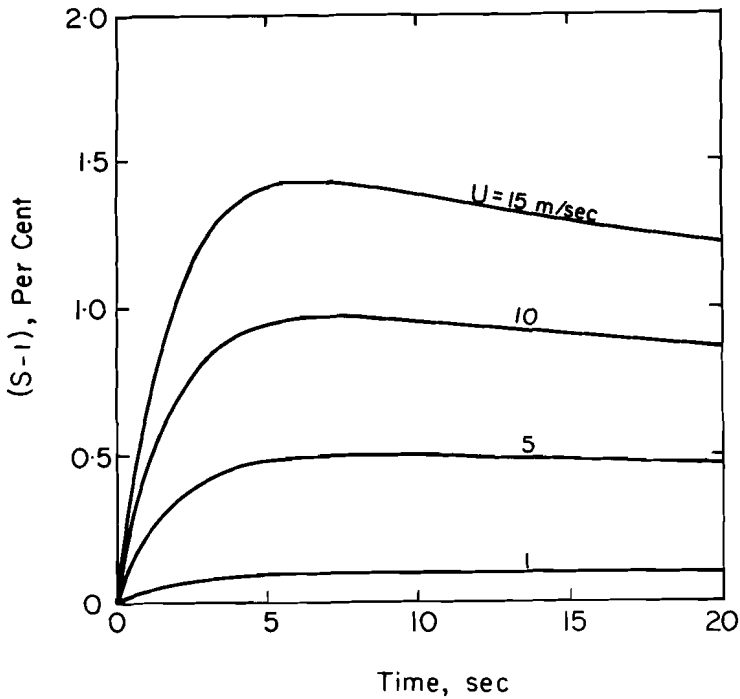


Fig. 5 The effect of updraft speed on the course of supersaturation.

response; this is seen to be a good approximation in all cases for the first few seconds. Thus, for short times, the supersaturation varies according to

$$(s - s_{\infty}) = (s_0 - s_{\infty})e^{-t/\tau} \quad (12)$$

where  $\tau$  is the "time constant" characterizing the approach of supersaturation to its limiting value. Table 1 summarizes the results, giving the values of  $s_{\infty}$  and  $\tau$  for each calculation.

#### 4 Approximate analytical solution

Using (1) and (2), the rate of change of liquid water content may be expressed

$$\frac{d\chi}{dt} = \frac{d}{dt}(\frac{4}{3}\pi\rho_L v_0 r^3) = \frac{4\pi\rho_L v_0}{F_k + F_d}(S - 1)r. \quad (13)$$

The equation (10) for saturation ratio then becomes

$$\frac{dS}{dt} = Q_1 U - \rho Q_2 (4\pi\rho_L v_0)(F_k + F_d)^{-1}(S - 1)r.$$

In terms of the supersaturation  $s = (S - 1)$  we may therefore write

$$\frac{ds}{dt} = A - Bs \quad (14)$$

where  $A = Q_1 U$  and  $B = 4\pi\rho\rho_L Q_2 v_0 r / (F_k + F_d)$ .

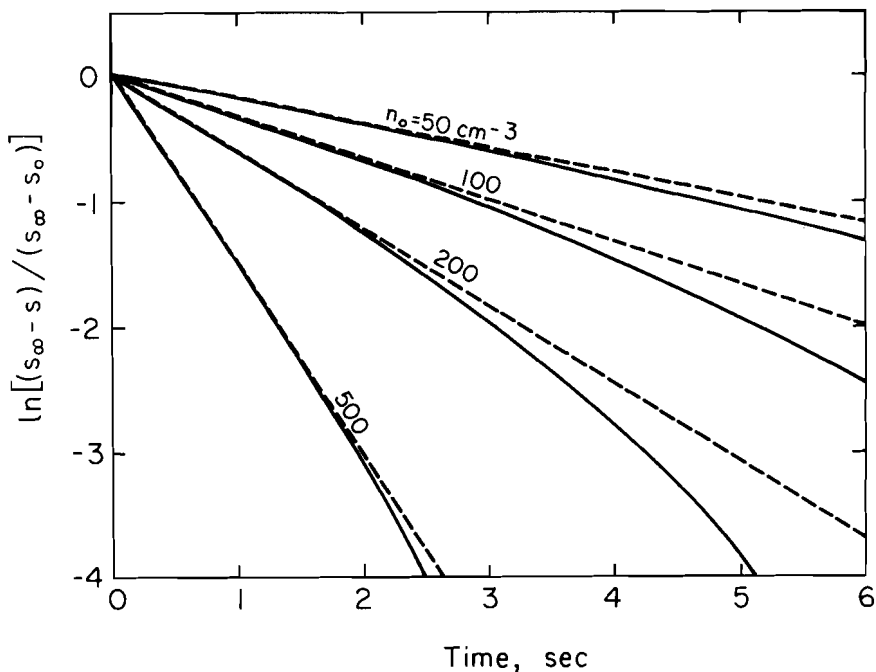


Fig. 6 The initial behavior of supersaturation, for various values of droplet concentration. On these coordinates the straight lines (dashed) would imply exact exponential response.

The calculations showed that the approach to the limiting value of supersaturation is quite rapid. As an approximation, pressure and temperature may therefore be regarded as constant during the short time required for the limiting supersaturation to be reached. If the small change in droplet radius is also neglected, it follows that  $A$  and  $B$  in (14) are constant. The appropriate solution of this equation is then

$$s = \left( s_0 - \frac{A}{B} \right) e^{-Bt} + \frac{A}{B}, \quad (15)$$

where  $s_0 = (S_0 - 1)$  is the initial supersaturation. The limiting supersaturation is therefore given by

$$s_\infty = (S_\infty - 1) = \frac{A}{B} = G(p, T) \frac{U}{rv_0}, \quad (16)$$

where

$$G(p, T) = \frac{Q_1 (F_k + F_d)}{Q_2 \frac{4\pi\rho_L\rho}{r}}. \quad (17)$$

Thus the limiting supersaturation is directly proportional to updraft speed and inversely proportional to the product of drop concentration times drop radius. As a matter of interest the function  $G(p, T)$  is plotted in Fig. 7.

TABLE 1. Values of the limiting supersaturation ( $S_\infty - 1$ ) and time constant  $\tau$  determined for the indicated initial conditions.

$P_0(\text{mb})$	$T_0(^{\circ}\text{C})$	$U(\text{m/s})$	$(S_0 - 1)(\%)$	$n_0(\text{cm}^{-3})$	$r_0(\mu\text{m})$	$(S_\infty - 1)(\%)$	$\tau(\text{sec})$
800	7	10	0	200	4	1.52	2.72
800	7	10	0	200	8	0.97	1.73
800	7	10	0	200	12	0.68	1.21
800	7	10	0	200	16	0.52	0.92
800	7	10	0	50	8	3.05	5.45
800	7	10	0	100	8	1.78	3.17
800	7	10	0	200	8	0.97	1.73
800	7	10	0	500	8	0.41	0.73
800	7	10	-2	200	8	0.99	1.85
800	7	10	-1	200	8	0.98	1.81
800	7	10	0	200	8	0.97	1.73
800	7	10	1	200	8	1.02	0.75
800	7	10	2	200	8	0.96	1.91
800	7	1	0	200	8	0.10	1.70
800	7	5	0	200	8	0.50	1.78
800	7	10	0	200	8	0.97	1.73
800	7	15	0	200	8	1.43	1.72
800	-3	10	0	200	8	1.11	1.84
800	7	10	0	200	8	0.97	1.73
800	17	10	0	200	8	0.86	1.68
600	7	10	0	200	8	0.75	1.34
800	7	10	0	200	8	0.97	1.73
1000	7	10	0	200	8	1.18	2.11

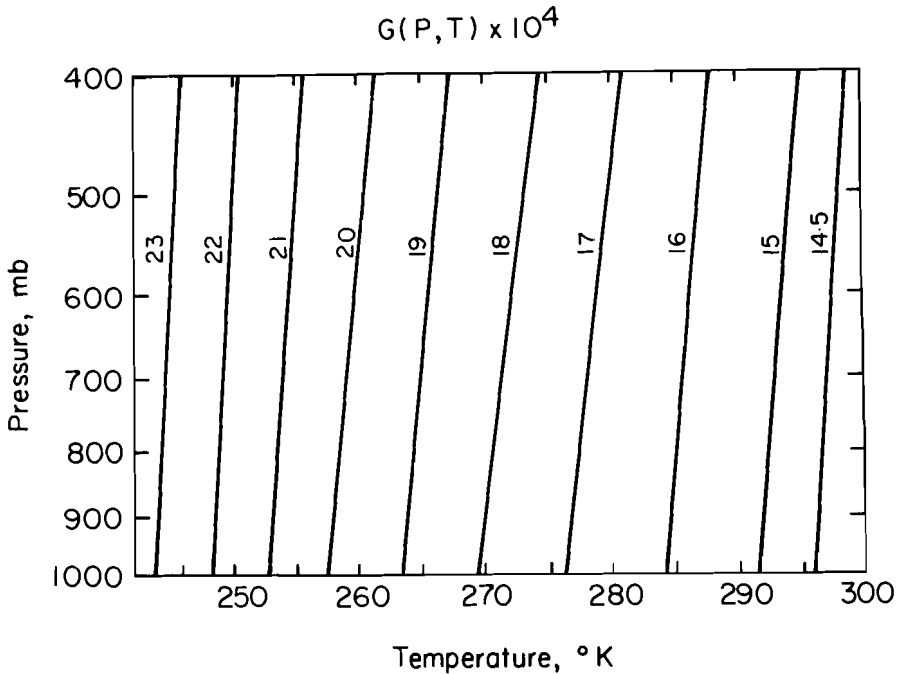


Fig. 7 The proportionality factor  $G(p, T)$ , in  $\text{s/g}$ , relating the limiting value of fractional supersaturation,  $s_\infty$ , with updraft, droplet size, and droplet concentration.

From (15), the time-constant characterizing the change in supersaturation is given by

$$\tau = B^{-1} = \frac{(S_{\infty} - 1)}{UQ_1} = \frac{G(p, T)}{Q_1 r \nu_0}. \quad (18)$$

Using (16) and (18),  $s_{\infty}$  and  $\tau$  were calculated for all cases listed in Table 1. In both equations the initial value of radius was used for  $r$ . The agreement between these approximate analytical results and the calculated values in Table 1 was found to be good. In the standard case, for example, (16) and (18) predict  $s_{\infty} = 1.04\%$  and  $\tau = 1.88$  s whereas the calculations gave  $s_{\infty} = 0.97\%$  and  $\tau = 1.73$  s. The analytical values of  $s_{\infty}$  and  $\tau$  consistently overestimate the computed values by an amount that averages about 10%. This discrepancy is explained almost entirely by the fact that the initial radius is used in the analytical evaluations, while in fact the radius has usually increased by about 10% by the time  $s_{\infty}$  is reached. The discrepancies are least for the cases in which  $r$  increases by only a small amount. The largest discrepancy occurs for the case in which the initial supersaturation was 1%. In this case the initial value is close to the limiting value and the changes in  $s$  are controlled primarily by changes in  $r$ . Consequently (18) is not a good approximation and overestimates  $\tau$  by about a factor 2.5.

The gradual decrease in supersaturation after the initial quasi-steady value is reached is explained by (16). As the radius continues to increase,  $s$  diminishes approximately as  $r^{-1}$ .

## 5 Discussion

In this elementary parcel model, the supersaturation rapidly tends to the equilibrium value that is determined by a balance between the rates of vapor production by the updraft and consumption by drop growth. The equilibrium value is given by (16), which is equivalent to the solution of (14) when  $ds/dt = 0$ , and the response time by (18), both to good approximation.

When the initial supersaturation is less than the limiting value, there is a significant difference between this simple model and an actual cloudy parcel. In the atmosphere condensation nuclei would be activated as the supersaturation increases and more droplets thereby produced. By consuming some moisture the additional droplets would be expected to reduce both the limiting supersaturation and response time. The values predicted by the model might thus be interpreted as upper limits of the steady supersaturation and response time in real clouds. In an exhaustive treatment of droplet growth by condensation, Squires (1952) took into account the activation of additional nuclei as well as ventilation effects. He found also an approximate exponential approach to the limiting supersaturation with time constants ranging from 1 to 10 s. He gave an approximate expression for the limiting supersaturation, corresponding approximately to the assumptions for the present model, that is entirely equivalent to (16), but with a proportionality factor which is appropriate for supersaturation expressed in degrees.

As ascent continues in actual clouds, the drops can become large enough for

coalescence to begin, in which case the product  $\nu r$  will decrease with time. As shown by Young (1974), coalescence can proceed rapidly enough to produce a substantial increase in the supersaturation. To allow for the possibility of changes in drop concentration, as caused for example by coalescence, the elementary model could be generalized somewhat by allowing  $B$  in (14) to vary with time. Thus,

$$\frac{ds}{dt} + B(t)s = A \quad (19)$$

expresses the behavior of  $s$  in the more general system. To give an indication of the effect on  $s$  of a rapidly decreasing  $B$ , an elementary solution is possible for  $B(t)$  of the form

$$B(t) = \frac{B_0 t_0}{t + t_0} \quad (20)$$

Clearly  $B(0) = B_0$ , and  $B$  falls to half its initial value at  $t = t_0$ . The solution is

$$s(t) = \frac{A}{B_0 t_0 + 1} (t + t_0) \quad (21)$$

Therefore  $s$  does not approach a steady value, but increases at the constant rate

$$\frac{ds}{dt} = \frac{A}{B_0 t_0 + 1} \quad (22)$$

For the initial conditions of the standard case, and for a half-time  $t_0 = 30$  s, the result is

$$\frac{ds}{dt} = 3.27 \times 10^{-4} \text{ s}^{-1} = 3.27 \times 10^{-2} \%/\text{s}.$$

Even for a seemingly rapid decrease in  $B$ , the rate of increase of supersaturation is thus only about 2% per minute. By comparison, Young (1974) found a rate of about 0.6%  $\text{min}^{-1}$  due to coalescence in an example for a maritime cloud.

The possibility of an accelerating updraft can be taken into account by allowing  $A$  in (14) to vary with time. For constant acceleration, for example, (14) becomes

$$\frac{ds}{dt} + Bs = Q_1 kt, \quad (23)$$

where  $k = dU/dt$ , with the solution

$$s = \left( s_0 + \frac{Q_1 k}{B^2} \right) e^{-Bt} + \frac{Q_1 k}{B^2} (Bt - 1).$$

The rate of change of supersaturation in this accelerating updraft is therefore

$$\frac{ds}{dt} = \frac{Q_1 k}{B} - B \left( s_0 + \frac{Q_1 k}{B^2} \right) e^{-Bt}.$$

If the initial supersaturation is zero (as in the standard case), this result reduces to

$$\frac{ds}{dt} = \frac{Q_1 k}{B} (1 - e^{-Bt}).$$

Because of the short time-constant, the rate of change of supersaturation will quickly tend to

$$\frac{ds}{dt} = \frac{Q_1}{B} k = \frac{Q_1}{B} \frac{dU}{dt} \approx \frac{d}{dt} s_\infty.$$

That is, in an accelerating updraft there will be a strong tendency for  $s$  to keep pace with changes in the limiting value of  $s$ , as defined by (16).

### Acknowledgments

I am grateful to Mary A. Rogers for the programming and to the students in Meteorology 321B for running the program and analyzing the results.

### Appendix I

#### Numerical Details

In the  $F_k$  and  $F_d$  terms that appear in (2), the coefficient of conductivity  $K$  and diffusion coefficient  $D$  are empirically related to temperature and pressure by

$$K(T) = 2.42 \times 10^3 \left( \frac{393}{T + 120} \right) \left( \frac{T}{273} \right)^{3/2} \quad (\text{A.1})$$

$$D(p, T) = 8.28 \times 10^2 \frac{T}{p} \left( \frac{393}{T + 120} \right) \left( \frac{T}{273} \right)^{3/2} \quad (\text{A.2})$$

where  $T$  is in  $^\circ\text{K}$  and  $p$  is in dynes/cm<sup>2</sup>. These expressions follow from the relations between  $K$  and  $D$  and the viscosity of the air, and the empirical dependence of viscosity on  $p$  and  $T$ , as explained in the *Smithsonian Meteorological Tables* (R.J. List, 1958). The latent heat of condensation  $L$  is taken as constant at  $2.5 \times 10^3$  J/g, its weak dependence on temperature being neglected. The equilibrium vapor pressure over bulk water  $e_s$  is obtained by integrating the Clausius-Clapeyron equation, holding  $L$  constant, and is therefore

$$e_s(T) = 2.75 \times 10^{12} \exp \left( - \frac{5.44 \times 10^3}{T} \right), \quad (\text{A.3})$$

where the constant of integration is chosen to make the vapor pressure equal 6.1 mb at  $0^\circ\text{C}$ .

The same approximations for  $L$  and  $e_s$  are used in evaluating the  $Q_1$  and  $Q_2$  factors that appear in (10).

### References

- FLETCHER, N.H., 1962: *The Physics of Rain-clouds*. Cambridge University Press, 386 pp.
- LIST, R.J. (ed.), 1958: *Smithsonian Meteorological Tables*. Smithsonian Institution, Washington, 527 pp.
- MASON, B.J., 1971: *The Physics of Clouds*. Clarendon Press, Oxford, 671 pp.
- SQUIRES, P., 1952: The growth of cloud drops by condensation. *Australian Journal of Scientific Research* 5, 59–86.
- YOUNG, K.C., 1974: The evolution of drop spectra due to condensation, coalescence and breakup. *Preprints, Conference on Cloud Physics*, Tucson, Ariz., pp. 95–98. American Meteorological Society, Boston.

---

## BOOK REVIEWS

---

GLOBAL CLIMATE. Keith Boucher. The English Universities Press Ltd., 1975, 326 pp., \$14.50.

Boucher of the Loughborough College of Education, England, has written a textbook on global climate in which he succeeds in his stated objective of introducing geography students to synoptic climatology.

The book is a reappraisal of global climate and has been written against the background of the many recent advances in climatology. Texts such as Stringer's *Foundations of Climatology* and *Synoptic Climatology* by Barry and Perry or even volumes of the recently completed *World Survey of Climatology* are unlikely to ever make it on lists of required textbooks for climatology courses, simply because they are beyond the financial reach of the average under-graduate. Boucher's book has obviously been written to fill this vacuum. Its first chapter, a brief general section on atmospheric processes, is by far its weakest. Whilst only dealing with "aspects of some climatic or global significance, necessary for an understanding of the atmospheric processes mentioned in the regional sections of the book", its treatment of topics such as atmospheric stability and meridional energy transfer (including the part played by ocean currents) is far from satisfactory and easily surpassed by several existing texts. Chapters 2-6 comprise the regional section of the book. They deal with tropical America and Africa (2); the tropical monsoon climates of India, S.E. Asia, the Pacific and northern Australia (3); the subtropical climates of China and Japan (4); the mid-latitudes (5); and the polar regions (6). Each regional chapter commences with well-documented sections on general climatic features of the regions. This is then followed by detailed regional climatic analyses, with a wealth of climatic data, drawing heavily on published data sources.

My main criticism concerns the lack of an adequate overview, which is so necessary in any book dealing extensively with regional climatic analyses. What reasoning led to the present organization of this book? What links the regional sections? The section on general circulation (pp. 43-53) is too brief and rather sketchy and does not really serve its purpose.

The book is well illustrated with some 30 satellite photographs and more than 150 drawings and maps. It has an excellent bibliography which is detailed and well organized. The glossary appears to be adequate.

Several minor points should be mentioned. I do not like the book's format (24 cm wide; 17½ cm high). It requires four knees or a wide desk. The lay-out is useful for reference to the many short tables with climatic data but less than adequate when referring to the book's many figures. I applaud the use of metric units throughout the book but why still use cal/cm<sup>2</sup>/min or langley/min rather than watt/m<sup>2</sup>? Appendix (4) with frequently used conversion factors does not even include energy units.

In conclusion, I warmly recommend this book and feel confident that it will soon find its way into many colleges and universities.

J.D. Kalma  
Department of Geography  
University of British Columbia

THE DYNAMIC METEOROLOGY OF THE STRATOSPHERE AND MESOSPHERE. James R. Holton. American Meteorological Society Meteorological Monographs. Volume 15, Number 37, 1975, 216 pp., \$30.00 (\$20.00 AMS members).

Its relatively small mass notwithstanding, the neutral atmosphere above the tropopause has received increased attention from meteorologists in recent years. Much productive work on the stratosphere has been motivated by the presence there of the protective layer of ozone which many scientists believe can be adversely affected by such diverse influences

as supersonic aircraft and the burgeoning production of artificial fertilizers. Dynamic meteorology plays a central role in determining the quantitative effects of man's activities on the ozone distribution. Thus, the practical motivation for studying the dynamics of the stratosphere and mesosphere is compelling. Moreover, the motions observed there provide an absorbing and varied study in themselves. These motions, rather than photochemistry, are the subject of Holton's book.

There is a brief account of observational evidence in the first chapter, but the bulk of the text is devoted to a discussion of mathematical models for the observed phenomena. The presentation of the models is lucid and in many cases the discussion of results is accompanied by figures. After introductory chapters on observations and the development of the equations, additional chapters treat baroclinic instability in the stratosphere and mesosphere, forced waves and wave-zonal flow interactions, and modelling of the general circulation of the stratosphere and mesosphere. One of the most interesting (and longest) chapters is that dealing with forced waves and wave-zonal flow interactions. Forced and free equatorial and extratropical planetary waves as well as the tidal motions of the stratosphere and mesosphere are discussed. These are then related to the most dramatic of the observed changes in the zonal mean state: the sudden stratospheric warmings and the quasi-biennial oscillation.

Most of the important theoretical results concerning the stratosphere are put forward, but this work is by no means an exhaustive review. In this sense it is an appropriate book for students or non-specialists in the field. One omission which appears significant is the effect of photochemistry on dynamics. This is an important dynamical effect which sets the stratosphere and mesosphere apart from the troposphere. Nonetheless, one of the virtues of this work may be that it does not attempt to present too much and thus dilute the significance of the most important advances made in the last 15 years. The author's perception of the substantial contributions and their interrelations is admirable.

Still, in a book which presents a record of the important results obtained over a number of years, one would expect the author to attempt a greater synthesis than is achieved here. There is no concluding chapter, just as there is no concluding section at the close of each chapter. For the most part, the reader is left to form his own opinion of the present level of our understanding of the observed stratosphere and mesosphere and his own outlook for future research. While these sorts of projections tend to become dated rather quickly and are not appreciated by some readers, to this reviewer the venturesome act of including a critical synopsis seems not only sporting but also worthwhile.

With this minor complaint aside, the book should be judged on its many merits. It presents a well-written up-to-date account of our present understanding of the chemically neutral dynamics of the stratosphere and mesosphere. All of the material included is of great interest and most of it is essential to a proper comprehension of the motions in these regions. A book of this type was not previously available and it will be of value to anyone concerned with the dynamic meteorology of the stratosphere and mesosphere.

Dennis L. Hartmann  
Department of Meteorology  
McGill University

# Atmosphere

Index to Volume 13, 1975

---

## Page Numbers of Issues

No. 1	1-36	No. 3	81-132
No. 2	37-80	No. 4	133-208
9th Annual Congress Issue	1-84		

Section A: Index of contributions by author

Section B: CMS subject index

Section C: General subject index

Figures in italics refer to 9th Annual Congress Issue

---

## Section A: Index of Contributions by Author

- ANGLE, R.P., Airflow from mustard to fallow, 110
- CHAUZY, S. (avec A. Elefterion et P. Sarthou), Une méthode d'étude expérimentale "in situ" de la zone d'échange entre les nuages convectifs et leur environnement, 49
- EAST, C., voir M.J.E. Gauthier
- ELEFTERION, A., voir S. Chauzy
- FLEER, H., see H. Flohn
- FLOHN, H. (with H. Fleer), Climatic teleconnections with the equatorial Pacific and the role of ocean/atmosphere coupling, 96
- FRASER, A.B., The green flash and clear air turbulence, 1
- GAUTHIER, M.J.E. (avec C. East), Techniques d'échantillonnage et d'analyse granulométrique des brouillards, 11
- HARTMANN, D., Review of *The Dynamic Meteorology of the Stratosphere and Mesosphere* (J.R. Holton), 205
- HAWKES, R.L., The 15-25  $\mu\text{m}$  barrier to drop growth in warm rain, 62
- KALMA, J.D., Review of *Global Climate* (K. Boucher), 205
- KHANDEKAR, M.L., see G.S. Strong
- LEAHEY, D.M., Review of *Atmospheric Diffusion* (F. Pasquill), 130
- MATEER, C.L., Review of *Actinometry, Atmospheric Optics, Ozonometry* (G.P. Gushchin, ed.), 34
- MCBEAN, G.A., Turbulent fluxes over Lake Ontario during a cold frontal passage, 37
- MEGAW, W.J., Review of *Nuclear Meteorology* (K.P. Makhon'ko and S.G. Malakhov, eds.), 132
- NEWARK, M.J., The relationship between forest fire occurrence and 500 mb longwave ridging, 26
- PETERSON, R.E., Snow devils - early observations, 77
- ROGERS, R.R., An elementary parcel model with explicit condensation and supersaturation, 192
- SARTHOU, P., voir S. Chauzy
- SIMONS, T.J., Effective wind stress over the Great Lakes derived from long-term numerical model simulations, 169
- STRONG, G.S. (with M.L. Khandekar), A note on fluctuations in the normal temperature trend at selected Canadian stations, 19
- SUNDQVIST, H., On truncation errors in sigma-system models, 81
- TABATA, S., The general circulation of the Pacific Ocean and a brief account of the oceanographic structure of the North Pacific Ocean, Part 1 - Circulation and volume transports, 133
- YAP, D., Review of *Review of Urban Climatology 1968-1973* (T.R. Oke), 130

## Section B: CMS Subject Index

- Annual Congress (9th), 28-30 May 1975,  
University of British Columbia, Van-  
couver  
Abstracts, 17  
Program, 3  
Summary of sessions, 1  
Annual General Meeting (9th), Agenda, 58  
Annual Reports for 1974  
Awards Committee, 65  
Centres, 70  
Citations Committee, 65  
Editorial Committee, 64  
Nominating Committee, 84  
President, 59  
Public Information Committee, 66  
Scientific Committee (SOMAS), 69  
Treasurer, 60  
Appel aux candidatures pour les prix et cita-  
tions 1975, 79, ibc no. 3  
Budget proposed for 1976, 63  
Call for nominations - 1975 awards, 76,  
ibc no. 3  
Call for papers - 10th Annual Congress,  
80, 125  
Contributions scientifiques au 10me  
Congrès Annuel, 80, 129  
Formule d'adhésion, 36  
Membership application form, 35  
Notice of motion for amendments to By-  
Laws, 82

## Section C: General Subject Index

- Airflow from mustard to fallow, 110  
Book reviews, by author of book  
Boucher, K., *Global Climate*, 205  
Gushchin, G.P., *Actinometry, Atmo-  
spheric Optics, Ozonometry*, 34  
Holton, J.R., *The Dynamic Meteorology  
of the Stratosphere and Mesosphere*,  
205  
Makhon'ko, K.P. and S.G. Malakhov,  
eds., *Nuclear Meteorology*, 132  
Oke, T.R., *Review of Urban Climatology*,  
130  
Pasquill, F., *Atmospheric Diffusion*, 130  
Brouillards, Techniques d'échantillonnage et  
d'analyse granulométrique des, 11  
Clear air turbulence, The green flash and, 1  
Climatic teleconnections with the equatorial  
Pacific and the role of ocean/atmo-  
sphere coupling, 96  
Condensation and supersaturation, An ele-  
mentary parcel model with explicit, 192  
Drop growth in warm rain, The 15-25  $\mu\text{m}$   
barrier to, 62  
Forest fire occurrence and 500 mb ridging,  
The relationship between, 26  
Fourier series on spheres, 180  
General circulation of the Pacific Ocean  
and a brief account of the ocean-  
ographic structure of the north Pacific  
Ocean, The, Part 1 - Circulation and  
volume transports, 133  
Green flash and clear air turbulence, The, 1  
Longwave ridging, The relationship between  
forest fire occurrence and 500 mb, 26  
Méthode d'étude expérimentale "in situ" de  
la zone d'échange entre les nuages  
convectifs et leur environnement, Une,  
49  
Notes and Correspondence  
Operation LEECAT, 126  
Snow devils - early observations, 77  
Nuages convectifs et leur environnement,  
Une méthode d'étude expérimentale  
"in situ" de la zone d'échange entre les,  
49  
Ocean/atmosphere coupling, Climatic tele-  
connections with the equatorial Pacific  
and the role of, 96  
Oceanographic structure of the north Pacific  
Ocean, The general circulation of the  
Pacific Ocean and a brief account of  
the, Part 1 - Circulation and volume  
transports, 133  
Parcel model with explicit condensation and  
supersaturation, An elementary, 92  
Sigma-system models, On truncation er-  
rors in, 81  
Techniques d'échantillonnage et d'analyse  
granulométrique des brouillards, 11  
Temperature trend at selected Canadian  
stations, A note on fluctuations of the  
normal, 19  
Truncation errors in sigma-system models,  
On, 81  
Turbulent fluxes over Lake Ontario during  
a cold frontal passage, 37  
Warm rain, The 15-25  $\mu\text{m}$  barrier to drop  
growth in, 62  
Wind stress over the Great Lakes derived  
from long term numerical model simu-  
lations, Effective, 169

## INFORMATION FOR AUTHORS

---

**Editorial policy.** *Atmosphere* is a medium for the publication of the results of original research, survey articles, essays and book reviews in all fields of atmospheric science. It is published quarterly by the CMS with the aid of a grant from the Canadian Government. Articles may be in either English or French. Contributors need not be members of the CMS nor need they be Canadian; foreign contributions are welcomed. All contributions will be subject to a critical review before acceptance. Because of space limitations articles should not exceed 16 printed pages and preferably should be shorter.

**Manuscripts** should be submitted to: the Editor, *Atmosphere*, West Isle Office Tower, 5th Floor, 2121 Trans-Canada Highway, Dorval, Quebec H9P 1J3. Three copies should be submitted, typewritten with double spacing and wide margins. Heading and sub-headings should be clearly designated. A concise, relevant and substantial abstract is required.

**Tables** should be prepared on separate sheets, each with concise headings.

**Figures** should be provided in the form of three copies of an original which should be retained by the author for later revision if required. A list of legends should be typed separately. Labelling should be made in generous size so that characters after reduction are easy to read. Line drawings should be drafted with India ink at least twice the final size on white paper or tracing cloth. Photographs (halftones) should be glossy prints at least twice the final size.

**Units.** The International System (SI) of metric units is preferred. Units should be abbreviated only if accompanied by numerals, e.g., '10 m', but 'several metres.'

**Footnotes** to the text should be avoided.

**Literature citations** should be indicated in the text by author and date. The list of references should be arranged alphabetically by author, and chronologically for each author, if necessary.

---

## RENSEIGNEMENTS POUR LES AUTEURS

---

**Politique éditoriale.** *Atmosphère* est un organe de publication de résultats de recherche originale d'articles sommaires, d'essais et de critiques dans n'importe lequel domaine des sciences de l'atmosphère. Il est publié par la SMC à l'aide d'une subvention accordée par le gouvernement canadien. Les articles peuvent être en anglais ou en français. Il n'est pas nécessaire que les auteurs soient membre de la SMC; les contributions étrangères sont bien-venues. A cause des limitations d'espace les articles ne doivent pas dépasser 16 pages dans le format final. Tout article sera soumis à un critique indépendant avant d'être accepté.

**Les manuscrits** doivent être envoyés à : le Rédacteur, *Atmosphère*, West Isle Office Tower, 5e étage, 2121 route Trans-canadienne, Dorval, Québec H9P 1J3. Ils doivent être soumis en trois exemplaires dactylographiés à double interlignes avec de larges marges. Les titres et sous-titres doivent être clairement indiqués. Chaque article doit comporter un résumé qui soit concis, pertinent et substantiel.

**Les tableaux** doivent être préparés et présentés séparément accompagnés d'un titre et d'un numéro explicatifs concis.

**Les graphiques** doivent être présentés en trois copies dont les originaux devraient être conservés par l'auteur au cas où ils seraient nécessaire de les reviser. Une liste des légendes des graphiques doit être dactylographiée séparément. L'étiquetage doit être de grand format de façon à ce qu'il soit facilement lisible après réduction du format. Le traçage des lignes doit s'effectuer au moyen d'encre de chine en doublant, au moins, le format final, le tout sur papier blanc ou sur papier à calquer et identifié adéquatement. Les photographies (demi-teintes) devraient être présentées sur épreuves glacées au double du format final.

**Les unités.** Le Système International (SI) d'unités métriques est préférable. Les unités devraient être abrégées seulement lorsqu'elles sont accompagnées de nombres, ex: "10m", mais "plusieurs mètres".

**Les notes de renvoi** au texte doivent être évitées.

**Les citations littéraires** doivent être indiquées dans le texte selon l'auteur et la date. La liste des références doit être présentée dans l'ordre alphabétique, par auteur et, si nécessaire, dans l'ordre chronologique pour chaque auteur.

---

## The Canadian Meteorological Society / La Société Météorologique du Canada

---

The Canadian Meteorological Society came into being on January 1, 1967, replacing the Canadian Branch of the Royal Meteorological Society, which had been established in 1940. The Society exists for the advancement of Meteorology, and membership is open to persons and organizations having an interest in Meteorology. At nine local centres of the Society, meetings are held on subjects of meteorological interest. *Atmosphere* as the scientific journal of the CMS is distributed free to all members. Each spring an annual congress is convened to serve as the National Meteorological Congress.

Correspondence regarding Society affairs should be directed to the Corresponding Secretary, Canadian Meteorological Society, c/o Dept. of Meteorology, McGill University, P.O. Box 6070, Montreal, P.Q. H3C 3G1

There are three types of membership – Member, Student Member and Sustaining Member. For 1975 the dues are \$20.00, \$5.00 and \$60.00 (min.), respectively. The annual Institutional subscription rate for *Atmosphere* is \$15.00.

Correspondence relating to CMS membership or to institutional subscriptions should be directed to the University of Toronto Press, Journals Department, 5201 Dufferin St., Downsview, Ontario, Canada, M3H 5T8. Cheques should be made payable to the University of Toronto Press.

---

La Société météorologique du Canada a été fondée le 1<sup>er</sup> janvier 1967, en remplacement de la Division canadienne de la Société royale de météorologie, établie en 1940. Cette société existe pour le progrès de la météorologie et toute personne ou organisation qui s'intéresse à la météorologie peut en faire partie. Aux neuf centres locaux de la Société, on peut y faire des conférences sur divers sujets d'intérêt météorologique. *Atmosphere*, la revue scientifique de la SMC, est distribuée gratuitement à tous les membres. À chaque printemps, la Société organise un congrès qui sert de Congrès national de météorologie.

Toute correspondance concernant les activités de la Société devrait être adressée au Secrétaire-correspondant, Société météorologique du Canada, Département de Météorologie, l'Université McGill, C.P. 6070, Montréal, P.Q. H3C 3G1

Il y a trois types de membres: Membre, Membre-étudiant, et Membre de soutien. La cotisation est, pour 1975, de \$20.00, \$5.00 et \$60.00 (min.) respectivement. Les Institutions peuvent souscrire à *Atmosphère* au coût de \$15.00 par année.

La correspondance concernant les souscriptions au SMC ou les souscriptions des institutions doit être envoyée aux Presses de l'Université de Toronto, Département des périodiques, 5201 Dufferin St., Downsview, Ontario, Canada, M3H 5T8. Les chèques doivent être payables aux Presses de l'Université de Toronto.

---

### Council / Conseil d'Administration: 1975-76

---

<i>President/Président</i>	– P.E. Merilees	<i>Councillors-at-large/Conseillers</i>
<i>Vice-President/Vice-Président</i>	– J.E. Hay	A.D.J. O'Neill
<i>Past President/Président sortant</i>	– A.J. Robert	R.M. Gagnon
<i>Corresponding Secretary/Secrétaire-correspondant</i>	– H.G. Leighton	D.B. Fraser
<i>Treasurer/Trésorier</i>	– J-G. Cantin	<i>Chairmen of Local Centres / Présidents des centres</i>
<i>Recording Secretary/Secrétaire d'assemblée</i>	– P.P. Zwack	<i>Chairman-Oceanography</i>
		C. Mann
		<i>Secretary-Oceanography</i>
		S. Smith

#### ATMOSPHERE

<i>Editorial Committee/Comité de rédaction</i>		
<i>Editor/Rédacteur</i>	I.D. Rutherford	
<i>Associate Editors/Rédacteurs Associés</i>	C. East	P.E. Merilees
	J.B. Gregory	R.R. Rogers
	W. Gutzman	V.R. Turner
	R. List	E.J. Truhlar
	C.L. Mateer	E. Vowinckel
	G.A. McBean	P.H. LeBlond
	D.N. McMullen	
<i>Sustaining Member/Membre de soutien</i>		Air Canada